

**Polymer-Based Hydrogen Carriers:
Their Synthesis and Electrolytic Hydrogenation**

高分子型水素キャリア：合成と電解水素化

February 2017

Waseda University
Graduate School of Advanced Science and Engineering
Department of Advanced Science and Engineering,
Research on Applied Chemistry A

Ryo KATO

加藤 遼

Promoter: Prof. Dr. Hiroyuki Nishide
Referees: Prof. Dr. Yasushi Sekine
Prof. Dr. Kenichi Oyaizu
Prof. Dr. Martin Sjödín
Dr. Hiroshi Mouri

Preface

Hydrogen is produced at chemical facilities and from a great variety of potential sources, subsequently stored and then delivered to an end-use application where water is the sole combustion or reaction product. Conventional storing and carrying methods of hydrogen use high pressure or cryogenic tanks; however, these methods intensively consume energy and are accompanied by inherent safety risks. Thus, hydrogen-storing and/or -carrying material systems with high safety, ease of handling and low energy loss during the hydrogen storing/carrying/releasing are highly demanded.

Recently, organic compounds with reversible hydrogen-storing capability have been intensively studied. These materials feature a high stability of the corresponding hydrogenated compounds due to the chemical bond formation and high hydrogen storage capacity. However, these compounds are mostly liquids or used as solutions and often suffer from safety issues of toxicity, flammability and volatility. Furthermore, their hydrogenation mostly proceeds at high pressure of hydrogen via highly energy-consuming processes. Although some of these liquid organic compounds have been tested as hydrogen storage materials on an industrial scale to be used in the existing infrastructure for oil storage and transportation, organic liquids are not always suitable to be examined in small-scale applications as hydrogen storage materials.

In this thesis, the author focused on electrolytic hydrogenation as a methodology of organic hydride production operated under mild conditions and only uses water as proton source. Furthermore, polymerized the organic hydrides and produced polymer-based hydrogen carriers having polymer's inherent advantages, such as mouldability, non-flammability and low toxicity. Chapter 1 describes the current trend of hydrogen storage materials and the reaction of the electrolytic hydrogenation. Chapter 2–6 describe the synthesis and hydrogen storage properties of polymer-based hydrogen carriers. The last chapter concludes this thesis and discusses the future prospects.

Ryo Kato

Contents

Preface

Chapter 1 General Introduction

| | | |
|-----|--|-------|
| 1.1 | Introduction | ...2 |
| 1.2 | Hydrogen Storage Materials | ...3 |
| 1.3 | Redox-Active Polymers for Charge Storage Materials | ...12 |
| 1.4 | Electrolytic Hydrogenation | ...17 |
| | References | ...20 |

Chapter 2 Synthesis of Fluorenone/FluorenoI Polymer for Cycle of Electrolytic Hydrogen-Fixing and -Releasing in Water

| | | |
|-----|---|-------|
| 2.1 | Introduction | ...28 |
| 2.2 | Redox and Hydrogen Storage Properties of Fluorenone | ...29 |
| 2.3 | Synthesis of Fluorenone/FluorenoI Polymer | ...34 |
| 2.4 | Hydrogen Storage Properties of Fluorenone/FluorenoI Polymer | ...38 |
| 2.5 | Experimental Section | ...45 |
| | References | ...53 |

Chapter 3 Poly(vinyl fluorenone/fluorenoI) for a Charge and Hydrogen Storage Material

| | | |
|-----|--|-------|
| 3.1 | Introduction | ...56 |
| 3.2 | Synthesis of Poly(vinyl fluorenone/fluorenoI) via Radical Polymerization | ...57 |
| 3.3 | Charge Storage Properties of Poly(vinyl fluorenone) | ...59 |
| 3.4 | Hydrogen Storage Properties of Poly(vinyl fluorenone) | ...61 |
| 3.5 | Experimental Section | ...65 |
| | References | ...68 |

Chapter 4 A Quinaldine Polymer: Ni-Electrodeposition-Assisted Hydrogenation and Hydrogen Evolution

| | | |
|-----|---|-------|
| 4.1 | Introduction | ...72 |
| 4.2 | Electrochemical Hydrogenation of Quinaldine | ...74 |
| 4.3 | Ni-Electrodeposition-Assisted Hydrogenation of Quinaldine Polymer | ...77 |
| 4.4 | Hydrogen Evolution from the Hydrogenated Quinaldine Polymer | ...79 |

| | | |
|--|--|--------|
| 4.5 | Experimental Section | ...81 |
| | References | ...83 |
| | | |
| <i>Chapter 5 Electrolytic Hydrogenation of Carbonyl Compounds with Water and Dehydrogenation Using the Iridium Catalyst</i> | | |
| 5.1 | Introduction | ...86 |
| 5.2 | Redox Properties of the Iridium Catalyst | ...87 |
| 5.3 | Hydrogen Storage Properties of the Carbonyl Compounds Using the Iridium Catalyst | ...89 |
| 5.4 | Experimental Section | ...94 |
| | References | ...101 |
| | | |
| <i>Chapter 6 Fixing of Redox-Active Hydroxy-TEMPO Radical for a Dye-Sensitized Solar Cell</i> | | |
| 6.1 | Introduction | ...104 |
| 6.2 | Redox Performance of the Fixed Hydroxy-TEMPO Radical in the Nafion Layer | ...106 |
| 6.3 | Aqueous Dye-Sensitized Solar Cell Performance using Nafion-Coated Electrode | ...108 |
| 6.4 | Experimental Section | ...109 |
| | References | ...110 |
| | | |
| <i>Chapter 7 Conclusion and Future Prospects</i> | | |
| 7.1 | Conclusion | ...114 |
| 7.2 | Future Prospects | ...115 |

List of publications

Acknowledgements

Chapter 1

General Introduction

Contents

1.1 Introduction

1.2 Hydrogen Storage Materials

1.3 Redox-Active Polymers for Charge Storage Materials

1.4 Electrolytic Hydrogenation

References

1.1 Introduction

Hydrogen is produced at chemical facilities and from a great variety of potential sources. These consist not only of fossil fuels but also as a by-product of chemical processes, biomass, and water¹⁻³. Furthermore, hydrogen can be directly converted into electric power using a high efficiency fuel cell, and in that case the by-product is only water. Because of these advantages, the application of hydrogen towards a clean and efficient fuel has gathered a lot of attention, and the construction of a new “hydrogen society”, which utilizes a system of delivering energy using hydrogen, is anticipated. However, hydrogen gas is difficult to handle because of its explosibility, permeability, and embrittlement. For many elements of the hydrogen society, such as production, storage, transportation, and utilization, the technological development of hydrogen storage and transportation are serious problems and create a bottleneck to expanding the society more widely⁴. Thus, safe and highly efficient hydrogen carrier or hydrogen storage materials are required.

Hydrogen storage materials have been studied in various fields and with various hydrogen storing and releasing systems, and these materials are suggested using some factors, such as gravimetric capacity, volumetric capacity, the condition of hydrogen storing and releasing, energy balance, safety, convenience, rate of hydrogen release, and so on. The usage requirements depend on the place and scale which they will be used.

In this thesis, the electrolytic hydrogenation of organic hydrogen carriers were applied to the hydrogen fixing or storage reaction as a methodology which does not require high temperature and pressure hydrogen gas. The organic hydrogen carriers were polymerized and demonstrated as a polymer-based hydrogen carriers, to apply the inherent advantages of the polymers, such as easy handling, mouldability, robustness, non-flammability and low toxicity, to the hydrogen storage materials.

In this chapter, three main topics, i.e., hydrogen storage materials (section 1.2), redox-active polymers for charged storage materials (section 1.3), and electrolytic hydrogenation (section 1.4) are reviewed to clarify the background of this thesis in terms of its application, materials, and approach. In section 1.2, the system of the hydrogen society and hydrogen storage materials are described. In section 1.3, redox-active polymers and their applications toward charged storage materials are summarized. In section 1.4, the basic concept and theory of electrolytic hydrogenation are described; and in particular, the electrochemical properties of conjugated carbonyl compounds are explained in detail.

1.2 Hydrogen Storage Materials

There are four steps, producing, storage, transportation, and utilization, necessary to use hydrogen as a fuel in the hydrogen economy (Figure 1.2.1), and the storage and transportation are the most important steps that currently constitute a bottleneck to using hydrogen more widely. The physical properties of hydrogen, such as explosibility, permeability, and embrittlement, present significant disadvantages for both storage and transporting⁵. Thus, storeable hydrogen materials containing high gravimetric density, high volumetric density, low energy loss for hydrogenation and dehydrogenation, high safety, and easy handling are most demanded to realize the hydrogen economy, as far as mobile applications are concerned.

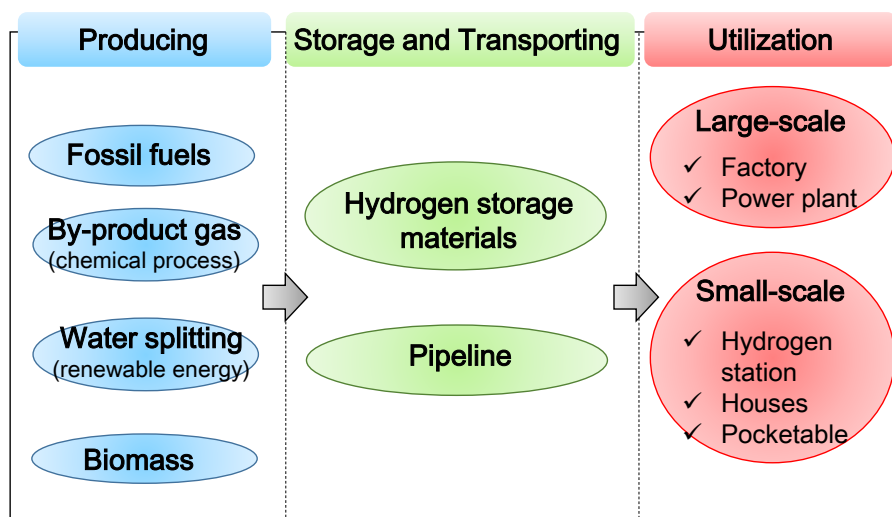
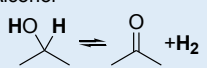
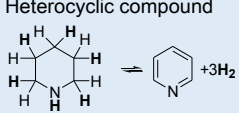


Figure 1.2.1 The system of the hydrogen economy

Recently, the definition of hydrogen storage materials has been expanded to not only consist of hydrogen tanks or porous materials, but also some hydrogen adducts, such as organic compounds, and the process or way of fixing hydrogen covers a lot of ground. Hydrogen storage materials are classified into two categories: physical storage and chemical storage. Physical storage materials include porous materials, such as zeolite, metal organic frame works (MOFs), porous carbons, and porous polymers, and high pressure and cryogenic tanks. Chemical storage materials include metal and organic hydride (Table 1.2.1)⁶. New hydrogen storage materials in each category are reviewed.

Table 1.2.1 Classification of hydrogen storage materials

| Physical storage | | Chemical storage | |
|--|--|---|--|
| High pressure and cryogenic tanks | Porous materials | Metal hydride alloys | Organic hydride |
| Compression | Adsorption (Physisorption) | Forming chemical bond or Solid solution | Forming chemical bond |
| <ul style="list-style-type: none"> ✓ High pressure tank ✓ Cryogenic tank | <ul style="list-style-type: none"> ✓ Zeolites ✓ MOFs ✓ Porous carbons ✓ Polymers | AB ₅ : LaNi ₅ (1 wt%), MmNi ₅ ... AB ₂ : MgZ ₂ , ZrNi ₂ ... AB: TiFe, TiCo... BCC: Ti-V, Ti-Cr... | Alcohol  Heterocyclic compound  |

1.2.1 Physical storage

(a) High pressure and cryogenic tanks

The most common storing and carrying methods of hydrogen are those using high pressure or cryogenic tanks. The gravimetric and volumetric density depended on the pressure and weight of tanks. Table 1.2.2 shows some common conditions and densities^{7,8}. High pressure tanks are now used widely in society: For example, fuel cell vehicles and hydrogen gas stations store hydrogen in high pressure tanks with a pressure of 35 and 70 MPa⁹. Liquid hydrogen can store hydrogen at a higher density than that of compressed hydrogen gas, however the tank should be kept at a very low temperature and intensively consume energy.

These methods are mostly accompanied by inherent safety risks, such as explosions (for example, by collisions), permeability of hydrogen and embrittlement of the tank walls⁵. Thus, hydrogen-storing and/or -carrying material systems with high safety, ease of handling and low energy loss during the hydrogen storing/ carrying/releasing are highly demanded.

Table 1.2.2 Hydrogen storage with high pressure and cryogenic tanks

| Storage method | Gravimetric density (wt%) | Volumetric density (kg H ₂ m ⁻³) | Temperature (°C) | Pressure (bar) |
|-----------------------------------|---------------------------|---|------------------|----------------|
| High pressure tank | ca.13 | < 40 | RT | 800 |
| | ca. 2.5 | 200 | 0 | 350 |
| Liquid hydrogen in cryogenic tank | Size dependent | 70.8 | -252 | 1 |

(b) Porous materialsPorous carbons

Activated carbon-based materials have a high degree of porosity and a larger surface area, for example, the pouring diameter size is usually less than 1 nm and the surface area can be up to $3000 \text{ m}^2 \text{ g}^{-1}$ ¹⁰. Because of the huge surface area, they have been studied as materials for the adsorption of gases.

Carbon nanotubes were also studied as hydrogen storage materials after they were discovered in 1993¹¹. The gravimetric and volumetric hydrogen density of carbon nanotubes depended on many factors such as storage pressure and temperature, geometry, purification, pretreatment, and structure. Table 1.2.3 shows some reports of hydrogen capacity in carbon nanotubes¹⁰⁻¹³.

Table 1.2.3 Hydrogen storage with carbon nanotubes

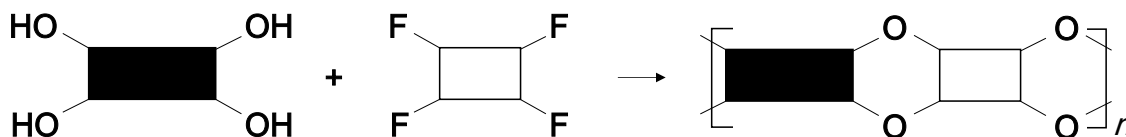
| Storage method | Gravimetric density (wt%) | Temperature (°C) | Pressure (MPa) |
|----------------|---------------------------|------------------|----------------|
| SWNT | 4.2 | 27 | 10.1 |
| | 8.2 | -193 | 7 |
| MWNT | 5-7 | 27 | 1 |
| | 13.8 ^{a)} | 27 | 1 |

a) Acid pretreatment

Porous polymers

Porous polymers for hydrogen storage are divided into three categories: polymers of intrinsic microporosity (PIMs), hyper-cross-linked polymers (HCPs), and covalent organic frameworks (COFs).

PIMs are mostly synthesized by using two or three rigid moieties in order to avoid making a planar structure in the final molecules. The most popular way of achieving this outcome is by introducing a spiro-center¹⁴⁻²⁰. The typical synthesis of PIMs is shown in Figure 1.2.2.

**Figure 1.2.2** Synthesis of PIMs

Hypercrosslinked polystyrene having a high surface area has been reported^{21–24}. Hypercrosslinked polystyrene is often prepared by suspension polymerization of a lightly crosslinked gel. The lightly crosslinked gel was swollen in some solvent and crosslinked via a Friedel-Crafts acylation of the chloromethyl groups. Figure 1.2.3 shows the typical scheme of the polymerization. The size of the pores of the polymer was mostly ca. 2 nm.

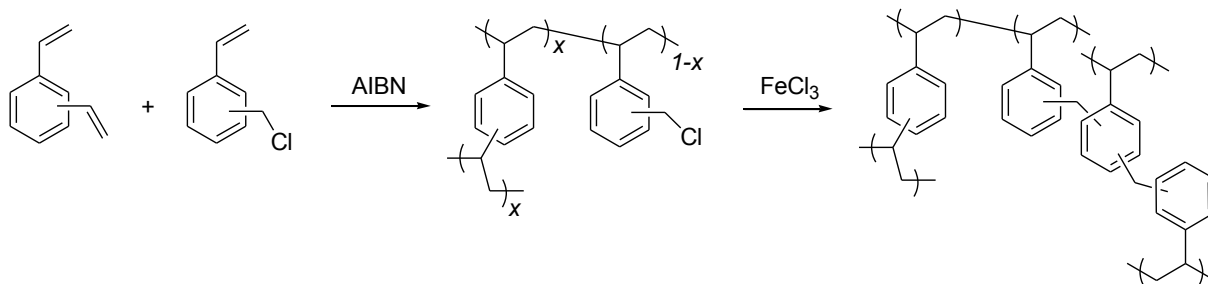


Figure 1.2.3 Scheme of the synthesis of HCP

The design of COFs allows for much finer control over the properties of crystallinity and porosity, compared to HCPs and PIMs. Table 1.2.4 shows an example of the hydrogen capacity of each porous polymer^{25–27}.

Table 1.2.4 Hydrogen storage with porous polymers

| Storage method | Gravimetric density (wt%) | Temperature (°C) | Pressure (MPa) |
|----------------|---------------------------|------------------|----------------|
| PIMs | 2.7 | -196 | 10 |
| HCPs | 3.7 | -196 | 15 |
| COFs | 7.2 | -196 | 70 |

MOFs

Mostly MOFs (metal-organic frameworks) and IRMOFs (isoreticular metal-organic frameworks) have very high surface areas and are often applied to materials for gas separation and storage^{28–30}. The first application of MOFs to hydrogen storage was reported by Yaghi's group in 2003³¹. The capacity of the reported MOF was 1 wt% at room temperature under 20 bars. Recently, many kinds of MOFs have been developed and the capacity of MOFs has increased³².

1.2.2 Chemical storage

(a) Metal hydride alloys

Metal hydride alloys are one of the most popular hydrogen storage materials and some of them have been used as particular materials in many contexts. Hydrogen is often fixed in place by forming a chemical bond or forming a solid solution, and the capacity of hydrogen depended on the temperature and pressure of hydrogen gas. Table 1.2.5 shows the categories of general metal hydride alloys³³.

Table 1.2.5 Categories of metal hydride alloys

| Category | Crystalline structure | Examples |
|------------------|-----------------------|--|
| AB ₅ | Hexagonal | LaNi ₅ , MmNi ₅ |
| AB ₂ | Hexagonal or cubic | MgZn ₂ , ZrNi ₂ |
| AB | Cubic | TiFe, TiCo |
| A ₂ B | Hexagonal | Mg ₂ Ni, Mg ₂ Cu |
| BCC | Body-centered cubic | Ti-V, Ti-Cr |

(b) Organic hydride

Recently, the number of papers about liquid organic hydrogen carriers or organic hydride, which stores hydrogen by forming chemical bonds, has been dramatically increasing. These materials exhibit a high degree of stability of the corresponding hydrogenated compounds due to chemical bond formation, and some of them were tested in large-scale environments, such as factories, because they can be used with existing infrastructure for oil storage and transportation.

Alcohols

Hydrogen evolution from alcohols and the hydrogenation of ketones was the most simple, reversible hydrogen storage reaction. Steam reforming of alcohols is one of the most popular reactions for bringing about hydrogen evolution. However, the reactions were often conducted under high temperatures. The wide distribution of products and the difficulty of separating the alcohol from the other products were also issues against using the reaction as hydrogen storage materials or in a larger system³⁴. To conduct hydrogen evolution from alcohols and the hydrogenation of ketones under mild conditions, metal complex catalysts for the reactions have been studied and developed.

Yamaguchi and Fujita's group reported a series of Cp*Ir complex catalysts bearing hydroxypyridine ligands for the dehydrogenation of alcohols and hydrogenation of ketones^{35,36}. Ir complexes exhibited well conversion efficiency and turnover numbers from alcohols to ketones under relatively mild conditions (ca. 120 °C, 1 atm) due to the ligand effect. Protic functional groups, such as hydroxyl groups, on the ligand promote the release of hydrogen gas from the metal hydride intermediate and the ligand (Figure 1.2.4). Particularly, the group developed water-soluble Cp*Ir complex using a bipyridine-based functional ligand, and the catalyst showed an over 80% conversion efficiency from alcohols to ketones in water at 100 °C in 1 atm³⁷. The hydrogen evolution reaction resulting from alcohols using water-soluble Ir complex was also based on the ligand effect (Figure 1.2.5).

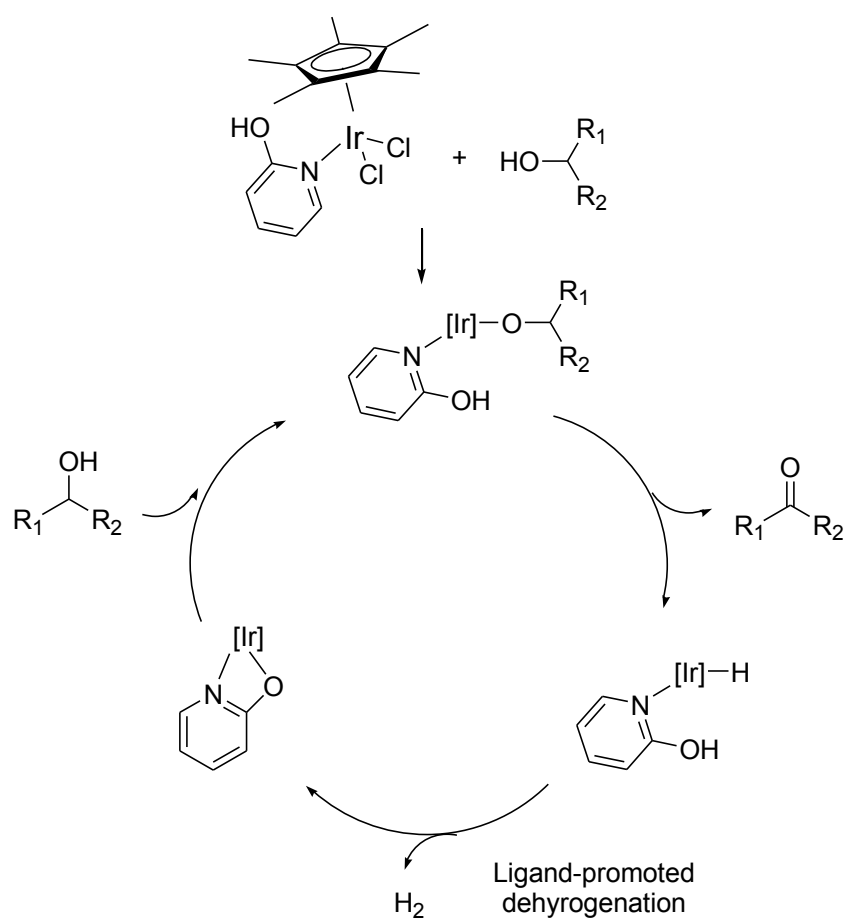


Figure 1.2.4 Mechanism for the dehydrogenation of alcohols catalyzed by Cp*Ir complex

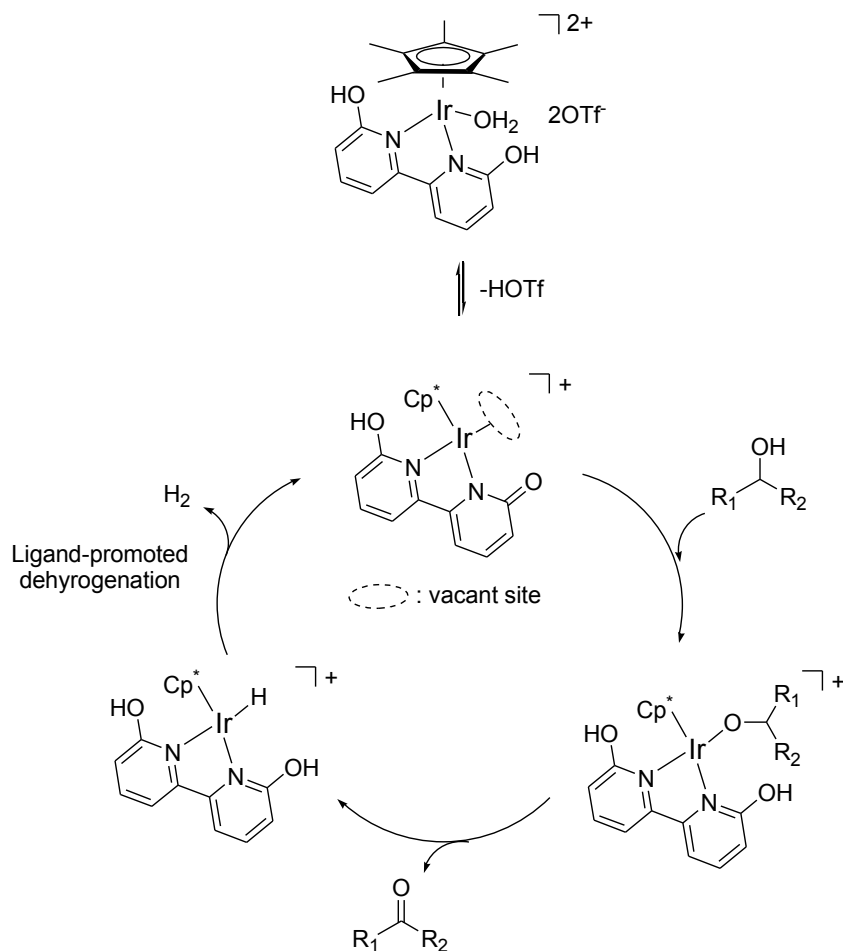


Figure 1.2.5 Mechanism for the dehydrogenation of alcohols in water catalyzed by Cp*Ir complex

Recently, Beller's group reported a successful hydrogen evolution from methanol with water using ruthenium complexes under mild conditions (65–95 °C)³⁸. The system was not reversible, but the hydrogen density was so high due to consuming water as an additional hydrogen source. The scheme was shown below:

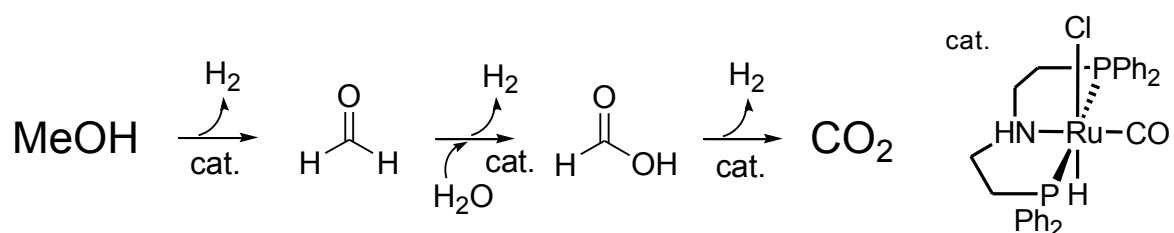
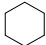
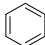
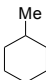
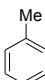
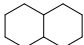
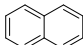


Figure 1.2.6 Scheme of the dehydrogenation of methanol with the Ru catalyst

Cycloalkanes

The hydrogenation and dehydrogenation of cycloalkanes has been studied as a basic foundation of organic chemistry, and recently has been applied to hydrogen storage materials and tested at a large-scale. The advantages of cycloalkanes as hydrogen storage materials are a relatively higher hydrogen capacity, being a liquid organic hydrogen carrier, and having a high boiling point. However, the disadvantage of using cycloalkanes as a hydrogen storage material is the limitations of their dehydrogenation conditions. Most cycloalkanes need high temperatures to release hydrogen, some as high as ca. 300 °C. Table 1.2.6 shows the hydrogen storage properties of cycloalkanes^{39–43}.

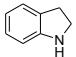
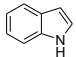
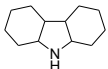
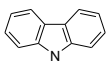
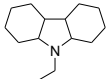
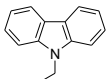
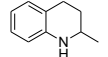
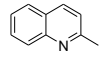
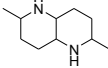
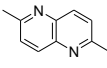
Table 1.2.6 Hydrogen storage properties of cycloalkanes

| Cycloalkanes | Product of dehydrogenation | Gravimetric density (wt%) | Heat of desorption ΔH (kJ/mol _{H₂}) | Dehydrogenation temperature (°C) |
|--|--|---------------------------|--|----------------------------------|
|  |  | 7.2 | 68.6 | 300 |
|  |  | 6.2 | 68.3 | ca. 300 |
|  |  | 7.3 | 63.9 | ca. 320 |

N-Heterocycles

Crabtree's group indicated that the hydrogen evolution temperature of cycloalkanes could be reduced by incorporating N atoms into the rings or ring substituents using thermodynamic calculations^{44–49}. The N–H bond and the neighboring C–H bonds are weaker than the C–H bonds of carbocycles and the heterocycles thermodynamically favor releasing hydrogen under relatively mild conditions. Table 1.2.7 shows some examples of the hydrogen storage properties of N-heterocycles^{50–53}.

Table 1.2.7 Hydrogen storage properties of N-heterocycles

| N-heterocycles | Product of dehydrogenation | Gravimetric density (wt%) | Calculated ΔH (kJ/mol _{H₂}) | Catalyst and activity |
|---|---|---------------------------|--|------------------------------------|
|  |  | 1.7 | 51.9 | Pd or Ru/C, 110 °C |
|  |  | 6.7 | 51.1 | Pd/C, 170 °C |
|  |  | 5.8 | 50.6 | Pd/C, 170 °C Ir complex, 200 °C |
|  |  | 2.7 | | Ir complex, 138 °C |
|  |  | 6.0 | | Ir complex, 138 °C |

Yamaguchi and Fujita's group reported the catalytic activity of the Cp*Ir complexes for reversible hydrogenation and dehydrogenation reactions of nitrogen heterocycles and applied the heterocycles to hydrogen storable organic compounds^{52,53}. The mechanism of the reaction between the Ir catalyst and nitrogen heterocycles was reposed by Zhang and Xi group's using theoretical calculations at the B3LYP level, and the group highlighted the importance of the ligand-promoted dehydrogenation process⁵⁴.

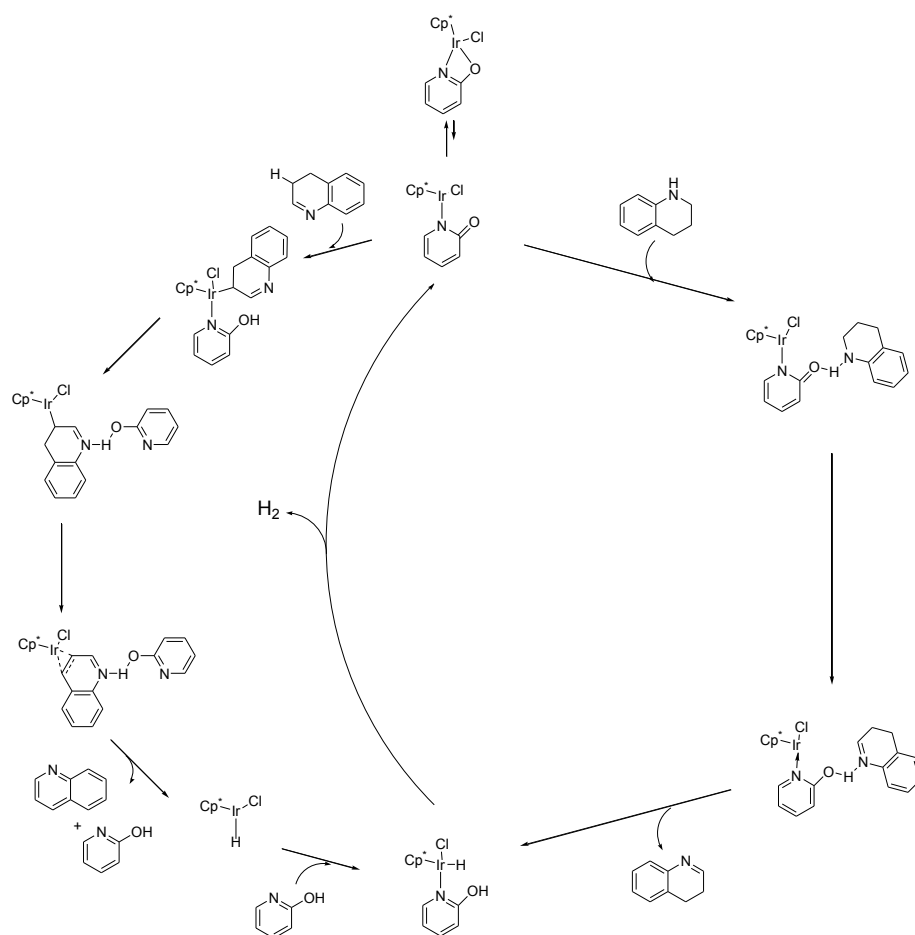


Figure 1.2.7 Mechanism for the dehydrogenation of nitrogen heterocycle catalyzed by Cp*Ir complex

1.3 Redox-Active Polymers for Charge Storage Materials

The system of charged storage materials, such as batteries, is controlled by a reversible redox reaction at each electrode. Redox-active polymers are polymers which have redox-active units in their backbones and/or side chain, and they have been studied as electrode active materials, that could be applied to the anode and/or cathode of a battery.

There are three types redox-active polymers: the p-type, n-type, and b-type, and they are classified depending on their redox reactions. For example, the p-type can be electrochemically oxidized (p-doped), the n-type can be electrochemically reduced (n-doped), and the b-type can be electrochemically oxidized and reduced⁵⁵.

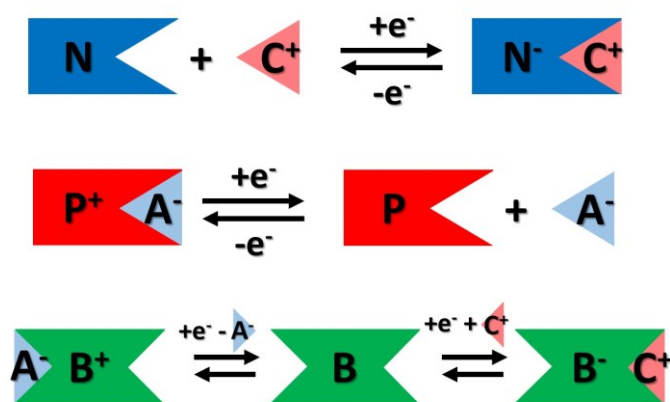


Figure 1.3.1 The redox reaction of three types: (a) n-type, (b) p-type, and (c) b-type.

Since the 1980s, conductive polymers, such as poly(pyrrole), poly(aniline), and poly(thiophene), have attracted a lot of attention and have been studied as the next generation of electrode-active materials⁵⁵⁻⁶⁹.

In the case of conjugated polymers, their electrochemical properties result from overlapping π -orbitals. Thus, their conductivity and redox properties depend on doping, and the one of the advantages of conductive polymers is their inherent conductivity. However, conductive polymers have some disadvantages in utilizing them for charged storage materials. The biggest issue is that their redox potential depends on the doping level and change during charging and discharging.

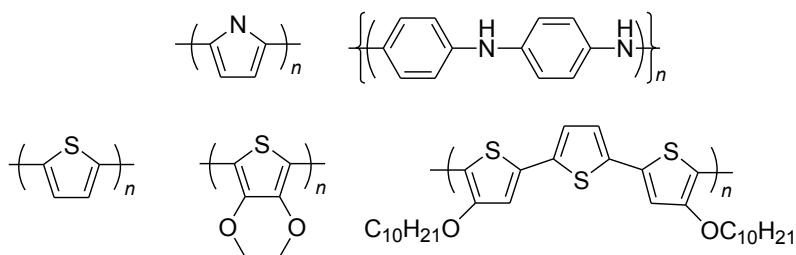


Figure 1.3.2 The conjugated polymers.

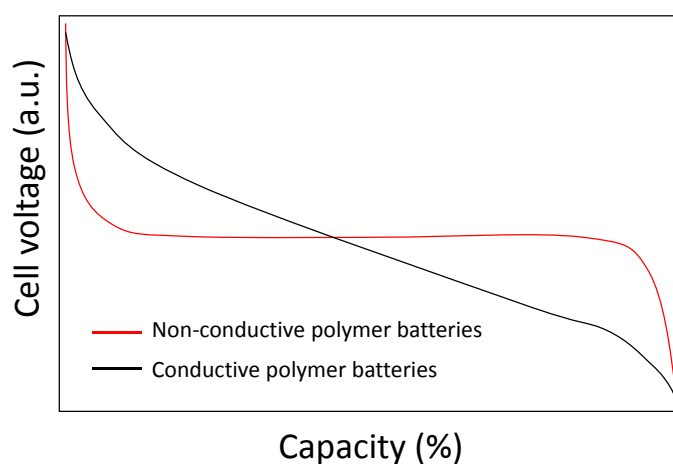


Figure 1.3.3 Comparison of the discharging behavior of batteries based on non-conductive and conductive polymers⁷⁰.

Because of some of the inherent disadvantages of conjugated polymers as charged storage materials, such as decreasing cell voltage depending on capacity and the limitation of the active moieties, studies have shifted to redox polymers for use as charged storage materials. The typical application of redox polymers were a kind of ion-exchanging resin. However, a redox polymer as defined here is a polymer which contains redox active moieties in their main and/or side chain and exhibits electrochemical redox behavior as an electro-active material. Most redox polymers consist of a non-conductive backbone and a number of electroactive pendant groups, thus sometimes the polymers were categorized as non-conductive polymers. A series of redox compounds, which have been reported as redox polymers for electroactive material, were shown below:

1.3.1 Conjugated carbonyl compound

Conjugated carbonyl compounds are a well-known type of organic compound with good electroactivity. Most could form stable anion radical and dianion states by electrolytic reduction (Figure 1.3.4), which can be augmented by a conjugated structure⁷¹⁻⁸⁶. Furthermore, because of their high theoretical capacity, fast reaction kinetics, as well as their structural diversity, they have been applied as anode-active materials for batteries. Typical small organic compounds made up of conjugated carbonyl compounds are shown in Figure 1.3.5.

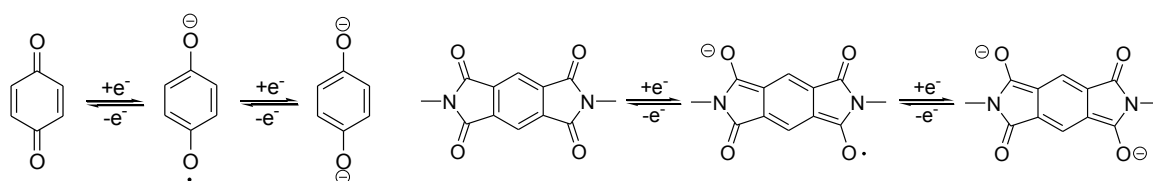


Figure 1.3.4 Redox reaction of quinone and imido

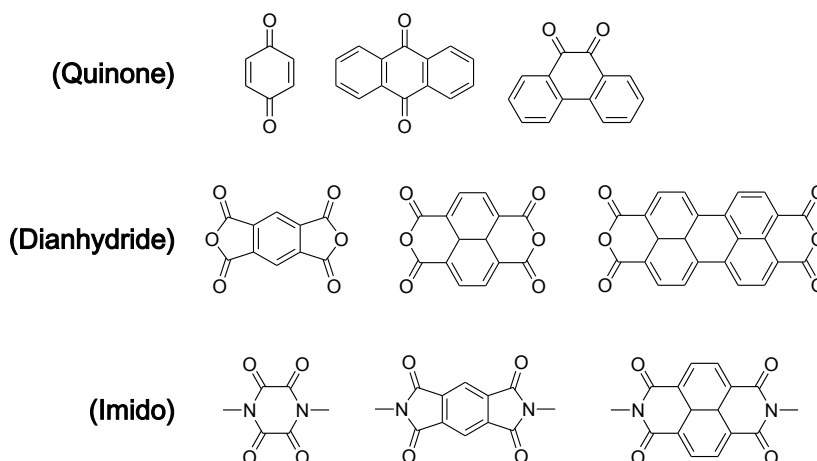


Figure 1.3.5 Typical conjugated carbonyl compounds

When the redox polymer was coated on a current corrector, it could exhibit reversible charging- and discharging-properties, and the plateau potential of the polymer coated electrode depended on the redox potential of the redox site in the polymer chain. The potential did not depend on the capacity or doping level, unlike the conductive polymer.

The charge was transported in the redox polymer layer resulting from the electron exchanging reaction between each redox site and the mass transfer process of ions (Figure 1.3.6). The diffusion coefficient of the charge depended on the self-electron-exchange rate constant (k_{ex}), the distance between the redox sites (δ), and the concentration of redox sites in the polymer layer (C) and then estimated using Laviron-Andrieux-Savéant equation as $D = k_{ex}\delta C/6$.

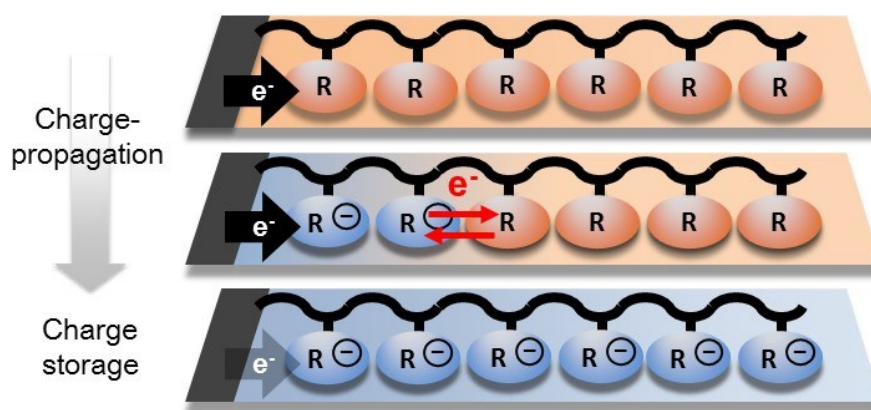


Figure 1.3.6 Charge propagation in redox polymer layer

1.3.2 Organic radical polymers

Organic radical polymers have been studied mostly as p-type redox-active materials. Some radical moieties were robust and stable, even though they had highly reactive, singly occupied molecular orbitals: Nitroxide, nitronyl nitroxide, phenoxy, and galvinoxyl radical were typical examples of stable organic radicals and were applied to redox-active sites in the polymers (Figure 1.3.7)⁸⁷⁻⁹⁹.

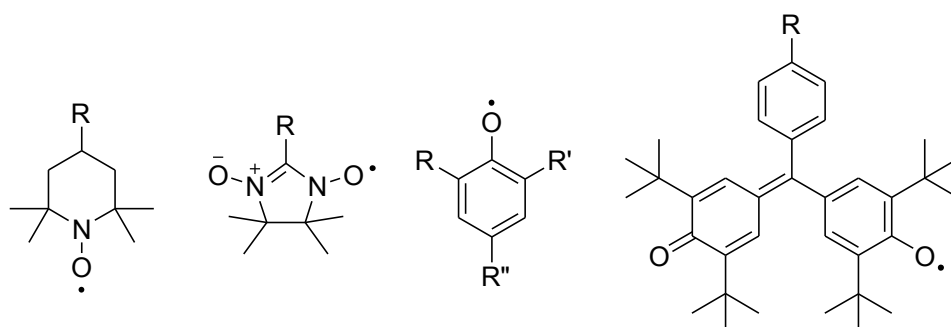


Figure 1.3.7 Typical examples of the stable organic radical molecules

The organic radical polymers containing radical units at high populations could store and propagate electrons by using the singly occupied molecular orbitals as hopping sites. Electron-propagation depended on the rapid electron exchange reaction between each organic radical site and the mass transfer process of ions. The driving force was a redox gradient in the polymer layer, and the current density (J) depended on Fick's laws (Figure 1.3.8). Thus, the population of radical sites in the polymer and the swellability of the polymer into the electrolyte could be of great importance for rapid charging- and discharging-properties and capacity. In most cases, the redox-active sites were introduced into the polymer as shown in Figure 1.3.9, in order to increase either the population or the capacity as well as to improve swellability.

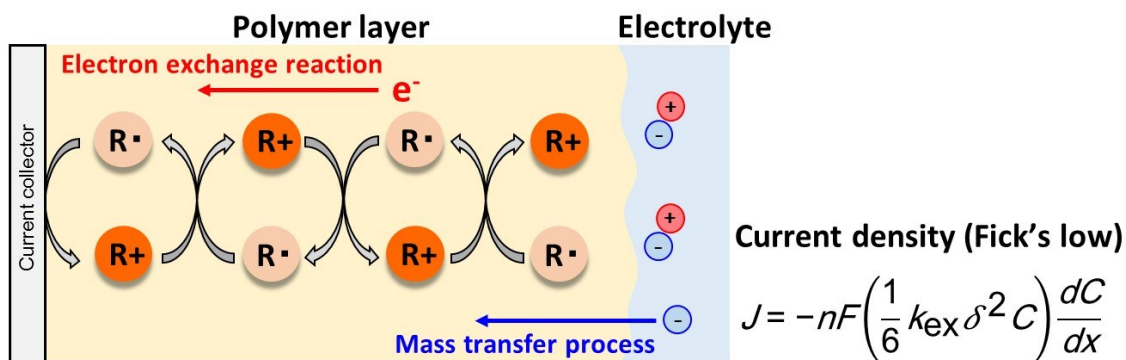


Figure 1.3.8 Charge transportation in the organic radical polymer layer

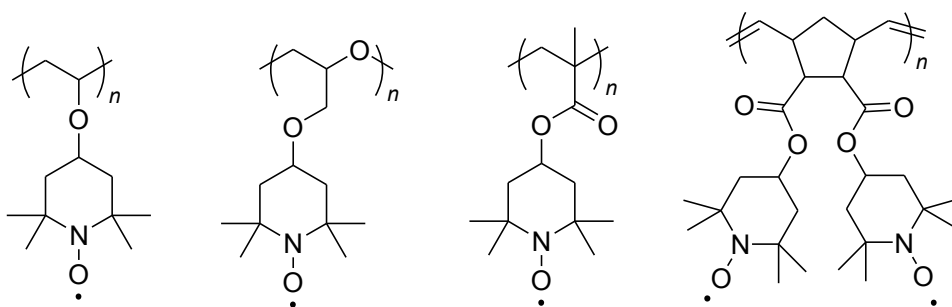


Figure 1.3.9 Structure of organic radical polymers

1.3.3 Application for charge storage materials

Redox polymer-coated electrodes have been applied to charge storage materials such as wet-type secondary batteries (Figure 1.3.10). P-type redox polymers act as cathode-active materials and can be applied to, for example, the cathodes of lithium-ion batteries. N-type redox polymers act as anode-active materials and can be applied to, for example, the anodes of air secondary batteries. Typical current collectors coated with redox polymers containing anthraquinone as a redox site in the side chain at high populations, such as poly(vinyl anthraquinone)¹⁰⁰ and poly(anthraquinone-substituted norbornene)¹⁰¹, have exhibited high energy densities, excellent rate performances, and good cycle performances of the polymer-air secondary battery resulting from rapid electron-exchange reactions between the anthraquinone sites and charge propagation.

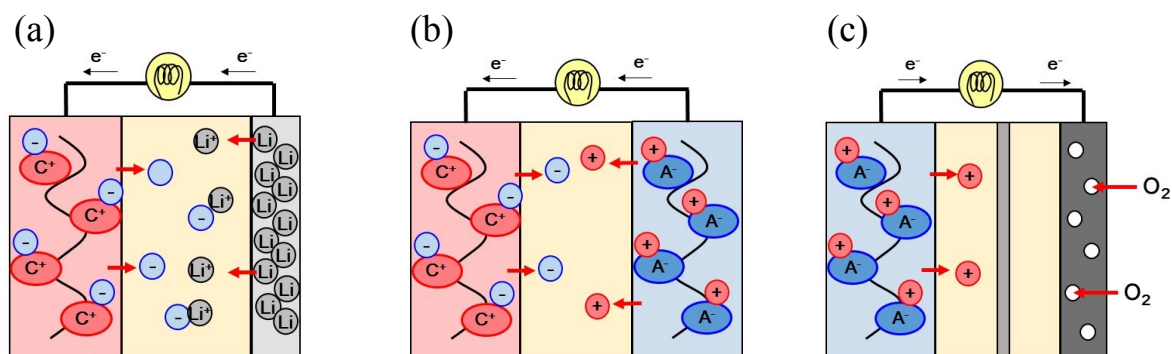


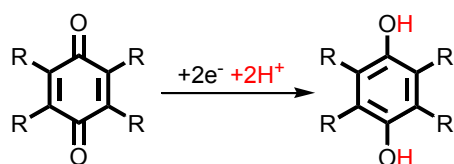
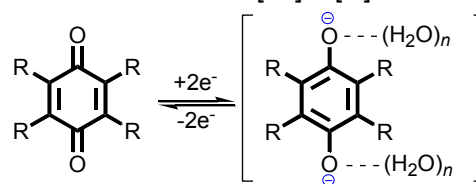
Figure 1.3.10 Schematic representations of the redox polymer in a (a) Li-ion battery, (b) polymer battery, and (c) polymer-air battery.

1.4 Electrolytic Hydrogenation

In situ electrochemical hydrogenation using electrons from a cathode and protons from water provides an alternative formation route of hydrogenated organic molecules at room temperature and an open-air atmosphere, with the advantages of being a simple experimental system and an electrochemically tunable reaction. The procedure of electrolytic hydrogenation is commonly divided into two categories: Hydrogenated compounds are produced by electrolytic reduction and protonation, and hydrogenated compounds are produced by using hydrogen activated by homogeneous or heterogeneous catalysts.

1.4.1 Electrolytic hydrogenation of quinone

The redox properties of quinones in a protic solvent, such as one which is buffered or unbuffered aqueous, have been studied as an electrochemistry of hydrogenation or protonation. The protonation or redox reaction of quinone in a protic solvent with $2e^-$ and $2H^+$ is the most popular description. However, there are some reports suggesting that the appearance of two redox waves of quinone in aprotic solvent, and that the number of waves depends on the concentration of protons and quinone^{102,103}. Figure 1.4.1 (b) shows another description of the redox reaction, which concerns pH dependence, and could bridge the redox properties of quinones in protic and aprotic solvents^{104–109}.

(a) Buffered water or unbuffered with $[H^+] > [Q]$ (b) Unbuffered water with $[H^+] < [Q]$ **Figure 1.4.1** Redox reaction of quinone in protic solvents

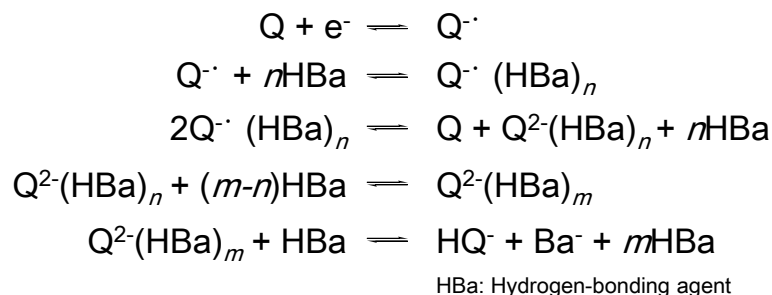
As the scheme of Figure 1.4.1 (b) shows, the strength of the hydrogen bonding of quinone largely effects its own redox properties. Many papers show that the second redox wave of quinone derivative, which was the redox reaction of $Q^{\cdot -}/Q^{2-}$, exhibited large positive shifts by adding weak hydrogen-bonding agents such as alcohols^{110–113}, and the difference in potential between the two redox waves became smaller. The positive shift of the potential increased with the concentration of additive agents. This result indicated the changing of the equilibrium constant for the comproportionation reaction K_c of scheme 1.4.1. The K_c can be calculated from the difference in redox potential between the two waves using the equation below (at 25 °C)¹¹⁴.

$$Q + Q^{2-} \rightleftharpoons 2Q^{\cdot -}$$

$$\log K_c = \frac{(E^0_{Q/Q^{\cdot -}} - E^0_{Q^{\cdot -}/Q^{2-}})}{0.0592 \text{ V}}$$

Scheme 1.4.1 The equilibrium constant for the comproportionation reaction

In the case of adding mild hydrogen-bonding agents such as trifluoroethanol to the electrolyte containing quinones, the form changing of the quinone redox waves was different compared to the changing of the redox wave of the quinone by adding weak hydrogen-bonding agents. The first wave not only shifted positive, but also changed shape irreversibly, and the current of the reduction peak increased by adding the hydrogen-bonding agents¹¹⁵. The increase of the first reduction peak showed the disproportionation of the semiquinone catalyzed by the hydrogen-bonding agent (Scheme 1.4.2)¹¹⁶. After the disproportionation, the dianion quinone could be protonated if the dianion quinone was a strong base.



Scheme 1.4.2 Disproportionation and protonation of quinone with hydrogen-bonding agent

1.4.2 Electrolytic hydrogenation with catalytic electrode

The redox-inactive organic compounds, including unsaturated compounds, could be electrochemically hydrogenated by using chemisorbed hydrogen on the catalytic electrode (Figure 1.4.1). In the electrolytic hydrogenation with catalytic electrode, the hydrogen source was mostly a solvent, such as water, and supporting electrolyte, and the potential for hydrogenation resulted from the reduction potential of both.

The process of electrocatalytic hydrogenation of unsaturated compounds is shown in Figure 1.4.2¹¹⁷. At first, the unsaturated compounds were adsorbed into the electrode and hydrogenated with the chemisorbed hydrogen. Then the hydrogen adducts were desorbed. During the electrolytic hydrogenation of unsaturated compounds, for the most part the hydrogen evolution reaction could also proceed, and the rate of hydrogenation of the organic compounds and of hydrogen evolution depended on many factors, including the solvent, electrolyte, substrate, metal of the electrode, applied potential, and so on^{118–121}.

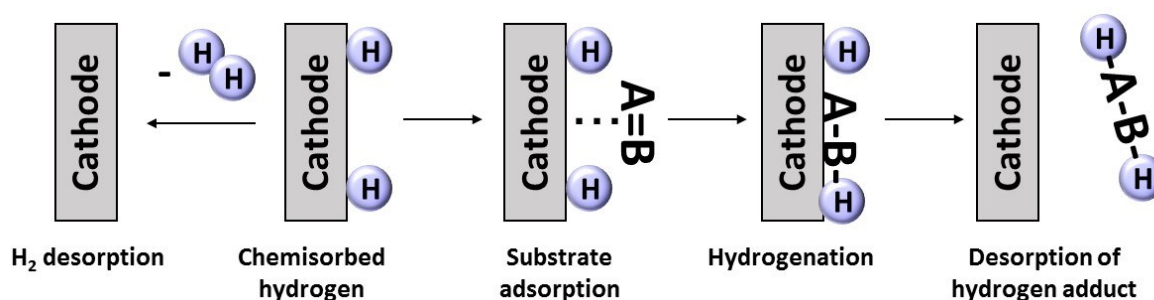


Figure 1.4.2 The mechanism of electrocatalytic hydrogenation of the unsaturated compound

The surface area of the cathode was one of the most important factors for the high catalytic activity to hydrogenate the unsaturated compounds in the bulk electrolyte solution. Metal electrodeposition on the polymer-coated cathode has been studied in order to prepare high surface area catalytic-electrodes^{122–128}. The polymer layer works as a scaffold for the

metal electrodeposition, leading to electrodeposition of well-dispersed metal microparticles.

The polymer layer worked not only to increase the surface area of the cathode, but also to improve the catalytic activity of the electrodeposited metal. A highly active water splitting using polypyrrole and an MoS_x copolymer coated electrode was reported by Li's group¹²⁹. The group suggested that the S-rich MoS_x was formed in the electrolytic polymerized pyrrole which led to the high activity for water splitting or the hydrogen evolution reaction.

The electrolytic hydrogenation of hydrogen-storable organic compounds, such as toluene, using water as a hydrogen source has also been investigated^{130,131}. Generally, cells of electrolytic hydrogenation were composed with a Pt-containing membrane electrode and a polymer electrolyte. Recently, the electrocatalytic hydrogenation of toluene using acid microemulsion electrolyte was reported, whose system was simpler and cheaper than the membrane electrode system¹³². The system achieved a Faradaic efficiency of 80%, but the side reaction of producing cyclohexane was an issue. The cell configuration and cell reaction are shown in Figure 1.4.3.

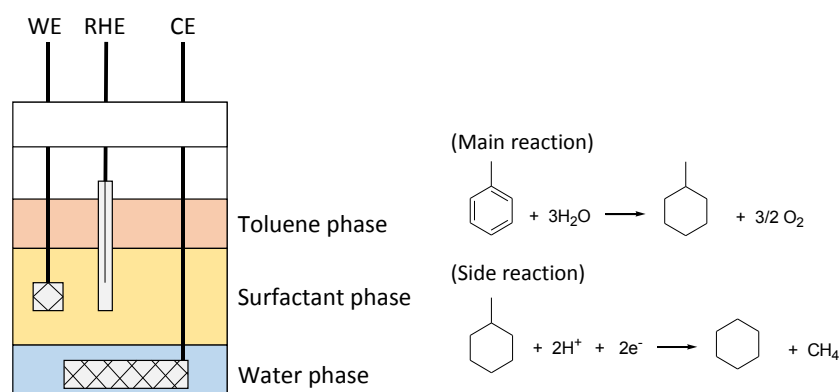


Figure 1.4.3 Schematic diagram of the electrolytic hydrogenation of toluene

References

- 1 R. C. Armstrong, C. Wolfram, K. P. Jong, R. Gross, N. S. Lewis, B. Boardman, A. J. Ragauskas, K. Martinez, G. Crabtree, M. V. Ramana, *Nat. Energy* **2016**, *1*, 1.
- 2 L. Schlapbach, A. Züttel, *Nature* **2001**, *414*, 353.
- 3 B. Steele, A. Heinzl, *Nature* **2001**, *414*, 345.
- 4 B. Liu, F. Li, L. Ma, H. Cheng, *Adv. Mater.* **2010**, *22*, E28.
- 5 J. Zheng, X. Liu, P. Xu, P. Liu, Y. Zhao, J. Yang, *Int. J. Hydrogen Energy* **2012**, *37*, 1048.
- 6 A. Dalebrook, W. Gan, M. Grasmann, S. Moret, G. Laurenczy, *Chem. Commun.* **2013**,

- 49, 8735.
- 7 A. Mazzucco, M. Dornheim, M. Sloth, T. Jensen, J. Jensen, M. Rokni, *International Journal of Hydrogen Energy* **2014**, *39*, 17054.
 - 8 A. Zuttel, *Naturwissenschaften* **2004**, *91*, 157.
 - 9 M. Felderhoff, C. Weidenthaler, R. Helmolt, U. Eberle, *Phys. Chem. Chem. Phys.* **2007**, *9*, 2643.
 - 10 Y. Ye, C.C. Ahn, C. Whitam, B. Fultz, L. Liu, A.G. Rinzler, D. Colbert, K.A. Smith, R.E. Smalley, *J. Appl. Phys. Lett.* **1999**, *74*, 2307.
 - 11 C. Liu, Y.Y. Fan, M. Liu, H.T. Cong, H. M. Cheng, M. Dresselhaus, *Science* **1999**, *286*, 1127.
 - 12 C. Liu, Q. H. Yang, Y. Tong, H. T. Cong, H. M. Cheng, *Appl. Phys. Lett.* **2002**, *80*, 2389.
 - 13 Y. Chen, D. T. Shaw, X. D. Bai, E. G. Wang, C. Lund, W. M. Lu, D. D. L. Chung, *Appl. Phys. Lett.* **2001**, *78*, 2128.
 - 14 N. B. McKeown, B. Gahnem, K. J. Msayib, P. M. Budd, C. E. Tattershall, K. Mahmood, S. Tan, D. Book, H. W. Langmi, A. Walton, *Angew. Chem, Int. Ed.* **2006**, *45*, 1804.
 - 15 P. M. Budd, E. S. Elabas, B. S. Ghanem, S. Makhseed, N. B. McKeown, K. J. Msayib, C. E. Tattershall, D. Wang, *Adv. Mater.* **2004**, *16*, 456.
 - 16 P. M. Budd, B. S. Ghanem, S. Makhseed, N. B. McKeown, K. J. Msayib, C. E. Tattershall, *Chem. Commun.* **2004**, 230.
 - 17 B. S. Ghanem, N. B. McKeown, P. M. Budd, D. Fritsch, *Macromolecules* **2008**, *41*, 1640.
 - 18 P. M. Budd, K. J. Msayib, C. E. Tattershall, B. S. Ghanem, K. J. Reynolds, N. B. McKeown, D. Fritsch, *J. Membr. Sci.* **2005**, *251*, 263.
 - 19 J. Weber, O. Su, M. Antonietti, A. Thomas, *Macromol. Rapid. Commun.* **2007**, *28*, 1871.
 - 20 B. S. Ghanem, N. B. McKeown, P. M. Budd, J. D. Selbie, D. Fritsch, *Adv. Mater.* **2008**, *20*, 2766.
 - 21 O. W. Webster, F. P. Gentry, R. D. Farlee, B. E. Smart, *Makromol. Chem, Macromol. Symp.* **1992**, *54*, 477.
 - 22 V. A. Davankov, M. M. Ilyin, M. P. Tsyurupa, G. I. Timofeeva, L. V. Dubrovina, *Macromolecules* **1996**, *29*, 8398.
 - 23 J. Hradil, E. Kralova, *Polymer* **1998**, *39*, 6041.
 - 24 J. Y. Lee, C. D. Wood, D. Bradshaw, M. J. Rosseinsky, A. I. Cooper, *Chem. Commun.* **2006**, 2670.
 - 25 P. M. Budd, A. Butler, J. Selbie, K. Mahmood, N. B. McKeown, B. Ghanem, K. Msayib, D. Book, A. Walton, *Phys. Chem. Chem. Phys.* **2007**, *9*, 1802.
 - 26 C. D. Wood, B. Tan, A. Trewin, H. J. Niu, D. Bradshaw, M. J. Rosseinsky, Y. Z.

- Khimyak, N. L. Campbell, R. Kirk, E. Stockel, A. I. Cooper, *Chem. Mater.* **2007**, *19*, 2034.
- 27 H. Furukawa, O. M. Yaghi, *J. Am. Chem. Soc.* **2009**, *131*, 8875.
- 28 U. Mueller, M. Schubert, F. Teich, H. Puetter, K. Arndt, J. Pastre, *J. Mater. Chem.* **2006**, *16*, 626.
- 29 G. Ferey, *Chem. Soc. Rev.* **2008**, *37*, 191.
- 30 H. Li, M. Eddaoudi, M. O’Keeffe, O. M. Yaghi, *Nature* **1999**, *402*, 276.
- 31 N. L. Rosi, J. Eckert, M. Eddaoudi, D. T. Vodak, J. Kim, M. O’Keeffe and O. M. Yaghi, *Science* **2003**, *300*, 1127.
- 32 J. L. C. Rowsell, A. R. Millward, K. S. Park, O. M. Yaghi, *J. Am. Chem. Soc.* **2004**, *126*, 5666.
- 33 D. Chandra, J. J. Reilly, R. Chellappa, *J. Met.* **2006**, *58*, 26.
- 34 S. Abate, G. Centi, P. Lanzafame, S. Perathoner, *J Energy Chemistry* **2015**, *24*, 535.
- 35 K. Fujita, T. Yoshida, Y. Imori, R. Yamaguchi, *Org. Lett.* **2011**, *13*, 2278.
- 36 K. Fujita, N. Tanino, R. Yamaguchi, *Org. Lett.* **2007**, *9*, 109.
- 37 R. Kawahara, K. Fujita, R. Yamaguchi, *J. Am. Chem. Soc.* **2012**, *134*, 3643.
- 38 M. Nielsen, E. Alberico, W. Baumann, H. Drexler, H. Junge, S. Gladiali, M. Beller, *Nature* **2013**, *7*, 85.
- 39 J. Yu, Q. Ge, W. Fang, H. Xu, *Appl. Catal.* **2011**, *114*, A395.
- 40 N. Kariya, A. Fukuoka, M. Ichikawa, *Appl. Catal.* **2002**, *91*, A233.
- 41 N. Kariya, A. Fukuoka, T. Utagawa, M. Sakuramoto, Y. Goto, M. Ichikawa, *Appl. Catal.* **2003**, *247*, A247.
- 42 A. A. Shukla, P. V. Gosavi, J. V. Pande, V. P. Kumar, K. V. R. Chary, R. B. Biniwale, *Int. J. Hydrogen Energy* **2010**, *35*, 4020.
- 43 B. Wang, D. W. Goodman, G. F. Froment, *J. Catal* **2008**, *253*, 229.
- 44 R. H. Crabtree, *Energy Environ. Sci.* **2008**, *1*, 134.
- 45 E. Clot, O. Eisenstein, R. H. Crabtree, *Chem. Commun.* **2007**, 2231.
- 46 A. Moores, M. Poyatos, Y. Luo, R. H. Crabtree, *New J. Chem.* **2006**, *30*, 1675.
- 47 R. B. Biniwale, S. Rayalu, S. Devotta, M. Ichikawa, *Int. J. Hydrogen Energy* **2008**, *33*, 360.
- 48 F. Sotoodeh, L. Zhao, K. Smith, *J. Appl. Catal.* **2009**, *155*, A362.
- 49 Z. Wang, I. Tonks, J. Belli, C. M. Jensen, *J. Organomet. Chem.* **2009**, *694*, 2854.
- 50 A. Moores, M. Poyatos, Y. Luo, R. H. Crabtree, *New J. Chem.* **2006**, *30*, 1675.
- 51 R. B. Biniwale, S. Rayalu, S. Devotta, M. Ichikawa, *Int. J. Hydrogen Energy* **2008**, *33*, 360.
- 52 R. Yamaguchi, C. Ikeda, Y. Takahashi, K. Fujita, *J. Am. Chem. Soc.* **2009**, *131*, 8410.
- 53 K. Fujita, Y. Tanaka, M. Kobayashi, R. Yamaguchi, *J. Am. Chem. Soc.* **2014**, *136*, 4829.

- 54 X. Zhang, Z. Xi, *Phys. Chem. Chem. Phys.* **2011**, *13*, 3997.
- 55 S. Muench, A. Wild, C. Friebe, B. Haupler, T. Janoschka, U. S. Schubert, *Chem. Rev.* **2016**, *116*, 9438.
- 56 G. Nystrom, A. Razaq, M. Stromme, L. Nyholm, A. Mihranyan, *Nano Lett.* **2009**, *9*, 3635.
- 57 J. Wang, S. Chou, H. Liu, G. Wang, C. Zhong, S. Chew, H. Liu, *Mater. Lett.* **2009**, *63*, 2352.
- 58 C. Wang, W. Zheng, Z. Yue, C. Too, G. Wallace, *Adv. Mater.* **2011**, *23*, 3580.
- 59 M. Zhou, J. Qian, X. Ai, H. Yang, *Adv. Mater.* **2011**, *23*, 4913.
- 60 S. Park, B. Schougaard, B. Goodenough, *Adv. Mater.* **2007**, *19*, 848.
- 61 C. Cui, G. Wu, H. Yang, S. She, J. Shen, B. Zhou, Z. Zhang, *Electrochim. Acta* **2010**, *55*, 8870.
- 62 H. Min, B. Park, L. Taherabadi, C. Wang, Y. Yeh, R. Zaouk, M. Madou, B. Dunn, *J. Power Sources* **2008**, *178*, 795.
- 63 E. Perez-Cappe, Y. Mosqueda, R. Martínez, C. Milian, O. Sanchez, J. Varela, A. Hortencia, E. Souza, P. Aranda, E. Ruiz-Hitzky, *J. Mater. Chem.* **2008**, *18*, 3965.
- 64 X. Huang, J. Tu, X. Xia, X. Wang, J. Xiang, *Electrochem. Commun.* **2008**, *10*, 1288.
- 65 X. Huang, J. Tu, X. Xia, X. Wang, J. Xiang, L. Zhang, *J. Power Sources* **2010**, *195*, 1207.
- 66 M. Gvozdenovic, B. Jugovic, T. Trisovic, J. Stevanovic, B. Grgur, *Mater. Chem. Phys.* **2011**, *125*, 601.
- 67 J. Wang, S. Chou, J. Chen, S. Chew, G. Wang, K. Konstantinov, J. Wu, S. Dou, H. Liu, *Electrochem. Commun.* **2008**, *10*, 1781.
- 68 Y. Jung, N. Singh, K. Choi, *Angew. Chem., Int. Ed.* **2009**, *48*, 8331.
- 69 W. Chen, L. Qie, L. Yuan, S. Xia, X. Hu, W. Zhang, Y. Huang, *Electrochim. Acta* **2011**, *56*, 2689.
- 70 T. Janoschka, M. D. Hager, U. S. Schubert, *Adv. Mater.* **2012**, *24*, 6397.
- 71 W. Xu, A. Read, K. Koech, H. Hu, M. Wang, J. Xiao, A. Padmaperuma, L. Graff, J. Liu, J. Zhang, *J. Mater. Chem.* **2012**, *22*, 4032.
- 72 Z. Song, T. Xu, L. Gordin, Y. Jiang, I. Bae, Q. Xiao, H. Zhan, J. Liu, D. Wang, *Nano Lett.* **2012**, *12*, 2205.
- 73 K. Liu, J. Zheng, G. Zhong, Y. Yang, *J. Mater. Chem.* **2011**, *21*, 4125.
- 74 Z. Song, Y. Qian, X. Liu, T. Zhang, Y. Zhu, H. Yu, M. Otani, H. Zhou, *Energy Environ. Sci.* **2014**, *7*, 4077.
- 75 D. Haringer, P. Novak, O. Haas, B. Piro, M. Pham, *J. Electrochem. Soc.* **1999**, *146*, 2393.
- 76 L. Zhao, W. Wang, A. Wang, K. Yuan, S. Chen, Y. Yang, *J. Power Sources* **2013**, *233*,

- 23.
- 77 W. Choi, D. Harada, K. Oyaizu, H. Nishide, *J. Am. Chem. Soc.* **2011**, *133*, 19839.
- 78 T. Kawai, K. Oyaizu, H. Nishide, *Macromolecules* **2015**, *48*, 2429.
- 79 T. Nokami, T. Matsuo, Y. Inatomi, N. Hojo, T. Tsukagoshi, H. Yoshizawa, A. Shimizu, H. Kuramoto, K. Komae, H. Tsuyama, *et al. J. Am. Chem. Soc.* **2012**, *134*, 19694.
- 80 K. Oyaizu, A. Hatemata, W. Choi, H. Nishide, *J. Mater. Chem.* **2010**, *20*, 5404.
- 81 Z. Song, H. Zhan, Y. Zhou, *Angew. Chem., Int. Ed.* **2010**, *49*, 8444.
- 82 Y. Meng, H. Wu, Y. Zhang, Z. Wei, *J. Mater. Chem. A* **2014**, *2*, 10842.
- 83 H. Wu, S. Shevlin, Q. Meng, W. Guo, Y. Meng, K. Lu, Z. Wei, Z. Guo, *Adv. Mater.* **2014**, *26*, 3338.
- 84 H. Wu, K. Wang, Y. Meng, K. Lu, Z. Wei, *J. Mater. Chem. A* **2013**, *1*, 6366.
- 85 P. Sharma, D. Damien, K. Nagarajan, M. Shaijumon, M. Hariharan, *J. Phys. Chem. Lett.* **2013**, *4*, 3192.
- 86 J. Geng, J. Bonnet, S. Renault, F. Dolhem, P. Poizot, *Energy Environ. Sci.* **2010**, *3*, 1929.
- 87 H. Nishide, K. Oyaizu, *Science* **2008**, *319*, 737.
- 88 H. Nishide, T. Suga, *Electrochem. Soc. Interface* **2005**, *14*, 32.
- 89 T. Suga, Y.-J. Pu, K. Oyaizu, H. Nishide, *Bull. Chem. Soc. Jpn.* **2004**, *77*, 2203.
- 90 K. Oyaizu, Y. Ando, H. Konishi, H. Nishide, *J. Am. Chem. Soc.* **2008**, *130*, 14459.
- 91 T. Suga, H. Konishi, H. Nishide, *Chem. Commun.* **2007**, 1730.
- 92 K. Oyaizu, T. Suga, K. Yoshimura, H. Nishide, *Macromolecules* **2008**, *41*, 6646.
- 93 Y. Takahashi, N. Hayashi, K. Oyaizu, K. Honda, H. Nishide, *Polym. J.* **2008**, *40*, 763.
- 94 H. Nishide, S. Iwasa, Y.-J. Pu, T. Suga, K. Nakahara, M. Satoh, *Electrochim. Acta* **2004**, *50*, 827.
- 95 K. Oyaizu, H. Nishide, *Adv. Mater.* **2009**, *21*, 2339.
- 96 T. Sukegawa, K. Sato, K. Oyaizu, H. Nishide, *RSC Advances*, **2015**, *5*, 15448.
- 97 T. Sukegawa, I. Masuko, K. Oyaizu, H. Nishide, *Macromolecules* **2014**, *47*, 8611.
- 98 I. S. Chae, M. Koyano, T. Sukegawa, K. Oyaizu, H. Nishide, *J. Mater. Chem. A*, **2013**, *1*, 9608.
- 99 T. Sukegawa, A. Kai, K. Oyaizu, H. Nishide, *Macromolecules* **2013**, *46*, 1361.
- 100 W. Choi, D. Harada, K. Oyaizu, H. Nishide, *J. Am. Chem. Soc.* **2011**, *133*, 19839.
- 101 T. Kawai, K. Oyaizu, H. Nishide, *Macromolecules* **2015**, *48*, 2429.
- 102 O. H. Muller, *J. Am. Chem. Soc.* **1940**, *62*, 2434.
- 103 S. I. Bailey, I. M. Ritchie, *Electrochim. Acta* **1985**, *30*, 3.
- 104 I. M. Kolthoff, E. F. Orlemann, *J. Am. Chem. Soc.* **1941**, *63*, 664.
- 105 J. C. Abbott, J. W. Collat, *Anal. Chem.* **1963**, *35*, 859.
- 106 R. T. Robertson, B. D. Pendley, *J. Electroanal. Chem.* **1994**, *374*, 173.
- 107 Y. Sato, M. Fujita, F. Mizutani, K. J. Uosaki, *Electroanal. Chem.* **1996**, *409*, 145.

- 108 Y. Shim, S. Park, *J. Electroanal. Chem.* **1997**, *425*, 201.
- 109 H. Park, M. Won, C. Cheong, Y. Shim, *Electroanalysis* **2002**, *14*, 1501.
- 110 M. F. Marcus, M. D. Hawley, *Biochim. Biophys. Acta* **1970**, *222*, 163.
- 111 P. H. Given, M. E. Peover, *J. Chem. Soc.* **1960**, 385.
- 112 H. Linschitz, J. Rennert, T. M. Korn, *J. Am. Chem. Soc.* **1954**, *76*, 5839.
- 113 M. Mastragostino, L. Nadjo, J. M. Saveant, *Electrochim. Acta* **1968**, *13*, 721.
- 114 M. Quan, D. Sanchez, M. F. Wasylkiw, D. K. Smith, *J. Am. Chem. Soc.* **2007**, *129*, 12847.
- 115 N. Gupta, H. Linschitz, *J. Am. Chem. Soc.* **1997**, *119*, 6384.
- 116 C. Costentin, *Chem. Rev.* **2008**, *108*, 2145.
- 117 M. Vilar, J. L. Oliveira, M. Navarro, *Applied Catalysis A* **2010**, *372*, 1.
- 118 G. Horanyi, K. Torkos, *J. Electroanal. Chem.* **1982**, *136*, 301.
- 119 M. V. F. Lima, F. D. Menezes, B. B. Neto, M. Navarro, *J. Electroanal. Chem.* **2008**, *613*, **58**.
- 120 D. S. Santana, M. V. F. Lima, J. R. R. Daniel, M. Navarro, *Tetrahedron Lett.* **2003**, *44*, 4725.
- 121 D. S. Santana, G. O. Melo, M. V. F. Lima, J. R. R. Daniel, M. C. C. Areias, M. Navarro, *J. Electroanal. Chem.* **2004**, *569*, 71.
- 122 K. Shigehara, N. Oyama, F. C. Anson, *Inorg Chem* **1981**, *20*, 518.
- 123 J. Roncali, *J Mater Chem* **1999**, *9*, 1875.
- 124 Y. Yu, C. Yan, Z. Zheng, *Adv Mater* **2014**, *26*, 5508.
- 125 W. Zhou, Y. Du, H. Zhang, J. Xu, P. Yang, *Electrochim Acta* **2010**, *55*, 2911.
- 126 A. Mourato, S. M. Wong, H. Siegenthaler, L. M. Abrantes, *J Solid State Electrochem* **2006**, *10*, 140.
- 127 A. Zouaoui, O. Stephan, A. Ourari, *J. Moute, Electrochim Acta* **2000**, *46*, 49.
- 128 N. Takano, A. Nakade, N. Takeno, *Bull Chem Soc Jpn* **1997**, *70*, 837.
- 129 T. Wang, J. Zhuo, K. Du, B. Chen, Z. Zhu, Y. Shao, M. Li, *Adv Mater* **2014**, *26*, 3761.
- 130 P. Wang, T. Minegishi, G. Ma, K. Takanabe, Y. Satou, S. Maekawa, Y. Kobori, J. Kubota, K. Domen, *J. Am. Chem. Soc.* **2012**, *134*, 2469.
- 131 V. Kalousek, P. Wang, T. Minegishi, T. Hisatomi, K. Nakagawa, S. Oshima, Y. Kobori, J. Kubota, K. Domen, *ChemSusChem* **2014**, *7*, 2690.
- 132 M. Wakisaka, M. Kunitake, *Electrochemistry Communications* **2016**, *64*, 5.

Chapter 2

Synthesis of Fluorenone/Fluorenol Polymer for Cycle of Electrolytic Hydrogen-Fixing and -Releasing in Water

Contents

- 2.1 Introduction
- 2.2 Redox and Hydrogen Storage Properties of Fluorenone
- 2.3 Synthesis of Fluorenone/Fluorenol Polymer
- 2.4 Hydrogen Storage Properties of Fluorenone/Fluorenol Polymer
- 2.5 Experimental Section

References

2.1 Introduction

As mentioned in the preceding chapter, hydrogen storage materials for the hydrogen society gather great deal of attentions¹⁻⁹. Organic compounds with reversible hydrogen-storing capability have been intensively studied; the typical examples are nitrogen heterocycles^{10,11}, formaldehyde water¹² and amide compounds¹³. These materials feature a high stability of the corresponding hydrogenated compounds due to the chemical bond formation and high hydrogen storage capacity of 2–6 wt% in the exemplified compounds. However, these compounds are mostly liquids or used as solutions and often suffer from safety issues of toxicity, flammability and volatility. Furthermore, their hydrogenation mostly proceeds at high pressure of hydrogen via highly energyconsuming processes. Although some of these liquid organic compounds have been tested as hydrogen storage materials on an industrial scale to be used in the existing infrastructure for oil storage and transportation, organic liquids are not always suitable to be examined in small-scale applications as hydrogen storage materials. They need vessels or sealed tanks operated at high pressure and/or temperature and often encounter difficulty in their separation from the evolved hydrogen gas. A pocketable and safe hydrogen carrier system, just similar to rechargeable batteries as a portable energy source, is anticipated. Alcohols have been studied as one-way hydrogen-supplying molecules^{14,15}, where iridium complexes were often used as effective catalysts for the hydrogen evolution under relatively mild conditions^{16,17}.

In this chapter, we focus on fluorenol, which is an alcohol derivative of fluorene and holds two hydrogen atoms with C–H and O–H chemical bonds. We note that fluorenol efficiently releases hydrogen with the iridium catalyst under mild conditions to yield fluorenone, the corresponding ketone form of fluorenol. We have found that fluorenone turned to the dianion species by electrolytic reduction and was protonated with water to return to the original fluorenol. This chapter refer to the paper of Nature Communications, 7, 13032 (2016) written by the author.

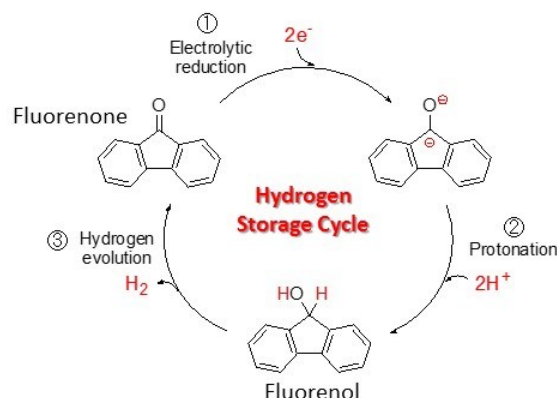


Figure 2.1.1 Schematic representation of hydrogen-fixing and -releasing cycle.

We have further extended the hydrogenation/dehydrogenation cycle of the fluorenone/fluorenol couple to the polymeric analogue, for example, a bendable polymer sheet, and examined electrolytic hydrogenation with water and the following hydrogen release from the polymer sheet by simply heating it in the presence of an aqueous catalyst. The fluorenone/fluorenol polymer was repeatedly hydrogenated and dehydrogenated with cyclability. Hydrogen is reversibly fixed in and released from the organic polymer (the bendable sheet) under mild conditions: easy handling, mouldability, robustness, non-flammability and low toxicity are inherent advantages of the polymers.

2.2 Redox and Hydrogen Storage Properties of Fluorenone

2.2.1 Redox properties of fluorenone in aprotic solvent

First, the redox properties of fluorenone in aprotic solvent were studied. A cyclic voltammogram of the fluorenone in acetonitrile (AN) electrolyte (Figure 2.2.1) gave two reversible redox waves at -1.3 and -1.9 V (vs. Ag/AgCl) ascribed to forming the anion radical and dianion fluorenone, respectively. The results of electron spin resonance (ESR) spectra of fluorenone after the electrolytic reduction applying at -1.0, -1.6, and -2.0 V (vs. Ag/AgCl) also indicated the producing of radical species (Figure 2.2.1 inset).

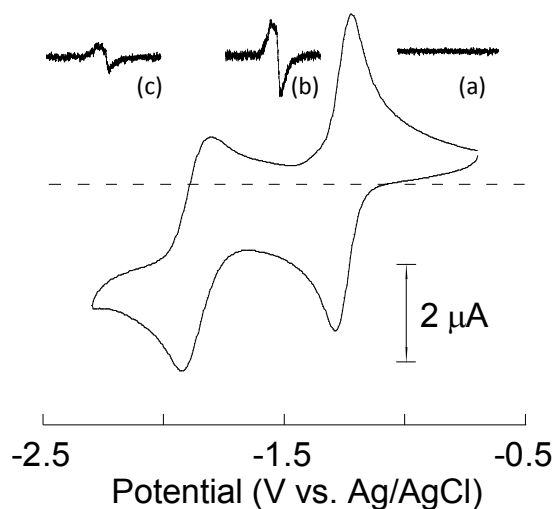


Figure 2.2.1 The cyclic voltammogram of 1 mM fluorenone scanned at 100 mV s⁻¹ in 0.1 M (C₄H₉)₄NPF₆ AN solution. Inset: ESR spectra of fluorenone after the electrolytic reduction applying at -1.0, -1.6, and -2.0 V.

UV-vis spectra of fluorenone after electrolytic reduction by applying -1.0, -1.7, and -2.1 V (vs. Ag/AgCl) exhibited the isosbestic points, suggesting the reversibility of the redox reaction of fluorenone in AN electrolyte (Figure 2.2.2).

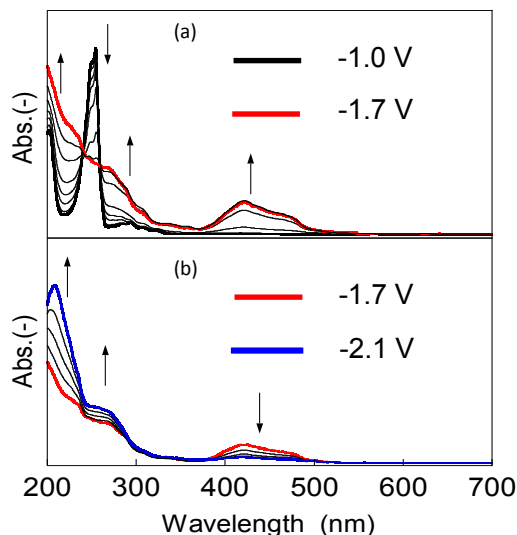


Figure 2.2.2 UV-vis spectra of fluorenone after the electrolysis by applying -1.0, -1.7, and -2.1 V in 0.1 M $(\text{C}_4\text{H}_9)_4\text{NPF}_6$ AN solution.

The diffusion coefficient ($D = 5.6 \times 10^{-5} \text{ cm}^2 \text{ s}^{-1}$) was determined from the Levich plots of fluorenone by using a rotating disk electrode (RDE) (Figure 2.2.3 (a)), and heterogeneous electron-transfer rate constants ($k_0 = 2.3 \times 10^{-2} \text{ cm s}^{-1}$) was calculated by using Nicholson's method (Figure 2.2.3 (b)), which numbers were comparable to another n-type redox-active organic compounds, such as anthraquinone ($k_0 = 2.2 \times 10^{-2} \text{ cm s}^{-1}$)¹⁸.

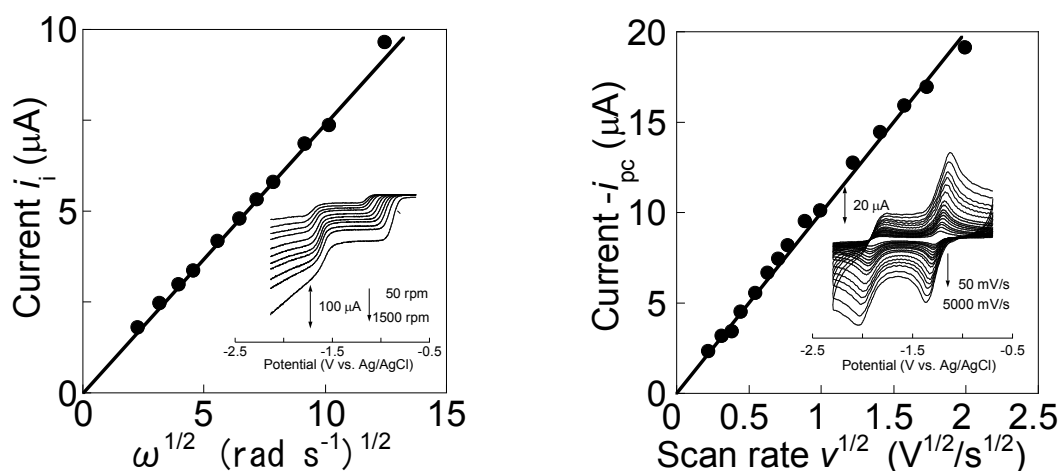


Figure 2.2.3 (a) Levich plots of fluorenone. Inset: Hydrodynamic voltammograms of 1 mM fluorenone in 0.1 M $(\text{C}_4\text{H}_9)_4\text{NPF}_6$ AN solution at a RDE ($\phi = 3.0 \text{ mm}$). (b) i_p vs. $v^{1/2}$ plots. Inset: Cyclic voltammograms of 0.1 mM fluorenone in 0.1 M $(\text{C}_4\text{H}_9)_4\text{NPF}_6$ AN solution.

2.2.2 Redox properties of fluorenone in protic solvent

To investigate the redox properties of fluorenone in protic solvent, the cyclic voltammograms of fluorenone in water/AN electrolyte were measured (Figure 2.2.4 (a)). While a cyclic voltammogram of the fluorenone in AN electrolyte gave two reversible redox waves, the oxidation peaks disappeared in the cyclic voltammogram in AN/water electrolyte and first reduction peak current became higher than that of second reduction peak. Furthermore, the two reduction waves shifted to positive by adding water (Figure 2.2.4 (b)). Similar results have been reported for protonation of quinones, which exhibit n-type redox like FN, in organic electrolyte containing acid^{19–30}.

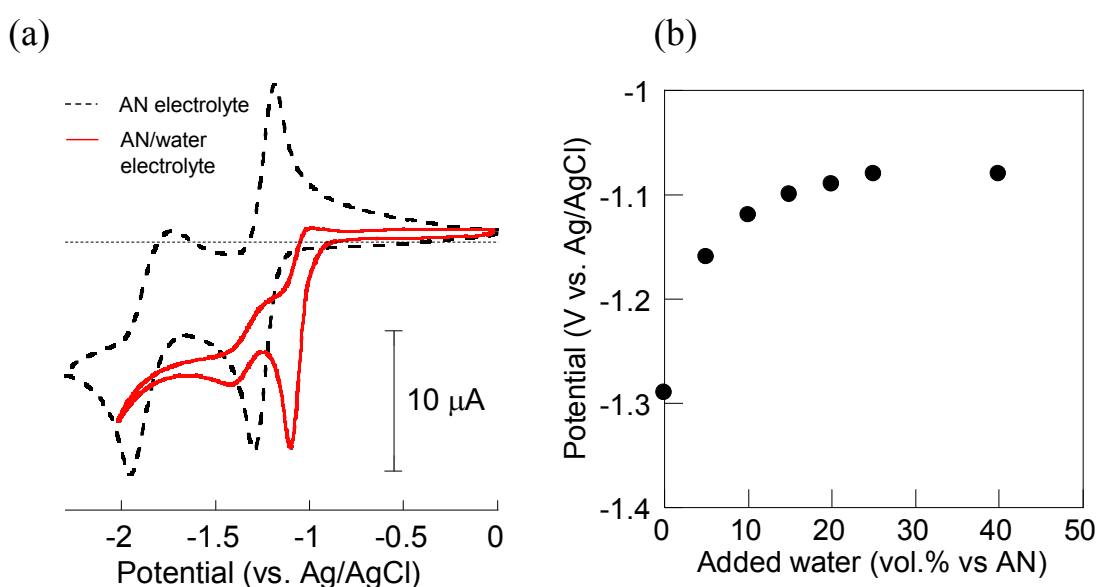


Figure 2.2.4 (a) The cyclic voltammogram of 1 mM fluorenone scanned at 100 mV s^{-1} in 0.1 M $(\text{C}_4\text{H}_9)_4\text{NPF}_6$ AN/water solution. (b) First anode peak potential of FN in acetonitrile electrolyte added water (scan rate = 50 mV/s).

The diffusion coefficient ($D = 1.7 \times 10^{-5} \text{ cm}^2 \text{ s}^{-1}$) was determined from the Levich plots of fluorenone by using a RDE (Figure 2.2.5), which numbers was lower than that of fluorenone in AN electrolyte. The number of electron for the first step reduction was calculated by using chronoamperogram of fluorenone in water/AN electrolyte, and the result indicated that fluorenone was reduced with two-electron by applying -1.1 V (vs. Ag/AgCl) (Figure 2.2.6).

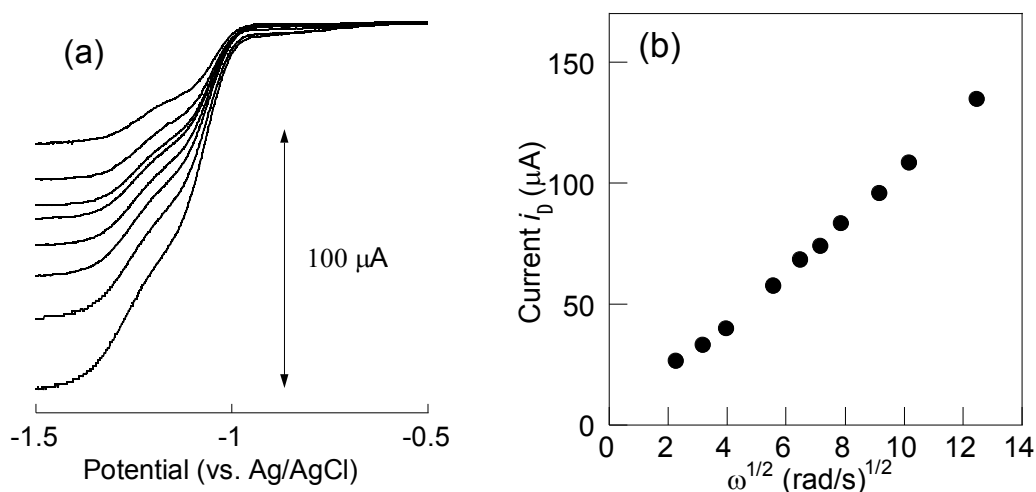


Figure 2.2.5 (a) Diffusion limit current for FN at a RDE in AN/water (= 1/1) electrolyte (b) Koutecky-Levich plot of FN in AN/water (= 1/1) electrolyte.

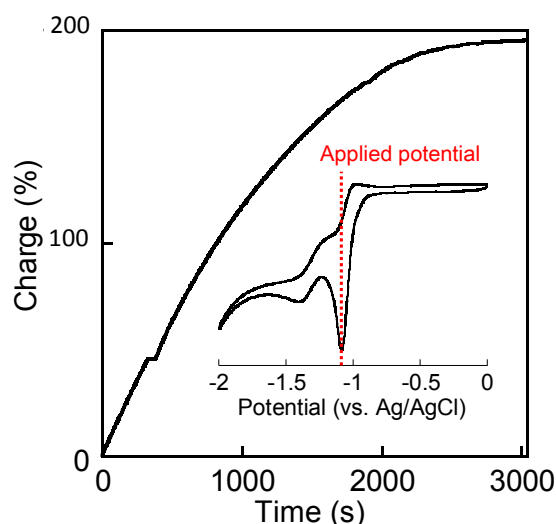


Figure 2.2.6 Bulk electrolysis curve of fluorenone in AN/water (= 4/1) containing 0.3 M $(\text{C}_4\text{H}_9)_4\text{NBF}_4$ at -1.1 V (vs. Ag/AgCl) Inset: Cyclic voltammogram of fluorenone in the same electrolyte.

Furthermore it was revealed that fluorenol, which is hydrogen adduct of fluorenone, was produced after the bulk electrolysis applying -1.5 V (Figure 2.2.7). The same reduction of fluorenone was carried out by using the AN/D₂O solution, to almost quantitatively yield two-deuterated fluorenol $\text{C}_{13}\text{OH}_8\text{D}_2$ ($m/z = \text{calcd for } 184.23$).

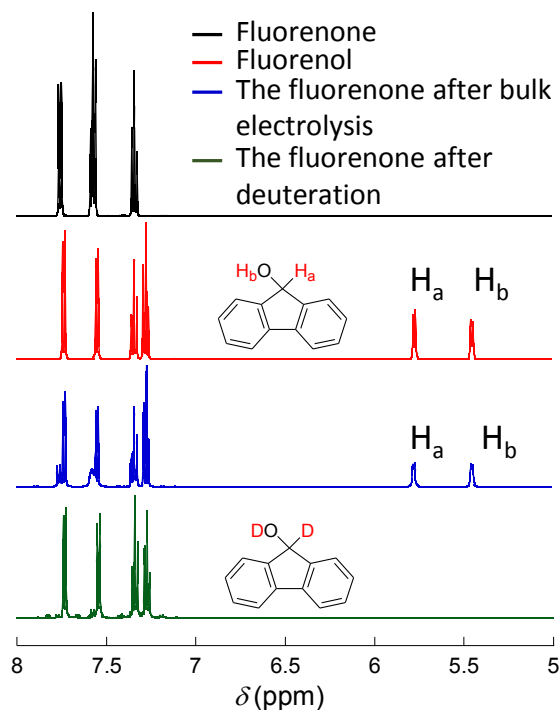


Figure 2.2.7 ^1H NMR spectra of fluorenone (black), fluorenoyl (red), the fluorenone after bulk electrolysis (blue), and the fluorenone after deuteration (green). The bulk electrolysis was carried out by applying potential of -1.5 V (vs. Ag/AgCl) in a solution of 1 mM fluorenone and 0.1 M $(\text{C}_4\text{H}_9)_4\text{NPF}_6$ in water or AN/ D_2O (vol 5/1).

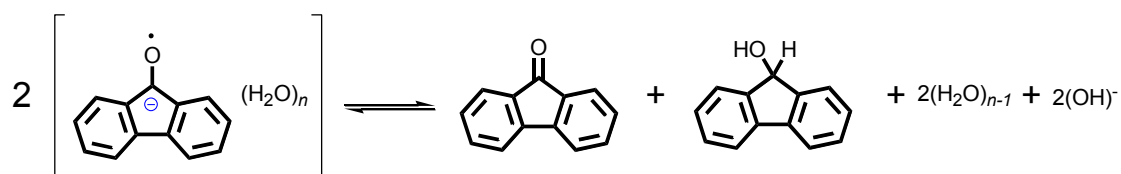
Peaks assigned to the hydroxyl (5.48 ppm), cyclopentane (5.81 ppm), and phenyl (7.77 , 7.59 , 7.38 , 7.31 ppm) protons of fluorenoyl appeared with the electrolytic reduction in AN/water. On the other hand, for the electrolytic reduction in AN/ D_2O , only the peaks assigned to the phenyl protons (7.77 , 7.58 , 7.38 , 7.31 ppm) of fluorenoyl appeared, which indicated 2D deuteration of the hydroxyl and cyclopentane protons of fluorenoyl.

Coulombic efficiency and conversion from fluorenone to fluorenoyl by the electrolytic hydrogenation applying each potential was investigated (Table 2.2.1). Fluorenoyl did not produced when -0.9 V applied which was more positive than the first reduction potential of fluorenone. Coulombic efficiency and conversion became the maximum by applying -1.1 V and they decreased by applying more negative potential. The decrease of coulombic efficiency and conversion could be resulted from the hydrogen evolution or water splitting.

Table 2.2.1 Conversion and coulombic efficiency of fluorenone to fluorenol

| applied potential (vs. Ag/AgCl) | conversion (%) | coulombic efficiency (%) |
|------------------------------------|-------------------|--------------------------------|
| -0.9 | 0 | 0 |
| -1.1 | 96 | 96 |
| -2.0 | 59 | 59 |

The two-electron reduction at -1.1 V and the results of ^1H NMR of the electrolysis product could suggest that disproportionation and protonation reaction occurred by applying the first reduction potential in water/AN electrolyte as below.

**Scheme 2.2.1** disproportionation and protonation of fluorenone

However, the first reduction peak current of fluorenone in water/AN was not higher than that of fluorenone in AN even though fluorenone was reduced with two-electron. To clear the reason of that, theoretical peak current was estimated from the diffusion coefficient. The peak current of cyclic voltammogram was estimated by using diffusion coefficient according to $i_p = 269 \times n^{3/2} A D^{1/2} C \nu^{1/2}$ (at 25 °C), where n , A , D , C and ν are stoichiometric numbers of electrons (two in this experiment), surface area of the electrode, diffusion coefficient, concentration, scan rate, respectively. According to the equation and the number of the diffusion coefficient, it was estimated that the first reduction peak current of fluorenone in water/AN electrolyte could be 0.53 times lower than that of fluorenone in AN electrolyte. Thus, the low reduction peak current of fluorenone in AN/water electrolyte could be due to the low diffusion coefficient in the electrolyte.

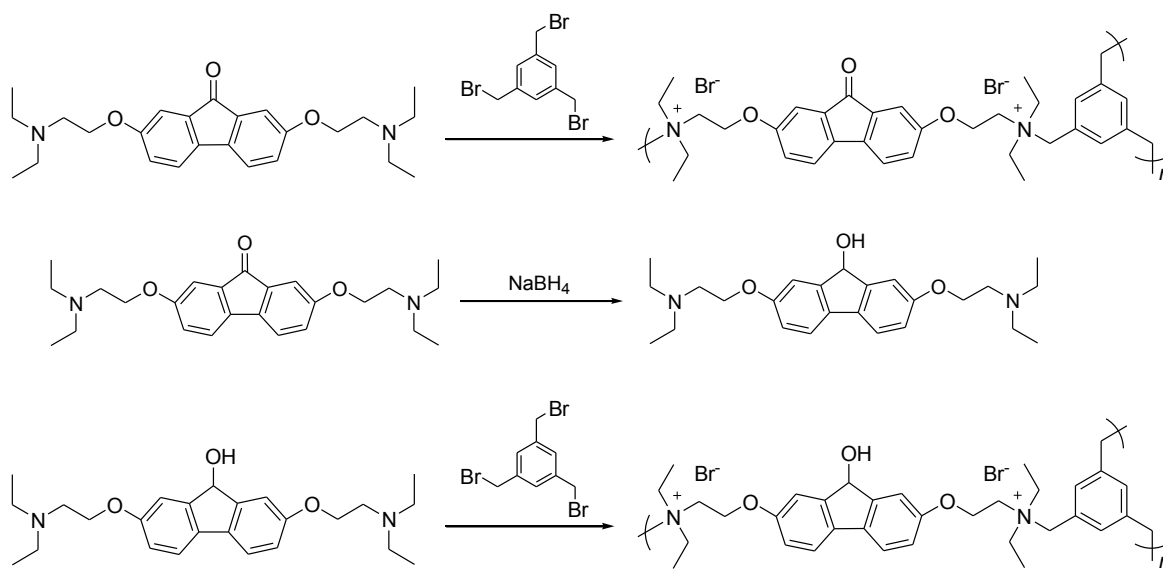
2.3 Synthesis of Fluorenone/Fluorenol Polymer

2.3.1 Preparation of the fluorenone and fluorenol polymer

The fluorenone and fluorenol polymers were moulded via a cross-linking reaction of a bifunctional fluorenone or fluorenol derivative, 2,7-bis[2-(diethylamino)ethoxy]-9-fluorenone

or -fluorenl, and a three-functional cross-linker, 1,3,5-tris (bromomethyl)benzene (Scheme 2.2; equimolar feed ratio of the functional groups), in a Teflon boat by simply heating (90 °C) their N-methylpyrrolidone solution and washing it with N-methylpyrrolidone, water and methyl alcohol. The polymer was kind of a hyperbranched polymer synthesized via Menshutkin reaction^{31–37}.

The polymers were yielded as bendable sheet (Figure 2.3.1), and a typical yield of the insoluble network or gel part (gel fraction) was 86% (the median of five specimens).



Scheme 2.3.1 Synthesis of fluorenone and fluorenl polymer

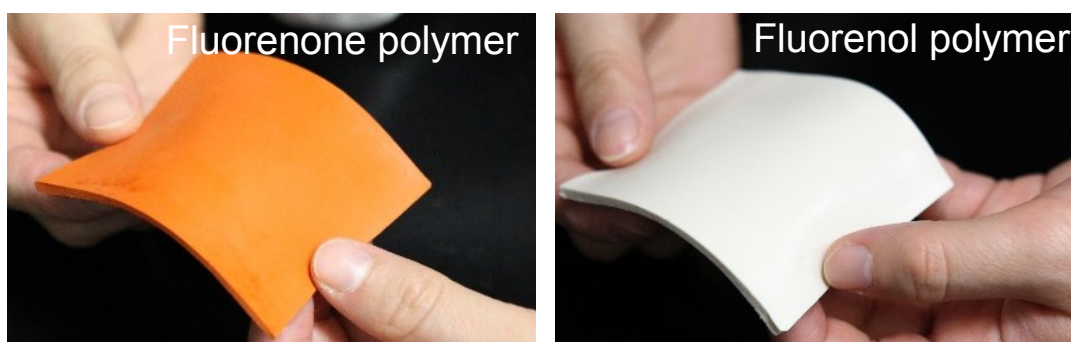


Figure 2.3.1 A sheet of the fluorenone and fluorenl polymer on a 5 g scale

The chemical structures of fluorenone, fluorenl and quaternized ammonium moieties represented in Scheme 2.3.1 were supported by ¹³C crosspolarization magic angle spinning–nuclear magnetic resonance (CP/MAS NMR) spectroscopy (Figure 2.3.2). Shifts of the methylene carbons of reactants in the bottom spectrum supported the polymerization progress. Standing experiments of the fluorenone and fluorenl polymers in an air atmosphere

at 80 °C for 30 days did not show any degradation or any chemical structure change detected in ^{13}C CP/MAS NMR spectroscopy (and the amount of evolved hydrogen gas from the fluorenone polymer was not significantly decreased after the standing), to support durability of the polymers as a hydrogen carrier. Neither the fluorenone nor fluorenone polymers were soluble in water, but were hydrophilic and swollen; they uptook water with 25–35 wt% on the air of a humidity of 30% and with 50–60 wt% in water to be the hydrogels.

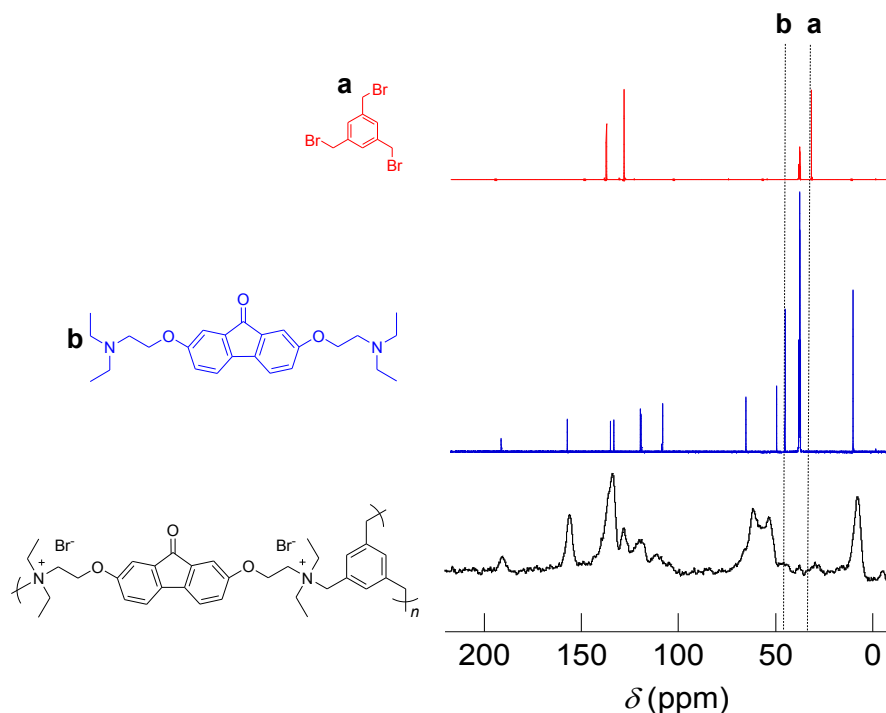


Figure 2.3.2 ^{13}C NMR spectrum of the fluorenone polymer and solution-state spectra of the reactants: 1,3,5-tris(bromomethyl)benzene and 2,7-bis[2-(diethylamino)ethoxy]-9-fluorenone in $\text{DMSO-}d_6$.

2.3.2 Mechanical properties of the fluorenone polymer

A network structure of the polymer was analysed by dynamic mechanical measurement (Figure 2.3.3). The storage modulus was much larger than the loss modulus, suggesting a mechanically tough gel formation with adequacy for a pocketable or a facile transportable hydrogen carrier (for the moulded example of a bendable sheet via the one-pot reaction).

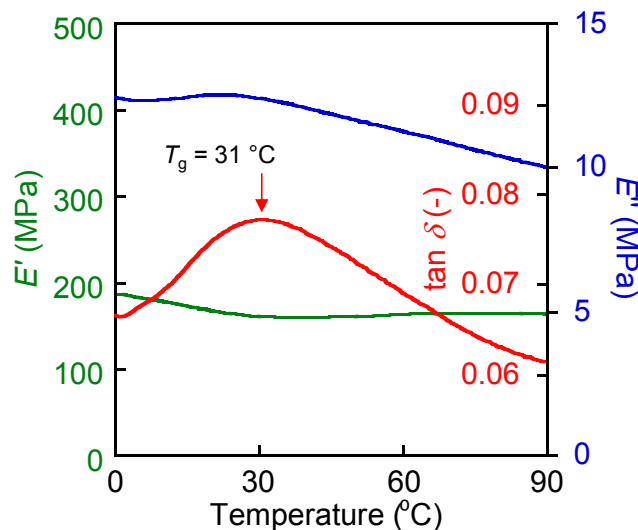


Figure 2.3.3 Dynamic mechanical measurement of the fluorenone polymer. Storage modulus (E'), loss modulus (E''), and tangent delta were analyzed by the dynamic mechanical measurement.

2.3.3 Scanning electron microscope observation of the fluorenone polymer

The fluorenone polymer was observed by using scanning electron microscope (SEM) (Figure 2.3.4). SEM images of the fluorenone polymer indicated the polymer was porous polymer, and the average of the pore size was several μm . The polymer was synthesized via polyaddition using the Menshutkin reaction, and a polarity of the backbone of polymer dramatically changed during the polymerization because of the ion group increasing. Thus, the construction of porous structure could be resulted from aggregation of the polymer chain during the polymerization.

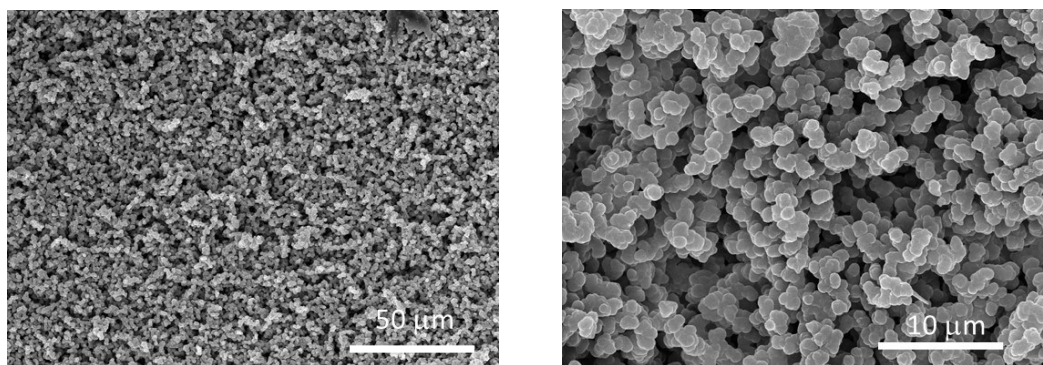


Figure 2.3.4 SEM images of the fluorenone polymer

2.4 Hydrogen Storage Properties of Fluorenone/Fluorenone Polymer

2.4.1 Redox properties of fluorenone polymer in aprotic electrolyte

In situ preparation of the fluorenone polymer on a glassy carbon substrate gave an electrode homogeneously coated with the fluorenone polymer with ca. 1 μm layer thickness. The fluorenone polymer layer was swollen but did not elute out in water, AN, or their mixtures. In the AN electrolyte (0.1 M $(\text{C}_4\text{H}_9)_4\text{NPF}_6$), the fluorenone polymer electrode exhibited two quasi-reversible redox waves at -1.3 and -1.7 V (vs. Ag/AgCl) in the cyclic voltammetry (Figure 2.4.1).

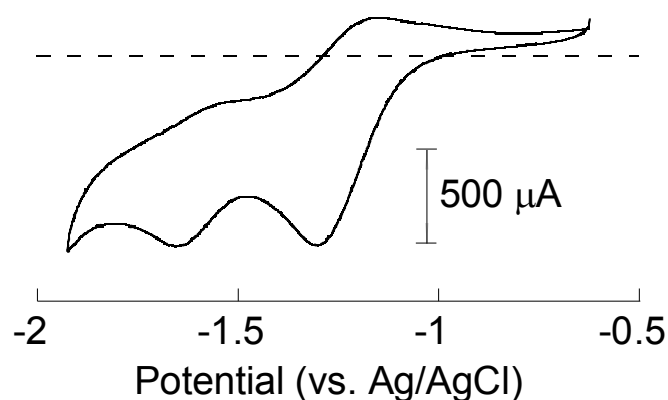


Figure 2.4.1 The cyclic voltammogram of fluorenone polymer-coated carbon scanned at 50 mV s^{-1} in 0.1 M $(\text{C}_4\text{H}_9)_4\text{NPF}_6$ AN solution.

The electrolytic reduction capacity of the fluorenone polymer layer reached 67 mA h g^{-1} , which was 92% of the calculated capacity for the two-electron reduction: Almost all fluorenone units stored two negative charges throughout the whole polymer layer (Figure 2.4.2). This charging proceeded quantitatively, even at a rapid charging rate of 10 C (or charging for 6 min), indicating that charge propagated efficiently throughout the polymer layer based on the redox gradient-driven and the rapid charge self-exchange reaction among the fluorenone units. (the author's group have previously described a similar charge propagation and storage for redox-active polymers³⁸⁻⁴⁵).

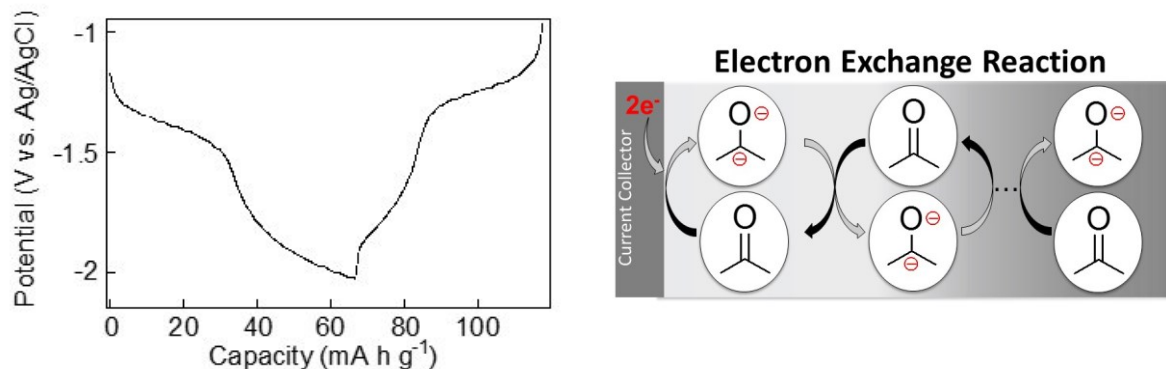


Figure 2.4.2 Charging/discharging curves of the fluorenone polymer at a rate of 10 C measured in the AN electrolyte (left), and schematic image of charge propagation in the polymer layer (right).

2.4.2 Redox properties of fluorenone polymer in protic electrolyte and hydrogenation

The addition of a drop of water to the AN electrolyte immediately caused, in the cyclic voltammogram, disappearance of the oxidation peaks at negative potential (Figure 2.4.3). The changing was similar to the peak change of fluorenone monomer, suggesting that the protonation of all fluorenone units in the polymer and producing of the fluorenol polymer.

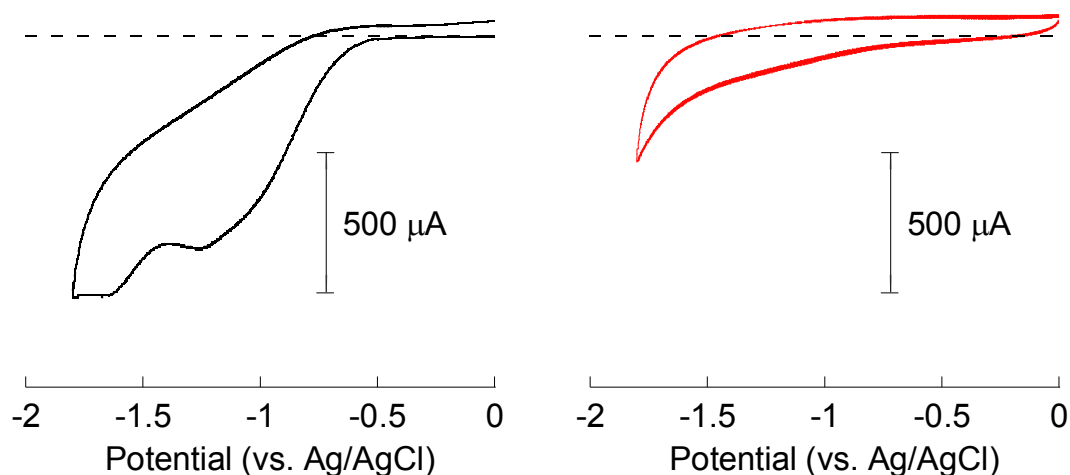


Figure 2.4.3 The cyclic voltammograms of the fluorenone polymer-coated carbon scanned at 50 mV s^{-1} in 0.1 M $(\text{C}_4\text{H}_9)_4\text{NPF}_6$ AN solution containing a drop of water (left), and after multiple potential cycles (right).

The fluorenone polymer layer was monitored with IR by applying -1.5 V in AN/water (vol 5/1) electrolyte: The absorption ascribed to $\nu_{C=O}$ at 1710 cm^{-1} decreased as the passed charge increased (Figure 2.4.4), indicating the decrease in fluorenone content in the polymer through the electrolytic reduction, or protonation or hydrogenation. The coulombic efficiency was, for example, 87% after the passage of equivalent charge, estimated with the conversion of the fluorenone unit.

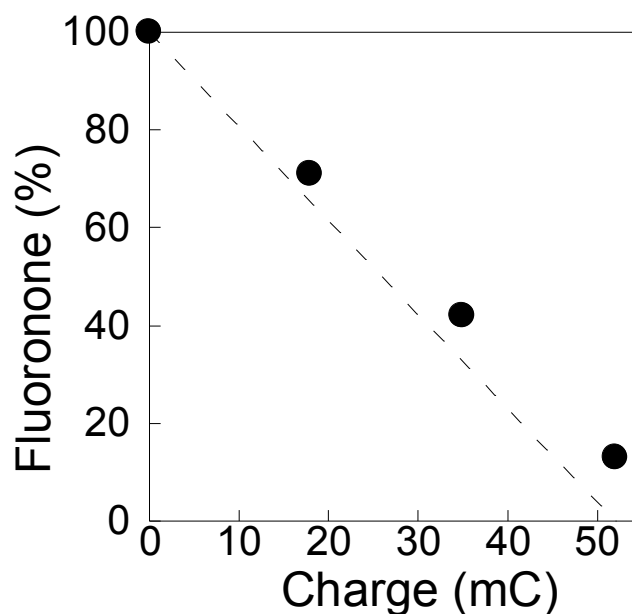


Figure 2.4.4 The conversion plots of the fluorenone to fluorenone unit in the fluorenone polymer layer electrolytically reduced in the AN/water electrolyte. Theoretical capacity of the fluorenone polymer-coated electrode was 52 mC per 0.2 mg polymer. The dashed line indicates the theoretical conversion with the passed charge.

2.4.3 Hydrogen evolution from fluorenone

The deuterated fluorenone was heated at $80\text{ }^{\circ}\text{C}$ with the aqueous iridium catalyst⁴⁶. The retention time of the gas evolved from the deuterated fluorenone was identical to that of D_2 in gas chromatography, clearly supporting the electrolytic deuteration (hydrogenation) of fluorenone with D_2O (water) and deuterium (hydrogen) evolution from the fluorenone (Figure 2.4.7).

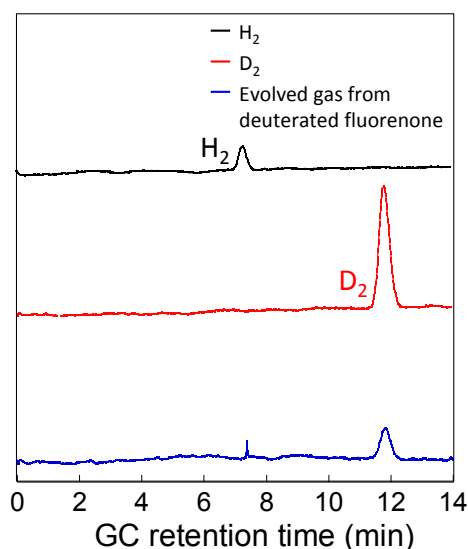


Figure 2.4.5 Gas chromatography of H₂, D₂, and evolved gas sample from deuterated fluorenol.

Among the alcoholic derivatives as hydrogen donors, fluorenol gave the higher rate of hydrogen evolution in comparison with those of other secondary alcohols (Table 2.4.1), although fluorenol is an aromatic alcohol.

Table 2.4.1 Hydrogen evolution rate and yield of alcohols

| entry | alcohol | solvent (alcohol concn, M) | initial hydrogen evolution (mL) ^{a)} | conversion (%) ^{b)} | conversion (%) ^{c)} |
|-------|---------|---|---|------------------------------|------------------------------|
| 1 | | H ₂ O/ <i>t</i> -C ₄ H ₉ OH (3/7) (0.01) | 67 | 28 | 82 |
| 2 | | H ₂ O/ <i>t</i> -C ₄ H ₉ OH (3/7) (0.01) | 44 | 18 | 76 |
| 3 | | H ₂ O/ <i>t</i> -C ₄ H ₉ OH (3/7) (0.01) | 31 | 13 | 63 |
| 4 | | H ₂ O/ <i>t</i> -C ₄ H ₉ OH (3/7) (0.01) | 17 | 6.9 | 35 |

a) Hydrogen evolution volume (mL) from 10 mmol of the fluorenol or alcohol derivative for the initial 1 h.

b) Conversion of alcohols to ketons after 1h was determined by GC.

c) The conversion after 5h.

X-ray crystallographic structures of fluorenol and fluorenone (Figure 2.4.6) depicted that the hydroxyl group and hydrogen atom bound to cyclopentane carbon are located out of the planar (slightly bent) fluorene skeleton, which is in contrast to the totally planar fluorenone structure. This suggests that the elimination of two hydrogens of the secondary alcohol fluorenol to form the π -conjugated planar fluorenone could be thermodynamically favourable.

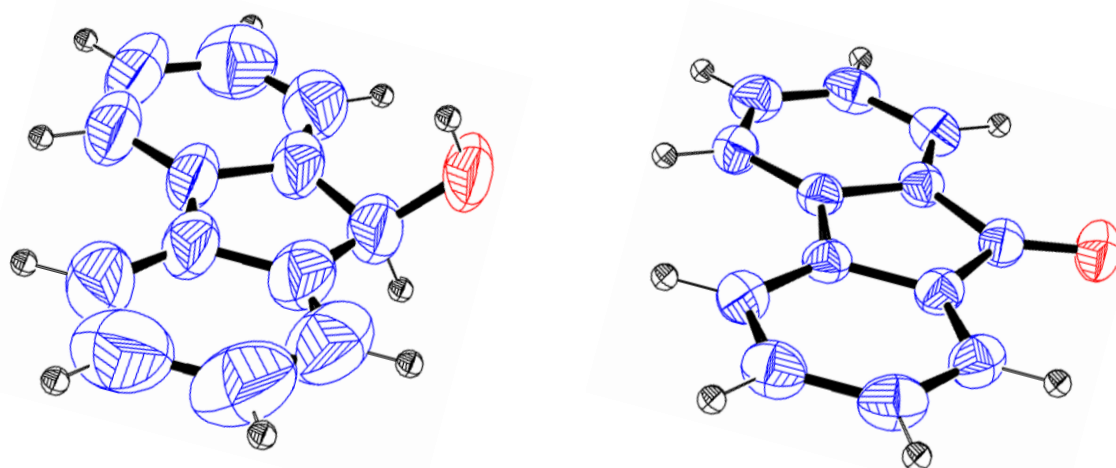


Figure 2.4.6 ORTEP view of fluorenol (left) and of fluorenone (right)

2.4.4 Hydrogen evolution from the fluorenol polymer

The fluorenol polymer (10 g) was soaked in an aqueous solution (15 mL) containing the iridium catalyst (157 mg of aqua (6,6'-dihydroxy-2,2'-bipyridine)(pentamethylcyclopentadienyl)iridium(III) bis(triflate) and heated at 80 °C. Rapid gas evolution from the polymer was ascribed to the elimination of H₂ by gas chromatography analysis, which amounted to 309 mL (94% of the formula weight-based mobile hydrogen amount) after 5 h (Table 2.4.2, Figure 2.4.7).

Table 2.4.2 Hydrogen evolution rate and yield of the fluorenol polymer

| entry | alcohol | solvent (alcohol concn, M) | initial hydrogen evolution (mL) ^{a)} | conversion (%) ^{b)} | conversion (%) ^{c)} |
|-----------------|---------|--|---|------------------------------|------------------------------|
| 1 ^{d)} | | H ₂ O (0.90 ^{e)}) | 86 | 36 | 94 ^{f)} |
| 2 ^{g)} | | H ₂ O (saturated) | 2.9 | 1.2 | 2.6 |
| 3 ^{h)} | | H ₂ O (0.90 ^{e)}) | 76 | 32 | 90 |

a) Hydrogen evolution volume (mL) from 10 mmol of the fluorenol or alcohol derivative for the initial 1 h.

b) Conversion of alcohols to ketones after 1h was determined by GC.

c) The conversion after 5h.

d) The polymer was swollen with the 60 wt% aqueous solution of the catalyst, which corresponded to 0.9 M in concentration of the fluorenol unit and was several thousand times higher than that of the aqueous solution saturated with fluorenone (ca. 0.2 mM).

e) Alcohol unit concentration was calculated by the molar mass of the repeating unit.

f) The conversion was on the average of 5 reactions with the standard deviation of 5.9%.

g) The aqueous solution was saturated with fluorenone (0.003 mmol) in water (15 mL) and involved the iridium catalyst (1.4 mol% vs. fluorenone).

h) The fluorenone/carbon composite (14.3 g) was prepared via hydrogenation with electrolytic reduction and protonation in the aqueous electrolyte.

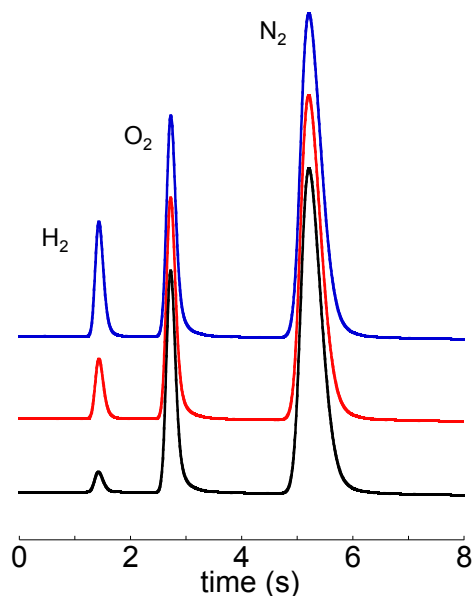


Figure 2.4.7 Gas chromatography of the gas evolved from the fluorenol polymer after the dehydrogenation reaction for 10 min (black), 20 min (red), and 30 min (blue). The peak of H₂ increased with the reaction time, indicating the pure hydrogen gas evolution from the polymer.

Hydrogen evolution rates from the polymer are listed in Table 2.4.2, along with those from the monomeric alcohols in the presence of the same iridium catalyst at 80 °C. The rate from the fluorenol polymer was 30 times larger than that from the monomeric fluorenol (entries 1 and 2), which is explained by the highly populated fluorenol units in the polymer and by the low solubility of fluorenol in the aqueous solution (Footnotes of Table 2.4.2).

After the hydrogen evolution, the colorless fluorenol polymer turned a reddish color (Figure 2.4.8). A strong IR absorption peak ($\nu_{\text{C=O}} = 1710 \text{ cm}^{-1}$) supported that almost all of the fluorenol units in the polymer turned into the fluorenone units through hydrogen evolution, to yield the fluorenone polymer (Figure 2.4.9).



Figure 2.4.8 Photograph of the fluorenol polymer specimen before (left) and after (right) the hydrogen evolution.

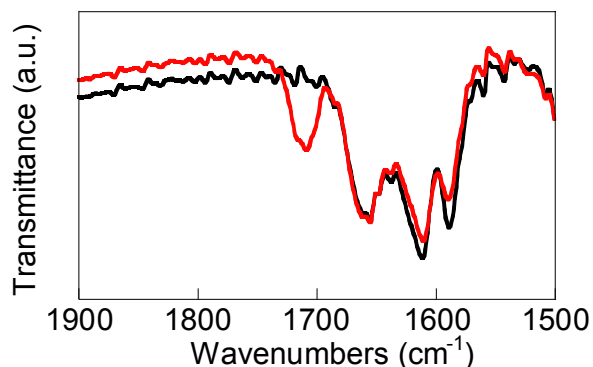


Figure 2.4.9 IR spectrum of the fluorene polymer before (black) and after (red) the hydrogen evolution.

2.4.5 Cycle of electrolytic hydrogenation and hydrogen evolution

A composite sheet (14.3 g) of the fluorene polymer with carbon nanofiber as a conductive additive was prepared, to perform the cycling of hydrogen-fixing and -releasing. The composite sheet was soaked in the AN/water electrolyte and -1.5 V was applied till a charge of 390 C per g polymer was passed. The sheet was transferred into 15 mL of water containing the iridium catalyst and heated at 80 °C for 5 h. The hydrogen evolution was almost similar to that of the neat fluorene polymer, and the evolved hydrogen (296 mL) almost reached the theoretical hydrogen density held in the composite sheet (entry 3 in Table 2.4.2). The composite sheet was then hydrogenated again, and this cycle was performed 50 times without any significant deterioration in the hydrogen evolution capacity (Figure 2.4.10).

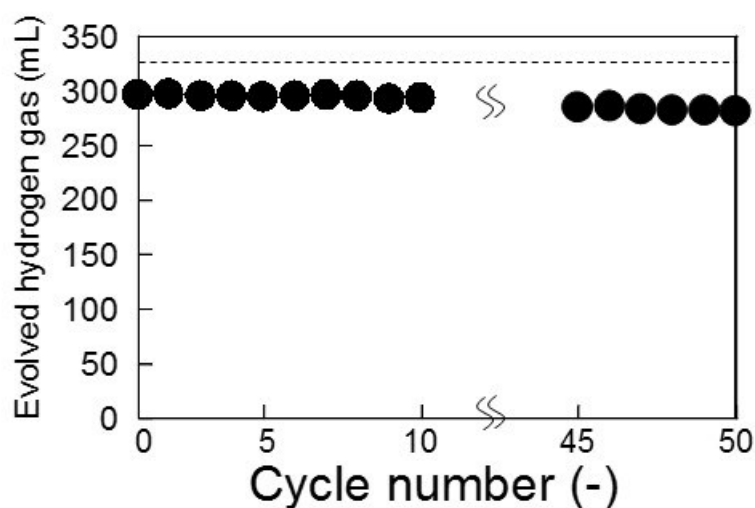


Figure 2.4.10 Evolved hydrogen gas plots from the fluorenone/carbon composite sheet after electrolytic hydrogenation. Dashed line represents the theoretical or formula weight-based calculated hydrogen gas volume. The cycle performance was tested in twice, and each gas volume was within the error limits.

2.5 Experimental Section

Methods

Fluorenone, fluorenoyl, and 2,7-bis[2-(diethylamino)ethoxy]-9-fluorenone dihydrochloride were purchased from Tokyo Chemical Industry Co. Aqua (6,6'-dihydroxy-2,2'-bipyridine)(pentamethylcyclopentadienyl)iridium(III)bis(triflate) was purchased from Kanto Chemical Co. ¹H NMR spectra were recorded on a JEOL ECX-500 spectrometer with chemical shifts downfield from tetramethylsilane as the internal standard, ¹³C CP/MAS NMR spectra on a JEOL ECX-600 spectrometer, IR spectra on a JASCO FT/IR-6100 spectrometer, UV-Vis spectra on a JASCO V-550 spectrometer, and X-ray crystallographic data on a R-Axis RAPID. Amount of evolved gas was determined using a gas chromatograph (Shimadzu GC-8AIT, Ar carrier) equipped with a 2 m long packed column of Molecular Sieve 5A and a recorder (Shimadzu C-R8A Chromatopac Data Processor). For H₂/D₂ detection, the gas samples were analyzed using a gas chromatograph (He carrier) equipped with a 3 m long packed column of Shinwa OGO-SP, that was immersed in liquid N₂ during the gas chromatograph measurements, and a thermal conductivity detector.

Mechanical testing of the polymer

The dynamic mechanical tests of a bar sample of 10 mm width and 40 mm length were performed using a Dynamic Mechanical Analyzer Q-800. Storage modulus, loss modulus, and tangent delta were analyzed at a frequency of 1 Hz with a ramp speed of 2 °C min⁻¹.

Electrochemical measurements

Cyclic voltammograms and chronopotentiograms were carried out with a fluorenone polymer-coated glassy carbon plate or disk electrode, a platinum wire, and an Ag/AgCl electrode as the working, the counter, and the reference electrode, respectively, using an ALS700 electrochemical analyzer. The formula weight-based theoretical capacity (in mA h g⁻¹) was calculated according to $1000 nFM^{-1} (3600)^{-1}$, where n , F , and M are stoichiometric numbers of electrons (two in this experiment), Faraday constant, and molar mass of the repeating unit, respectively. The redox capacity (in mA h g⁻¹) was given by the formula of $1000 Qm^{-1} (3600)^{-1}$, where Q and m are charges passed in electrolysis and the loading weight of the fluorenone polymer which was determined by weighing the anode.

Synthesis of 2,7-bis[2-(diethylamino)ethoxy]-9-fluorenoyl

2,7-Bis[2-(diethylamino)ethoxy]-9-fluorenone (17.0 g, 41.4 mmol) and sodium borohydride (11.3 g, 299 mmol) were dissolved and stirred in methyl alcohol (400 mL). Aqueous hydrochloric acid was added to neutralize the solution, evaporated, and the residue

was extracted with chloroform. The organic layer was washed with brine, dried over anhydrous sodium sulfate, evaporated to remove the solvent, and dried: Color-less powder (2,7-bis[2-(diethylamino)ethoxy]-9-fluorenol, 15.8 g). ^1H NMR (500 MHz, $(\text{CD}_3)_2\text{SO}$): δ 7.51 (d, 2H), 7.10 (s, 2H), 6.89 (d, 2H), 5.78 (d, 1H), 5.37 (d, 1H), 4.03 (t, 4H), 2.78 (t, 4H), 2.55 (q, 8H), 0.98 (t, 12H); ^{13}C NMR (500 MHz, $(\text{CD}_3)_2\text{SO}$): δ 157.8, 148.3, 132.2, 119.8, 114.5, 111.4, 73.5, 66.6, 51.4, 47.0, 11.9; FAB-MS (m/z): $[\text{M}]^+$ calcd for $\text{C}_{25}\text{H}_{36}\text{N}_2\text{O}_3$, 412.6; found, 412.7; Analysis (calcd, found for $\text{C}_{25}\text{H}_{36}\text{N}_2\text{O}_3$): C (72.8, 72.8), H (8.8, 8.8), O (11.6, 11.7).

Synthesis of the fluorenol polymer

2,7-Bis[2-(diethylamino)ethoxy]-9-fluorenol (12.8 g, 31.1 mmol) and 1,3,5-tris(bromomethyl)benzene (7.39 g, 20.7 mmol) were dissolved in NMP (60 ml). The mixture was heated on a boat ($10 \times 21 \text{ cm}^2$) of TeflonTM at 80 °C for 5 h. The obtained polymer was washed with NMP, water, and methyl alcohol, and dried. Solid-state ^{13}C NMR spectrum of the obtained polymer gave the peaks (156.5, 147.5, 132.4, 118.3, 114.6, 111.8, 72.4 ppm) assigned to the fluorenol moiety, and the peaks (46.9, 33.2 ppm) ascribed to the methylene carbons of the reactants were shifted.

Preparation of the fluorenone polymer/carbon composite

To prepare the fluorenone polymer/carbon composite, 2,7-bis[2-(diethylamino)ethoxy]-9-fluorenone (9.50 g, 23.1 mmol) and 1,3,5-tris(bromomethyl)benzene (5.50 g, 15.4 mmol) were mixed with multi-wall carbon nanotube (6.43 g, Sigma-Aldrich) in NMP. The mixture was heated on a boat of TeflonTM at 80 °C for 5 h. The obtained fluorenone polymer/carbon composite sheet was washed with NMP, water, and methyl alcohol, and dried. The composite sheet was cut (14.2 g) and applied to the working electrode in the electrolytic hydrogenation.

Crystal data and structure refinement for fluorenol

| | |
|----------------------|---|
| Empirical Formula | C ₁₃ H ₁₀ O |
| Formula Weight | 182.22 |
| Crystal Color, Habit | colorless, platelet |
| Crystal Dimensions | 0.550 X 0.550 X 0.300 mm |
| Crystal System | monoclinic |
| Lattice Type | Primitive |
| Lattice Parameters | a = 13.86571 Å b = 24.04798 Å c = 19.32089 Å β = 88.46200 ° V = 6440.08142 Å ³ |
| Space Group | P2 ₁ /n (#14) |
| Z value | 24 |
| D _{calc} | 1.128 g/cm ³ |
| F ₀₀₀ | 2304.00 |
| μ(CuKα) | 5.520 cm ⁻¹ |

Chapter 2

| | |
|--|--|
| Diffractometer | R-AXIS RAPID |
| Radiation | CuK α ($\lambda = 1.54187 \text{ \AA}$) graphite monochromated |
| Voltage, Current | 50kV, 100mA |
| Temperature | -100.0°C |
| Detector Aperture | 460.0 x 256.0 mm |
| Data Images | 180 exposures |
| ω oscillation Range ($\chi=54.0, \phi=0.0$) | 80.0 - 260.0° |
| Exposure Rate | 10.0 sec./° |
| ω oscillation Range ($\chi=54.0, \phi=90.0$) | 80.0 - 260.0° |
| Exposure Rate | 10.0 sec./° |
| ω oscillation Range ($\chi=54.0, \phi=180.0$) | 80.0 - 260.0° |
| Exposure Rate | 10.0 sec./° |
| ω oscillation Range ($\chi=54.0, \phi=285.0$) | 80.0 - 260.0° |
| Exposure Rate | 10.0 sec./° |
| ω oscillation Range ($\chi=10.0, \phi=60.0$) | 80.0 - 260.0° |
| Exposure Rate | 10.0 sec./° |
| Detector Position | 127.40 mm |
| Pixel Size | 0.100 mm |

| | |
|---------------------------------------|--|
| Structure Solution | Direct Methods (SIR92) |
| Refinement | Full-matrix least-squares on F ² |
| Function Minimized | $\sum w (F_o^2 - F_c^2)^2$ |
| Least Squares Weights | $w = 1 / [\sigma^2(F_o^2) + (0.4000 \cdot P)^2 + 0.0000 \cdot P]$ where $P = (\text{Max}(F_o^2, 0) + 2F_c^2)/3$ |
| $2\theta_{\text{max}}$ cutoff | 142.6° |
| Anomalous Dispersion | All non-hydrogen atoms |
| No. Observations (All reflections) | 11741 |
| No. Variables | 811 |
| Reflection/Parameter Ratio | 14.48 |
| Residuals: R1 ($I > 2.00\sigma(I)$) | 0.1715 |
| Residuals: R (All reflections) | 0.2352 |
| Residuals: wR2 (All reflections) | 0.5447 |
| Goodness of Fit Indicator | 0.999 |
| Max Shift/Error in Final Cycle | 0.006 |
| Maximum peak in Final Diff. Map | 0.67 e ⁻ /Å ³ |
| Minimum peak in Final Diff. Map | -0.49 e ⁻ /Å ³ |

Crystal data and structure refinement for fluorenone

| | |
|----------------------|--|
| Empirical Formula | C ₁₃ H ₈ O |
| Formula Weight | 180.21 |
| Crystal Color, Habit | yellow, platelet |
| Crystal Dimensions | 0.500 X 0.200 X 0.100 mm |
| Crystal System | orthorhombic |
| Lattice Type | Primitive |
| Lattice Parameters | a = 15.9263(3) Å b = 12.4384(2) Å c = 18.5790(3) Å V = 3680.44(12) Å ³ |
| Space Group | Pbca (#61) |
| Z value | 16 |
| D _{calc} | 1.301 g/cm ³ |
| F ₀₀₀ | 1504.00 |
| μ(CuKα) | 6.434 cm ⁻¹ |

| | |
|--|--|
| Diffractometer | R-AXIS RAPID |
| Radiation | CuK α ($\lambda = 1.54187 \text{ \AA}$) graphite monochromated |
| Voltage, Current | 50kV, 100mA |
| Temperature | -100.0°C |
| Detector Aperture | 460.0 x 256.0 mm |
| Data Images | 90 exposures |
| ω oscillation Range ($\chi=54.0, \phi=0.0$) | 80.0 - 260.0° |
| Exposure Rate | 10.0 sec./° |
| ω oscillation Range ($\chi=54.0, \phi=90.0$) | 80.0 - 260.0° |
| Exposure Rate | 10.0 sec./° |
| ω oscillation Range ($\chi=54.0, \phi=180.0$) | 80.0 - 260.0° |
| Exposure Rate | 10.0 sec./° |
| ω oscillation Range ($\chi=54.0, \phi=270.0$) | 80.0 - 260.0° |
| Exposure Rate | 10.0 sec./° |
| ω oscillation Range ($\chi=10.0, \phi=60.0$) | 80.0 - 260.0° |
| Exposure Rate | 10.0 sec./° |
| Detector Position | 127.40 mm |
| Pixel Size | 0.100 mm |

| | |
|---------------------------------------|--|
| Structure Solution | Direct Methods (SIR92) |
| Refinement | Full-matrix least-squares on F^2 |
| Function Minimized | $\sum w (F_o^2 - F_c^2)^2$ |
| Least Squares Weights | $w = 1 / [\sigma^2(F_o^2) + (0.0591 \cdot P)^2 + 0.4288 \cdot P]$ where $P = (\text{Max}(F_o^2, 0) + 2F_c^2)/3$ |
| $2\theta_{\text{max}}$ cutoff | 136.5° |
| Anomalous Dispersion | All non-hydrogen atoms |
| No. Observations (All reflections) | 3361 |
| No. Variables | 253 |
| Reflection/Parameter Ratio | 13.28 |
| Residuals: R1 ($I > 2.00\sigma(I)$) | 0.0381 |
| Residuals: R (All reflections) | 0.0440 |
| Residuals: wR2 (All reflections) | 0.1020 |
| Goodness of Fit Indicator | 1.083 |
| Max Shift/Error in Final Cycle | 0.000 |
| Maximum peak in Final Diff. Map | 0.18 e ⁻ /Å ³ |
| Minimum peak in Final Diff. Map | -0.26 e ⁻ /Å ³ |

References

- 1 R. C. Armstrong, C. Wolfram, K. P. Jong, R. Gross, N. S. Lewis, B. Boardman, A. J. Ragauskas, K. Martinez, G. Crabtree, M. V. Ramana, *Nat. Energy* **2016**, *1*, 1.
- 2 L. Schlapbach, A. Züttel, *Nature* **2001**, *414*, 353.
- 3 B. C. H. Steele, A. Heinzl, *Nature* **2001**, 345.
- 4 J. Zheng, X. Liu, P. Xu, P. Liu, Y. Zhao, J. Yang, *Int. J. Hydrogen Energy* **2012**, *37*, 1048.
- 5 A. Ströbel, J. Garche, P. T. Moseley, L. Jörissen, G. Wolf, *J. Power Sources* **2006**, *159*, 781.
- 6 S. Patchkovskii, J. S. Tse, S. N. Yurchenko, L. Zhechkov, T. Heine, G. Seifert, *Proc. Natl. Acad. Sci. USA* **2005**, *102*, 10439.
- 7 L. J. Murray, M. Dincă, J. R. Long, *Chem. Soc. Rev.* **2009**, *38*, 1294.
- 8 J. R. Li, J. Sculley, H. Zhou, *Chem. Rev.* **2012**, *112*, 869.
- 9 A. F. Dalebrook, W. Gan, M. Grasmann, S. Moret, G. Laurenczy, *Chem. Commun.* **2013**, *49*, 8735.
- 10 G. E. Döbereiner, A. Nova, N. D. Schley, N. Hazari, S. J. Miller, O. Eisenstein, R. H. Crabtree, *J. Am. Chem. Soc.* **2011**, *133*, 7547.
- 11 K. Fujita, Y. Tanaka, M. Kobayashi, R. Yamaguchi, *J. Am. Chem. Soc.* **2014**, *136*, 4829.
- 12 L. E. Heim, N. E. Schlörer, J. -H. Choi, M. H. G. Precht, *Nat. Commun.* **2014**, *5*, 3621.
- 13 P. Hu, E. Fogler, Y. Diskin-Posner, M. A. Iron, D. Milstein, *Nat. Commun.* **2015**, *6*, 6859.
- 14 G. A. Deluga, J. R. Salge, L. D. Schmidt, X. E. Verykios, *Science* **2004**, *303*, 993.
- 15 M. Nielsen, E. Alberico, W. Baumann, H. Drexler, H. Junge, S. Gladiali, M. Beller, *Nature* **2013**, *495*, 85.
- 16 S. Musa, I. Shaposhnikov, S. Cohen, D. Gelman, *Angew. Chem. Int. Ed.* **2011**, *50*, 3533.
- 17 T. Suzuki, *Chem. Rev.* **2011**, *111*, 1825.
- 18 K. Oyaizu, W. Choi, H. Nishide, *Polym. Adv. Technol.* **2011**, *22*, 1242.
- 19 N. Gupta, H. Linschitz, *J. Am. Chem. Soc.* **1997**, *119*, 6384.
- 20 M. W. Lehmann, D. H. Evans, *J. Electroanal. Chem.* **2001**, *500*, 12.
- 21 M. W. Lehmann, D. H. Evans, *J. Phys. Chem. B* **2001**, *105*, 8877.
- 22 M. Salas, M. Gomez, F. J. Gonzalez, B. Gordillo, *J. Electroanal. Chem.* **2003**, *543*, 73.
- 23 Y. Ge, L. Miller, T. Ouimet, D. K. Smith, *J. Org. Chem.* **2000**, *65*, 8831.
- 24 Y. Ge, D. K. Smith, *Anal. Chem.* **2000**, *72*, 1860.
- 25 Y. Hui, E. L. K. Chng, C. Y. L. Chng, H. L. Poh, R. D. Webster, *J. Am. Chem. Soc.* **2009**, *131*, 1523.
- 26 M. D. Stallings, M. M. Morrison, D. T. Sawyer, *Inorg. Chem.* **1981**, *20*, 2655.
- 27 M. D. Greaves, A. Niemz, V. M. Rotello, *J. Am. Chem. Soc.* **1999**, *121*, 266.
- 28 B. R. Eggins, J. Q. Chambers, *J. Electrochem. Soc.* **1970**, *117*, 186.

- 29 J. Garza, R. Vargas, M. Gomez, I. Gonzalez, F. J. Gonzalez, *J. Phys. Chem. A* **2003**, *107*, 11161.
- 30 M. Gomez, I. Gonzalez, F. J. Gonzalez, R. Vargas, J. Garza, *Electrochem. Commun.* **2003**, *5*, 12.
- 31 N. Menshutkin. *Physik. Chem.* **1890**, *5*, 589.
- 32 N. Menshutkin. *Physik. Chem.* **1890**, *6*, 41.
- 33 Y. Zheng, S. Li, Z. Wenga, C. Gao, *Chem. Soc. Rev.* **2015**, *44*, 4091.
- 34 D. Schmaljohann, B. Voit, *Macromol. Theory Simul.* **2003**, *12*, 679.
- 35 J. Han, S. Li, A. Tang, C. Gao, *Macromolecules*, **2012**, *45*, 4966.
- 36 S. Li, C. Gao, *Polym. Chem.* **2013**, *4*, 4450.
- 37 Z. L. Weng, Y. C. Zheng, A. J. Tang, C. Gao, *Aust. J. Chem.* **2014**, *67*, 103.
- 38 W. Choi, D. Harada, K. Oyaizu, H. Nishide, *J. Am. Chem. Soc.* **2011**, *133*, 19839.
- 39 T. Kawai, K. Oyaizu, H. Nishide, *Macromolecules*, **2015**, *48*, 2429.
- 40 K. Oyaizu, W. Choi, H. Nishide, *Polym. Adv. Technol.* **2011**, *22*, 1242.
- 41 K. Oyaizu, Y. Niibori, A. Takahashi, H. Nishide, *J. Inorg. Organomet. Polym.* **2013**, *23*, 243.
- 42 D. S. Canby, G. T. Cheek, *ECS Transactions*, **2007**, *3*, 609.
- 43 H. Nishide, K. Oyaizu, *Science* **2008**, *319*, 737.
- 44 K. Oyaizu, T. Kawamoto, T. Suga, H. Nishide, *Macromolecules* **2010**, *43*, 10382.
- 45 K. Oyaizu, Y. Ando, H. Konishi, H. Nishide, *J. Am. Chem. Soc.* **2008**, *130*, 14459.
- 46 R. Kawahara, K. Fujita, R. Yamaguchi, *J. Am. Chem. Soc.* **2012**, *134*, 3643.

Chapter 3

Poly(vinyl fluorenone/fluore nol) for a Charge and Hydrogen Storage Material

Contents

- 3.1 Introduction
- 3.2 Synthesis of Poly(vinyl fluorenone/fluore nol) via Radical Polymerization
- 3.3 Charge Storage Properties of Poly(vinyl fluorenone)
- 3.4 Hydrogen Storage Properties of Poly(vinyl fluorenone)
- 3.5 Experimental Section

References

3.1 Introduction

Conjugated carbonyl compounds have attracted much attention as a charge storage materials, such as an anode active materials, based on their reversible multi-electron-transfer capability, fast reaction kinetics, and structural diversity.¹⁻¹⁶ Fluorenone, one of the conjugated carbonyl compound, is a fluorene derivative with an oxygen atom at the 9-position, and it has been well studied as electroluminescence materials or probes for studying DNA because of some unique spectroscopic, photophysical, and electrochemical properties due to the fluorene structure¹⁷⁻²⁵. Especially, in the case of the electrochemical properties, the presence of ketone, which is electron-withdrawing group, reduce the reduction potential, but the cyclopentadiene nature of the central ring of fluorenone gives high stability to the reductants. In fact, fluorenone exhibits reversible $2e^-$ redox property in aprotic electrolyte solution, and the electrochemical reduction of fluorenone gives high stable anion radical or dianion state because of the resonance stabilization and formation of aromatic sextet²⁶. Furthermore, fluorenol, which is the hydrogen reductant of fluorenone, has a hydroxyl group at the 9-position of the internal cycle array and it is stable secondary alcohol.

Reversible charge storage performance is required for organic electrode-active materials, especially for anode materials in organic batteries possessing negative redox potentials to increase the electromotive force. Our laboratory have found that the polymers containing highly packed population of the redox-active units as pendant groups transport charge with large current densities, giving large redox capacities²⁷⁻³⁹. The driving force of the characteristics is redox gradient, and charges are transported by the electron self-exchange reaction between the each other redox units.

In this chapter, we synthesized poly(vinyl fluorenone) (PFN) as a n-type redox polymer and electrochemical properties of it in aprotic electrolyte was investigated. Furthermore, the redox and protonation properties of PFN in water electrolyte were declared by electrochemical measurements and repeatedly fix and release hydrogen through the three steps as follows: (1) Electrolysis reduction, (2) protonation, and (3) dehydrogenation. PFN was applied to not only the charge but hydrogen storage materials.

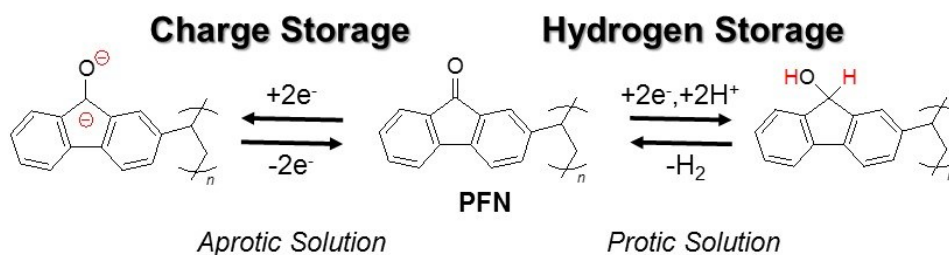
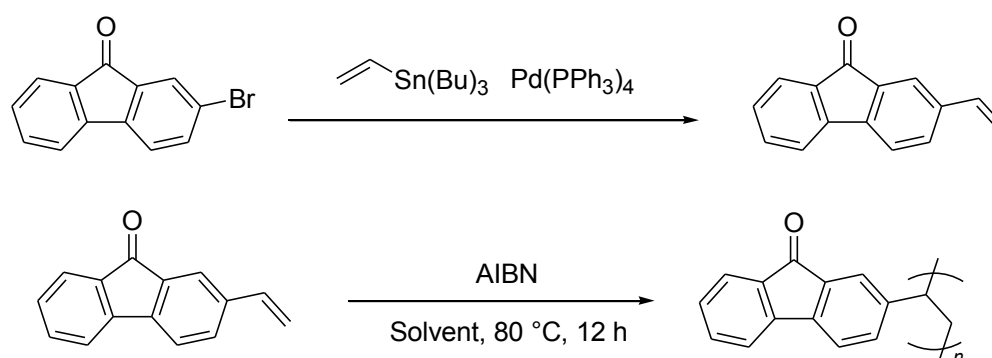


Figure 3.1.1 Schematic representation of charge and hydrogen storage

3.2 Synthesis of Poly(vinyl fluorenone/fluorenol) via Radical Polymerization

3.2.1 Synthesis of poly(vinyl fluorenone) via solution polymerization

Poly(vinyl fluorenone) (PFN) was synthesized via radical polymerization by using an azobisisobutyronitrile (AIBN) as initiator in different solvent. The results of the polymerization are summarized in run 1–6 of Table 3.2.1. The obtained polymers were analyzed by infrared. All polymers indicated the absorption ascribed to ν_{C-H} at 3000 cm^{-1} and $\nu_{C=O}$ at 1710 cm^{-1} , suggesting that the progress of the polymerization. 2-vinyl-fluorenone has the relatively higher solubility in the 1,2-dichloroethane. Thus we increased the monomer concentration in the solvent to obtain high molecular weight polymer.



Scheme 3.2.1 Synthesis of poly(vinyl fluorenone) via solution polymerization

Table 3.2.1 Solution polymerization of 2-vinyl-fluorenone

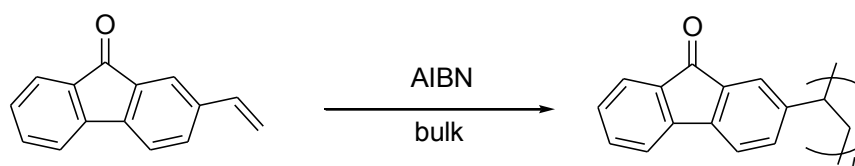
| Run | Solvent | Monomer conc. (M) | M_w ($\times 10^4$) | PDI | Yield (%) |
|-----|--------------------|-------------------|-------------------------|-----|-----------|
| 1 | 1,2-dichloroethane | 0.1 | 0.86 | 1.4 | 29 |
| 2 | 1,2-dichloroethane | 1 | 1.5 | 2.4 | 46 |
| 3 | 1,2-dichloroethane | 1.5 | 2.6 | 2 | 69 |
| 4 | toluene | 0.1 | 0.84 | 1.8 | 21 |
| 5 | THF | 0.1 | 0.61 | 1.6 | 22 |
| 6 | benzene | 0.1 | 0.81 | 1.6 | 22 |

Higher molecular weight polymer was obtained by using 1,2-dichloroethane as a solvent, and the molecular weight increased with the concentration of monomer.

3.2.2 Synthesis of Poly(vinyl fluorenone) via bulk polymerization

To obtain the high molecular weight polymer, PFN was synthesized via bulk polymerization. 2-vinyl-fluorenone is a liquid at room temperature, and AIBN has a good solubility to the monomer. The results of the polymerization are summarized in Run 7–12 of

Table 3.2.2. The obtained polymers were analyzed by infrared. All polymers indicated the absorption ascribed to $\nu_{\text{C-H}}$ at 3000 cm^{-1} and $\nu_{\text{C=O}}$ at 1710 cm^{-1} , suggesting that the progress of the polymerization.



Scheme 3.2.2 Synthesis of poly(vinyl fluorenone) via bulk polymerization

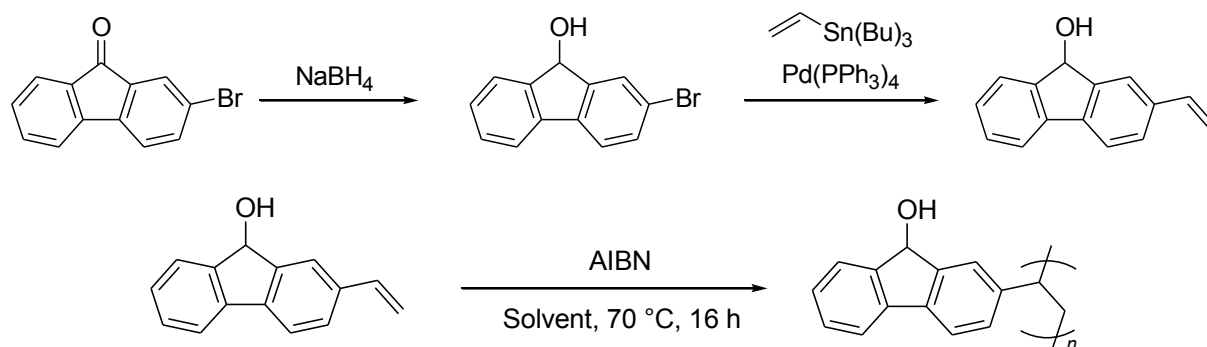
Table 3.2.2 Bulk polymerization of 2-vinyl-fluorenone

| Run | Temperature (°C) | AIBN (mol%) | M_w ($\times 10^4$) | PDI | Yield (%) |
|-----|------------------|-------------|-------------------------|-----|-----------|
| 7 | 75 | 0.75 | 8.4 | 2.5 | 7 |
| 8 | 80 | 0.75 | 32 | 7.6 | 35 |
| 9 | 80 | 2.5 | 15 | 2.6 | 36 |
| 10 | 80 | 5 | 12 | 2.7 | 46 |
| 11 | 85 | 0.75 | - | - | 29 |
| 12 | 90 | 0.75 | - | - | 49 |

The molecular weight of PFN increased with the reaction temperature, and the obtained polymer became too high molecular weight to solve in chloroform, which was the GPC solvent, by conducting the polymerization at over $85\text{ }^\circ\text{C}$ (Run 11 and 12). As a result of considering the PDI, we concluded that the polymer yielded by using the condition of Run 9 was the best and applied the polymer to electrochemical analysis.

3.2.3 Synthesis of Poly(vinyl fluorenone) via solution polymerization

2-Bromo-fluorenone was reduced by chemical reduction with sodium borohydride and polymerized via radical polymerization for the hydrogen evolution experiments. The results of the polymerization are summarized in Run 13–17 of Table 3.2.3.



Scheme 3.2.3 Synthesis of poly(vinyl fluorenone) via radical polymerization

Table 3.2.3 Radical polymerization of 2-vinyl-fluorenel

| Run | AIBN (mol%) | Monomer conc. (M) | M_w ($\times 10^3$) | PDI |
|-----|-------------|-------------------|-------------------------|-----|
| 13 | 1 | 0.5 | 5.1 | 1.3 |
| 14 | 0.75 | 0.5 | 8.2 | 1.3 |
| 15 | 0.75 | 1 | 9.8 | 1.4 |
| 16 | 0.75 | 2 | 15 | 1.5 |
| 17 | 0.75 | 3.5 | 20 | 1.6 |

The molecular weight increased with the concentration of monomer, and the polymer yielded by using the condition of Run 17 was applied to the hydrogen evolution analysis.

3.3 Charge Storage Properties of Poly(vinyl fluorenone)

3.3.1 Electrochemical properties of poly(vinyl fluorenone)

To investigate the behavior of poly(vinyl fluorenone) (PFN), a composite electrode of PFN with carbon nanofibre as a conductive additive was prepared. The composite electrode exhibited two reversible redox waves at -1.3 and -1.9 V (vs. Ag/AgCl) ascribed to the redox reaction of fluorenone units in the PFN. The peak current did not decrease after long cycles, revealing the robustness for the redox process of the PFN and the reaction proceeded without side reactions.

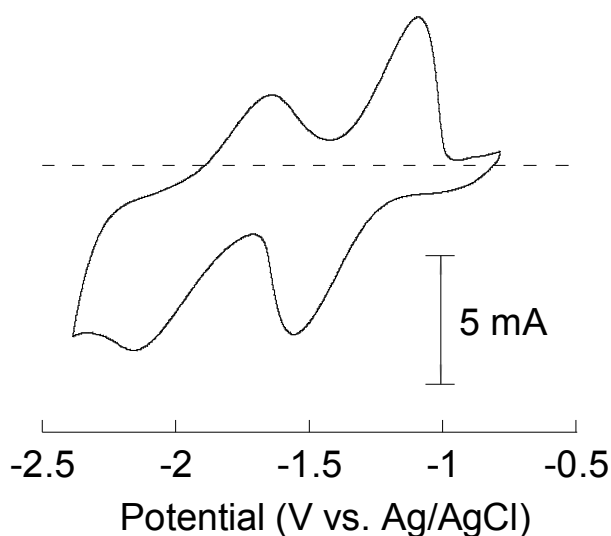


Figure 3.3.1 The cyclic voltammogram of PFN/carbon composite electrode in scanned at 10 mV s⁻¹ in 0.1 M (C₄H₉)₄NCIO₄ AN solution.

To examine the charge transport in the polymer layer, the PFN-coated electrode (thickness = 100 nm) was prepared. The chronoamperogram was measured by using the PFN-coated electrode and Cottrell plots were earned. The diffusion coefficient and the rate constant for the electron self-exchange reaction were calculated according to Laviron-Andrieux-Savéant equation.

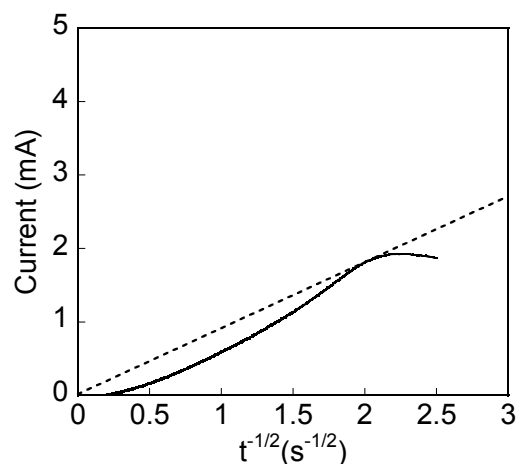


Figure 3.3.2 Chronoamperometric Cottrell plots obtained for the PFN-coated electrode in 0.1 M $(C_4H_9)_4NClO_4$ AN solution.

3.3.2 Charging/discharging property of poly(vinyl fluorenone)

The charging/discharging properties of PFN/carbon composite electrode was investigated by chronopotentiometry. Two plateaus were shown and the voltage region were observed about -1.3 and -1.9 V referring to the galvanostatic electrolysis of the PFN/carbon composite electrode, respectively. The charge capacities amounted to 244 mAh/g (94% of the formula weight-based theoretical density) and high discharge capacities, indicating that most of the fluorenone groups in the repeating unit underwent the two electron redox reaction (Figure 3.3.3).

The rate performance of the PFN/carbon composite electrode was also investigated. The electrode exhibited high discharge capacity even at a rapid discharging of 10 A/g, suggesting that rapid charge transport in the PFN layer.

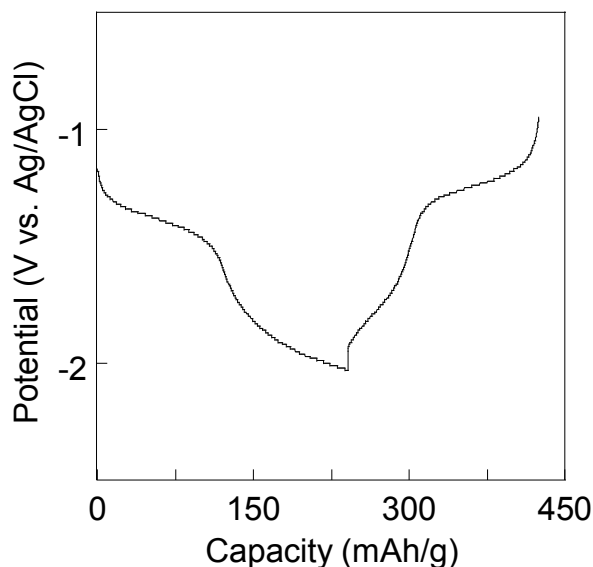


Figure 3.3.3 Charge–discharge curve of PFN/carbon composite electrode in 0.05 M $(C_4H_9)_4NBF_4$ AN/*t*-BuOH (vol =1/1) solution.

3.4 Hydrogen Storage Properties of Poly(vinyl fluorenone)

3.4.1 Electrolytic hydrogenation of Poly(vinyl fluorenone)

We have found the electrolytic hydrogenation of fluorenone in chapter 2. According to that result, the electrolytic hydrogenation of the PFN-coated electrode in protic electrolyte was investigated.

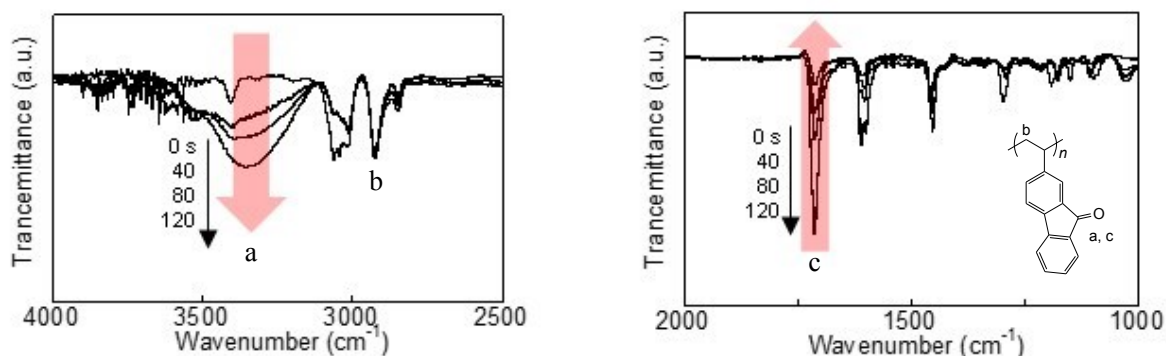


Figure 3.4.1 IR spectra of PFN layer during the electrolytic hydrogenation by applying -2.0 V in 0.05 M $(C_4H_9)_4NBF_4$ AN/water *t*-BuOH/AN/water (vol = 1/1/1) electrolyte.

PFN-coated carbon electrode (thickness = 100 nm) was prepared and applied -2.0 V (vs. Ag/AgCl), which potential was more negative than the reduction potential of fluorenone, in *t*-BuOH/AN/water (vol = 1/1/1) electrolyte. The PFN layer was monitored with infrared: The absorption ascribed to ν_{OH} at 3400 cm^{-1} increased and $\nu_{\text{C=O}}$ at 1710 cm^{-1} decreased as the passed charge increased, indicating the decrease in fluorenone content and increase in fluorenoneol content in the polymer through the electrolytic reduction, or protonation or hydrogenation (Figure 3.4.2). The coulombic efficiency was, for example, over 95% after the passage of equivalent charge, estimated with the conversion of the fluorenoneol unit.

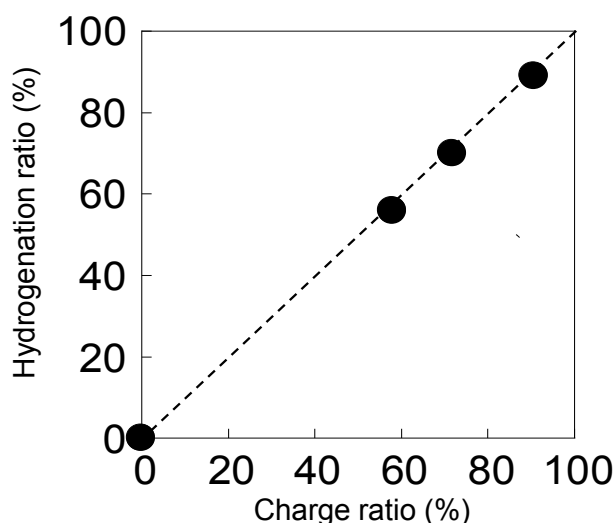


Figure 3.4.2 The conversion plots of the fluorenone to fluorenoneol unit in the PFN layer electrochemically reduced by applying -2.0 V in 0.05 M $(\text{C}_4\text{H}_9)_4\text{NBF}_4$ AN/water *t*-BuOH/AN/water (vol = 1/1/1) electrolyte.

3.4.2 Proton exchange reaction and proton-propagation

To discuss the rapid and quantitative hydrogenation reaction in the fluorenone polymer layer, we investigated the ^1H NMR of the mixture of fluorenoneol and the fluorenone dianion (the latter was prepared by the electrolytic reduction of fluorenone) (Figure 3.4.3). The peaks of hydroxyl (H^{a}) and cyclopentane (H^{b}) protons of fluorenoneol were broadened and shifted downfield by increasing the dianion content, indicating a proton exchange reaction between the fluorenoneol and the fluorenone dianion. The rate constants of the exchange were estimated with the relaxation time (T). These proton-exchanging rate constants are in the order of 10^3 – $10^4\text{ M}^{-1}\text{ s}^{-1}$ for fluorenoneol/fluorenone dianion and were large enough to explain the proton exchange in the fluorenone polymer layer (Figure 3.4.4).

The dianion of fluorenone was prepared by bulk electrolysis, by applying potential of -1.5

V (vs. Ag/AgCl) in the solution of 5 mM fluorenone and 0.1 M $(C_4H_9)_4NPF_6$ in $AN-d_3$. Mixtures of the dianion fluorenone and fluorenel (mol ratio 1/15–10000) were prepared in a N_2 glove box for NMR measurement. The rate constant of proton-exchanging (k_{ex}) was calculated by using equation $k_{app} = k_{ex} [FN \text{ dianion}]$ and $1/T^{obs} = 1/T + k_{app}$, where T is the relaxation time of each proton. Plots of k_{app} vs. $[FN \text{ dianion}]$ gave straight lines with the slopes of k_{ex} (Figure 3.4.5, Table 3.4.1).

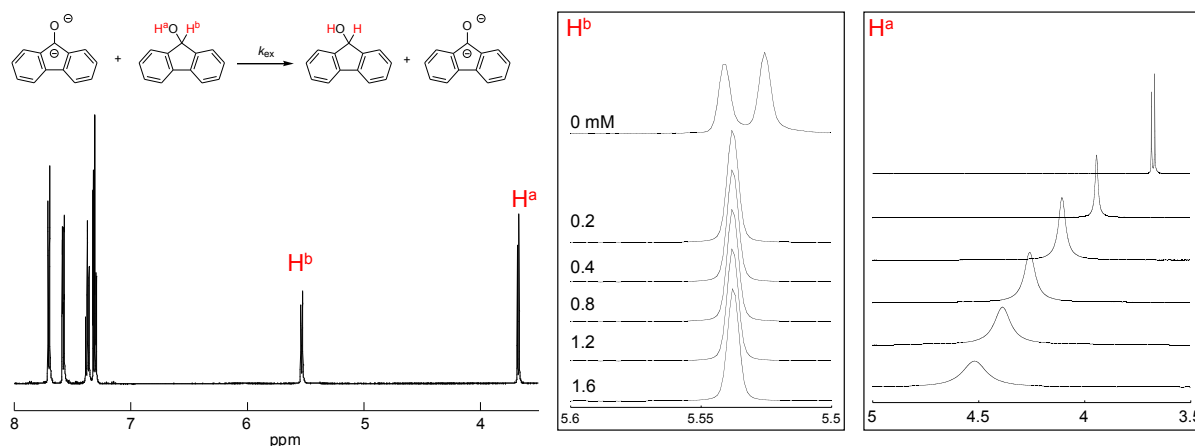


Figure 3.4.3 1H NMR measurements of fluorenel in the presence of the fluorenone dianion were conducted in $AN-d_3$ (left), expanded cyclopentane proton spectra of fluorenel (center), and hydroxyl proton spectra of fluorenel (right).

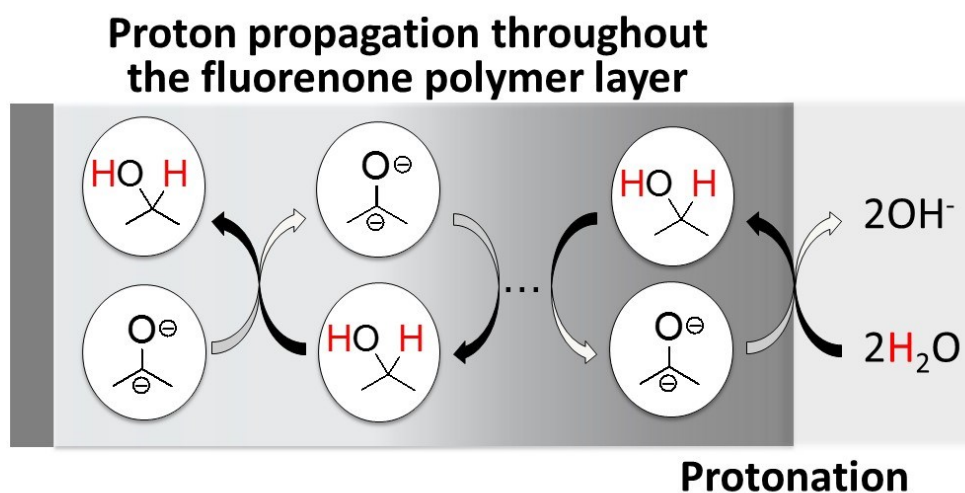


Figure 3.4.4 Schematic image of proton propagation in the polymer layer

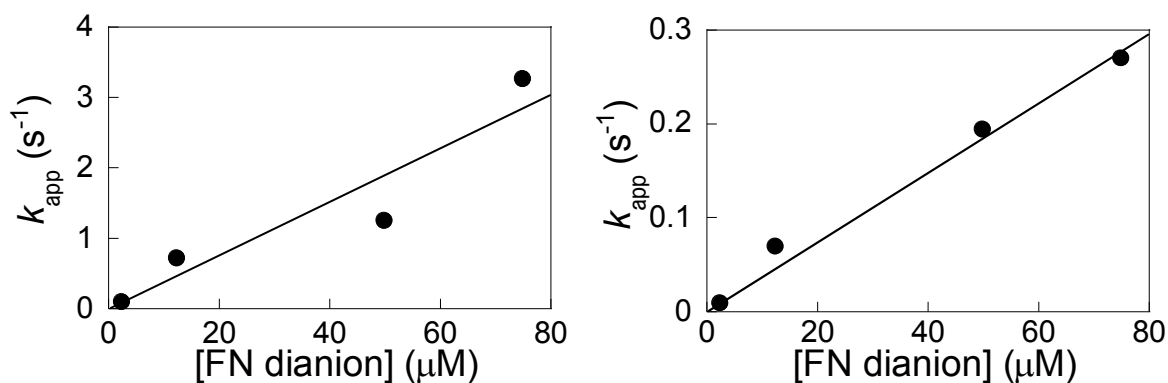


Figure 3.4.5 k_{app} plots of hydroxyl (right) and cyclopentane (left) protons of fluorenone.

Table 3.4.1 Rate constants of the proton-exchanging reaction

| Proton | k_{ex} ($\text{M}^{-1}\text{s}^{-1}$) |
|----------------|--|
| H ^a | 3.8×10^4 |
| H ^b | 3.7×10^3 |

Similar proton propagation had been examined using hydroquinone polymers^{40,41}; however, most of those were electrochemically inactive in aqueous media because of the very slow electron/proton hopping and of hydrophobic property of the polymers, and the redox active examples have been restricted only to the very thin quinone layer coated on a glassy carbon⁴¹. The fluorenone polymer hydrogel caused both an electrochemically effective charge and proton propagation or the hoppings, probably due to an appropriate network structure of the fluorenone units and the hydrophilic gel state. It should be noted here that the electrolytic reduction and the successive hydrogenation of the fluorenone polymer progressed in the presence of aqueous electrolyte at room temperature.

3.4.3 Hydrogen evolution from poly(vinyl fluorenone)

The poly(vinyl fluorenone) (PFNO) was dissolved in *t*-BuOH containing the iridium catalyst ((6,6'-dihydroxy-2,2'-bipyridine)(pentamethylcyclopentadienyl)iridium(III) bis(triflate))⁴² and heated at 82 °C. Rapid gas evolution from the polymer was ascribed to the

elimination of H₂ by gas chromatography analysis, which amounted to 93% of the formula weight-based mobile hydrogen amount after 5 h (Figure 3.4.6).

Hydrogen evolution rates from the PFNO was almost same as that from the monomeric fluoreenol, indicating that fluoreenol units in the PFNO oxidized and released hydrogen by reacting with the Ir catalyst without any side-reactions and steric hindrance of the polymer chain. IR spectra supported that almost all fluoreenol units in the polymer turned into fluorenone units through the dehydrogenation, to yield the PFN.

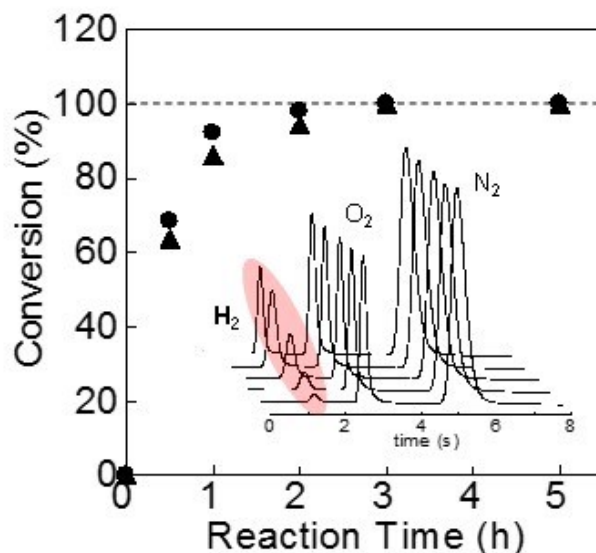


Figure 3.4.6 Time shift conversion of the dehydrogenation from fluoreenol (●) and PFNO (▲). Inset: Gas chromatograph for evolved gas from the PFNO.

3.5 Experimental Section

Methods

Fluorenone, fluoreenol, 2-bromo-9-fluorenone, tributyl(vinyl)tin, tetrakis(triphenylphosphine)palladium (0), sodium borohydride, and azobisisobutyronitrile were purchased from Tokyo Chemical Industry Co. Aqua (6,6'-dihydroxy-2,2'-bipyridine)(pentamethylcyclopentadienyl)iridium(III)bis(triflate) was purchased from Kanto Chemical Co. ¹H NMR spectra were recorded on a JEOL ECX-500 spectrometer with chemical shifts downfield from tetramethylsilane as the internal standard and IR spectra on a JASCO FT/IR-6100 spectrometer. Amount of evolved gas was determined using a gas chromatograph (Shimadzu GC-8AIT, Ar carrier) equipped with a 2 m long packed column of Molecular Sieve 5A and a recorder (Shimadzu C-R8A Chromatopac Data Processor).

Synthesis of 2-vinylfluorenone

2-Vinylfluorenone was synthesized via the Stille coupling reaction as follows. 2-Bromofluorenone (1.5 g, 5.79 mmol), tetrakis(triphenylphosphine)palladium(0) (201 mg, 0.174 mmol), and a proper amount of 2,6-di-*tert*-butyl-4-methylphenol were purged in dried vessel with N₂. Anhydrous toluene (60 mL) and tributyl(vinyl)tin (2.55 mL, 8.69 mmol) were added via syringe to the mixture under N₂. The resulting mixture was stirred at 100 °C for 14 h. After cooling to room temperature and evaporating the solvent, the mixture was extracted with chloroform and purified by silica gel column chromatography using chloroform/hexane (4:1 in v/v) as an eluent. The obtained solid was recrystallized from hexane to yield a yellow crystal. Yield: 60%. FAB-MS (m/z): M⁺ 206.1. Found 207.1. IR (KBr, cm⁻¹): 1709 (ν_{C=O}). Anal. Calcd for C₁₅H₁₀O: C, 87.4; H, 4.9%. Found: C, 87.2; H, 4.7%. ¹H NMR (CDCl₃, 500 MHz, ppm, TMS): δ 5.31 (d, 1H, vinyl), 5.79 (d, 1H, vinyl), 6.68 (t, 1H, vinyl), 7.29 (t, 1H, Ph), 7.74 (m, 4H, Ph), 7.64(d, 1H, Ph), 7.73 (s, 1H, Ph). ¹³C NMR (CDCl₃, 150 MHz, ppm, TMS): δ 115.1, 120.4, 121.6, 124.5, 129.1, 132.9, 134.6, 134.7, 134.9, 135.9, 138.9, 143.6, 144.4, 193.9.

Synthesis of poly(vinyl fluorenone) via solution polymerization

The 2-vinylfluorenone was polymerized to PFN using 2,2'-azobisisobutyronitrile (AIBN) as an initiator. Polymers obtained from the reactions in 1,2-dichloroethane, toluene, THF, and benzene. A sufficiently large molecular weight was accomplished by employing 1,2-dichloroethane as the solvent. After the polymerization, the solution was poured into methanol to precipitate the product which was purified by reprecipitation from chloroform to methanol to yield PFN as a yellow powder. Yield: 21–69%. GPC (chloroform eluent, polystyrene standard): $M_w = 0.86\text{--}2.6 \times 10^4$, $M_w/M_n = 1.4\text{--}2.4$, IR (KBr, cm⁻¹): 1709 (ν_{C=O}). Results were shown in Table 3.2.1.

Synthesis of poly(vinyl fluorenone) via bulk polymerization

The 2-vinylfluorenone was polymerized to PFN using 2,2'-azobisisobutyronitrile (AIBN) as an initiator. After the polymerization, the solution was poured into methanol to precipitate the product which was purified by reprecipitation from chloroform to methanol to yield PFN as a yellow powder. Yield: 7–49%. GPC (chloroform eluent, polystyrene standard): $M_w = 8.4\text{--}32 \times 10^4$, $M_w/M_n = 2.5\text{--}7.6$, IR (KBr, cm⁻¹): 1709 (ν_{C=O}). Results were shown in Table 3.2.2.

Synthesis of 2-bromofluorenone

2-Bromofluorenone (300 mg, 1.16 mmol) was dissolved in THF and ethanol co-solvent (16.6 mL, vol = 3/2). Sodium borohydride (44 mg, 1.16 mmol) was added to the mixture and

stirred at room temperature for overnight. After evaporating the solvent, the mixture was extracted with chloroform and purified by silica gel column chromatography using chloroform as an eluent. The obtained solid was recrystallized from acetone/hexane to yield a white powder. Yield: 86%. FAB-MS (m/z): M^+ 260.0, 262.0. Found 260.0, 261.9. Anal. Calcd for $C_{13}H_9BrO$: C, 59.8; H, 3.5%. Found: C, 59.6; H, 3.4%. 1H NMR ($CDCl_3$, 500 MHz, ppm, TMS): δ 1.85–1.87 (d, 1H, alcohol), 5.56–5.59 (d, 1H, fluorene), 7.32–7.37 (m, 1H, fluorenone), 7.39–7.41 (m, 1H, fluorene), 7.51–7.54 (m, 2H, fluorene), 7.61–7.64 (m, 2H, fluorene), 7.77 (d, 1H, fluorene). ^{13}C NMR ($CDCl_3$, 150 MHz, ppm, TMS): δ 75.0, 120.2, 121.6, 125.3, 128.3, 128.7, 129.1, 132.2, 139.1, 139.8, 145.4, 147.7.

Synthesis of 2-vinylfluorenel

2-Vinylfluorenel was synthesized via the Stille coupling reaction as follows. 2-Bromofluorenel (300 mg, 1.15 mmol), tetrakis(triphenylphosphine)palladium(0) (40 mg, 0.0345 mmol), and a proper amount of 2,6-di-*tert*-butyl-4-methylphenol were purged in dried vessel with N_2 . Anhydrous toluene (7.7 mL) and tributyl(vinyl)tin (0.51 mL, 1.73 mmol) were added via syringe to the mixture under N_2 . The resulting mixture was stirred at 100 °C for 14 h. After cooling to room temperature and evaporating the solvent, the mixture was extracted with chloroform and purified by silica gel column chromatography using chloroform as an eluent. The obtained solid was recrystallized from chloroform to yield a white powder. Yield: 72%. FAB-MS (m/z): M^+ 208.3. Found 208.1. Anal. Calcd for $C_{15}H_{12}O$: C, 86.5; H, 5.8%. Found: C, 86.9; H, 5.9%. 1H NMR ($CDCl_3$, 500 MHz, ppm, TMS): δ 1.84–1.86 (d, 1H, alcohol), 5.26–5.29 (d, 1H, vinyl), 5.57–5.59 (d, 1H, fluorene), 5.79–5.83 (d, 1H, vinyl), 6.77–6.71 (m, 1H, vinyl), 7.30–7.33 (m, 1H, fluorenone), 7.37–7.45 (m, 2H, fluorene), 7.58–7.62 (m, 1H, fluorene), 7.62–7.64 (m, 2H, fluorene), 7.72–7.74 (d, 1H, fluorene). ^{13}C NMR ($CDCl_3$, 150 MHz, ppm, TMS): δ 75.2, 113.9, 120.1, 122.7, 125.2, 127.7, 127.9, 129.2, 136.8, 137.5, 139.7, 139.8, 146.0, 146.2.

Polymerization of poly(vinyl fluorenel)

The 2-vinylfluorenel was polymerized to PFNO using 2,2'-azobisisobutyronitrile (AIBN) as an initiator. Polymers obtained from the reactions in THF. After the polymerization, the solution was poured into methanol to precipitate the product which was purified by reprecipitation from chloroform to methanol to yield PFNO as a white powder. Results of the polymers properties are shown in Table 3.2.3.

References

1. W. Xu, A. Read, K. Koech, H. Hu, M. Wang, J. Xiao, A. Padmaperuma, L. Graff, J. Liu, J. Zhang, *J. Mater. Chem.* **2012**, *22*, 4032.
2. Z. Song, T. Xu, L. Gordin, Y. Jiang, I. Bae, Q. Xiao, H. Zhan, J. Liu, D. Wang, *Nano Lett.* **2012**, *12*, 2205.
3. K. Liu, J. Zheng, G. Zhong, Y. Yang, *J. Mater. Chem.* **2011**, *21*, 4125.
4. Z. Song, Y. Qian, X. Liu, T. Zhang, Y. Zhu, H. Yu, M. Otani, H. Zhou, *Energy Environ. Sci.* **2014**, *7*, 4077.
5. D. Haringer, P. Novak, O. Haas, B. Piro, M. Pham, *J. Electrochem. Soc.* **1999**, *146*, 2393.
6. L. Zhao, W. Wang, A. Wang, K. Yuan, S. Chen, Y. Yang, *J. Power Sources* **2013**, *233*, 23.
7. W. Choi, D. Harada, K. Oyaizu, H. Nishide, *J. Am. Chem. Soc.* **2011**, *133*, 19839.
8. T. Kawai, K. Oyaizu, H. Nishide, *Macromolecules* **2015**, *48*, 2429.
9. T. Nokami, T. Matsuo, Y. Inatomi, N. Hojo, T. Tsukagoshi, H. Yoshizawa, A. Shimizu, H. Kuramoto, K. Komae, H. Tsuyama, *et al. J. Am. Chem. Soc.* **2012**, *134*, 19694.
10. K. Oyaizu, A. Hatemata, W. Choi, H. Nishide, *J. Mater. Chem.* **2010**, *20*, 5404.
11. Z. Song, H. Zhan, Y. Zhou, *Angew. Chem., Int. Ed.* **2010**, *49*, 8444.
12. Y. Meng, H. Wu, Y. Zhang, Z. Wei, *J. Mater. Chem. A* **2014**, *2*, 10842.
13. H. Wu, S. Shevlin, Q. Meng, W. Guo, Y. Meng, K. Lu, Z. Wei, Z. Guo, *Adv. Mater.* **2014**, *26*, 3338.
14. H. Wu, K. Wang, Y. Meng, K. Lu, Z. Wei, *J. Mater. Chem. A* **2013**, *1*, 6366.
15. P. Sharma, D. Damien, K. Nagarajan, M. Shaijumon, M. Hariharan, *J. Phys. Chem. Lett.* **2013**, *4*, 3192.
16. J. Geng, J. Bonnet, S. Renault, F. Dolhem, P. Poizot, *Energy Environ. Sci.* **2010**, *3*, 1929.
17. G. Zhao, K. Han, *J. Phys. Chem. A* **2007**, *111*, 9218.
18. H. Li, R. Zhu, W. Shi, K. He, Z. Shi, *Org. Lett.* **2012**, *14*, 4850.
19. L. A. Estrada, J. E. Yarnell, D. C. Neckers, *J. Phys. Chem. A*, **2011**, *115*, 6366.
20. J. A. McCubbin, X. Tong, Y. Zhao, V. Snieckus, R. P. Lemieux, *Chem. Mater.*, **2005**, *17*, 2574.
21. G. G. Gurzadyan, S. Steenken, *Chem. Eur. J.* **2001**, *7*, 1808.
22. P. Wan, E. Krogh, *J. Am. Chem. Soc.* **1989**, *111*, 4887.
23. J. A. McCubbin, X. Tong, R. Wang, Y. Zhao, V. Snieckus, R. P. Lemieux, *J. Am. Chem. Soc.* **2004**, *126*, 1161.
24. B. Wei, H. Li, W. Zhang, Z. Xi, *Organometallics*, **2015**, *34*, 1339.
25. A. P. Kulkarni, X. Kong, S. A. Jenekhe, *J. Phys. Chem. B*, **2004**, *108*, 8689.
26. D. S. Canby, G. T. Cheek, *ECS Transactions*, **2007**, *3*, 609.
27. H. Nishide, K. Oyaizu, *Science* **2008**, *319*, 737.

28. H. Nishide, T. Suga, *Electrochem. Soc. Interface* **2005**, *14*, 32.
29. T. Suga, Y.-J. Pu, K. Oyaizu, H. Nishide, *Bull. Chem. Soc. Jpn.* **2004**, *77*, 2203.
30. K. Oyaizu, Y. Ando, H. Konishi, H. Nishide, *J. Am. Chem. Soc.* **2008**, *130*, 14459.
31. T. Suga, H. Konishi, H. Nishide, *Chem. Commun.* **2007**, 1730.
32. K. Oyaizu, T. Suga, K. Yoshimura, H. Nishide, *Macromolecules* **2008**, *41*, 6646.
33. Y. Takahashi, N. Hayashi, K. Oyaizu, K. Honda, H. Nishide, *Polym. J.* **2008**, *40*, 763.
34. H. Nishide, S. Iwasa, Y.-J. Pu, T. Suga, K. Nakahara, M. Satoh, *Electrochim. Acta* **2004**, *50*, 827.
35. K. Oyaizu, H. Nishide, *Adv. Mater.* **2009**, *21*, 2339.
36. T. Sukegawa, K. Sato, K. Oyaizu, H. Nishide, *RSC Advances*, **2015**, *5*, 15448.
37. T. Sukegawa, I. Masuko, K. Oyaizu, H. Nishide, *Macromolecules* **2014**, *47*, 8611.
38. I. S. Chae, M. Koyano, T. Sukegawa, K. Oyaizu, H. Nishide, *J. Mater. Chem. A*, **2013**, *1*, 9608.
39. T. Sukegawa, A. Kai, K. Oyaizu, H. Nishide, *Macromolecules* **2013**, *46*, 1361.
40. C. Karlsson, H. Huang, M. Strømme, A. Gogoll, M. Sjödin, *M. J. Electroanal. Chem.* **2014**, *735*, 95.
41. K. Takada, P. Gopalan, C. K. Ober, H. D. Abruña, *Chem. Mater.* **2001**, *13*, 2928.
42. R. Kawahara, K. Fujita, R. Yamaguchi, *J. Am. Chem. Soc.* **2012**, *134*, 3643.

Chapter 4

A Quinaldine Polymer: Ni-Electrodeposition-Assisted Hydrogenation and Hydrogen Evolution

Contents

- 4.1 Introduction
- 4.2 Electrochemical Hydrogenation of Quinaldine
- 4.3 Ni-Electrodeposition-Assisted Hydrogenation of Quinaldine Polymer
- 4.4 Hydrogen Evolution from the Hydrogenated Quinaldine Polymer
- 4.5 Experimental Section

References

4.1 Introduction

Quinaldine (QD), or 2-methylquinoline, is one of the typical *N*-heterocycles, and is widely involved in natural products, anesthetics, dyes, and fluorescent substances.¹⁻⁵ Recently QD and its derivatives have been examined as a hydrogen storage material which stores two hydrogen molecules by forming chemical bonds to yield 1,2,3,4-tetrahydroquinaldine (HQD)⁶⁻⁹ (Scheme 1). While the hydrogen-storage form or HQD is characterized with high stability in comparison with those of the physical adsorption-based porous materials, the N–H bond and the neighboring C–H bonds are weaker than the C–H bonds of carbocycles and the HQD ring thermodynamically favors to release hydrogen to return to the QD under relatively mild conditions.¹⁰ However, the chemical bond formation or hydrogenation of QDs with hydrogen gas proceeds only in specific solvents and/or at high temperatures and under high hydrogen pressures, to be an energy-consuming process and often accompanied with a by-product.^{8,9}

In situ electrochemical hydrogenation using electrons from a cathode and protons of water¹¹⁻¹³ provides an alternative formation route of hydrogenated organic molecules at room temperature and open-air atmosphere, with advantages of a simple experimental system and an electrochemically tunable reaction. The electrochemical hydrogenation has been described to be initiated with the generation of a so-called chemisorbed hydrogen on the electrode, which comes from the solvent including water and/or the supporting electrolyte through electrochemical reduction, and is followed by reaction of the chemisorbed hydrogen with an unsaturated organic molecule.¹⁴ Although hydrogen gas evolution by electrolysis of water is a competitive reaction, the hydrogenation of organic molecule has been reported to become predominant in conjunction with the reduction of a metal ion or the electrodeposition of metal.^{12,15}

Current efficiency of the electrochemical hydrogenation depends on the metal species, concentration and species of the unsaturated organic compounds, and surface area and property of the cathode electrode. *N*-Heterocycles, such as pyridine derivatives, and nickel ion have been studied as the unsaturated compound and the metal ion for the electrochemical hydrogenation, respectively.^{16,17} Polymer-coated or -modified carbon substrates have been studied as electrochemically active electrodes.¹⁸⁻²⁴ The carbon substrates coated with conductive polymers were examined as a cathode for the metal electrodeposition, where the polymers acted as a scaffold for the electrodeposition of metal.²⁵⁻²⁷ The conductive polymer layers on the electrode have been considered to provide large specific areas and to contribute to the formation of well-dispersed metal microparticles with a diameter of several hundred nanometers in the polymer layer, leading to the high catalytic ability of the deposited metal for hydrogenation of the unsaturated organic compounds dissolved in the bulk electrolyte

solution.^{28–31} However, to the best of our knowledge, there have been no report on either extension of the unsaturated organic compounds or *N*-heterocycles including QD as the hydrogen-fixing unit to their polymeric analogues, and on application of the polymers as the scaffold for the electrodeposition of metal for the efficient electrochemical hydrogenation. In this paper, we anticipated that the electrode coated with the polymer containing a hydrogen-storable and unsaturated moiety works as a reversible hydrogenation system with both the effective electrochemical hydrogenation assisted with the metal microparticle deposition and the hydrogen-releasing from the hydrogenated organic polymer. We prepared a HQD- and QD-substituted poly(acrylic acid) (PHQD and PQD, respectively) and applied them as a hydrogen storage material. The PHQD evolved hydrogen by simply warming it in water containing the iridium complex catalyst, and the PQD layer coated on a carbon substrate was hydrogenated with the electrodeposition of nickel microparticles in the polymer layer and stored hydrogen by forming the chemical bonds using water as a hydrogen source. The QD unit in the polymer turned to the original HQD. The cycle of the hydrogen-evolution and hydrogen-fixing from and in the polymer was described as a new example of hydrogen-fixing and -releasing system using organic polymers.

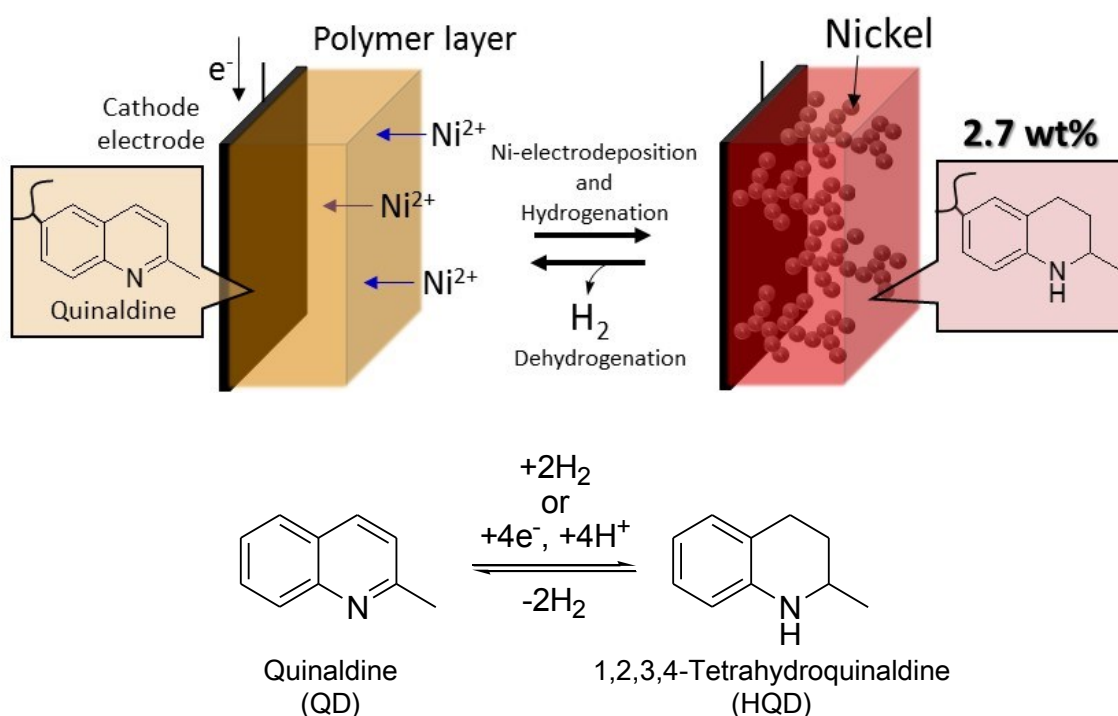


Figure 4.1.1 Schematic representation and scheme of hydrogen storage with quinaldine.

4.2 Electrochemical Hydrogenation of Quinaldine

Electrochemical hydrogenation of the monomeric QD associated with the electrodeposition of nickel microparticles was conducted as the control experiment. Cyclic voltammograms of 5 mM NiCl in 2.5 M NH₄Cl water/methyl alcohol (vol 4/1) solution with a carbon disk electrode are shown in Figure 4.2.1. The small reduction peak at -0.72 V (vs. Ag/AgCl, inset) and the cathodic current at -1.0 V have been ascribed, in the previous paper,²⁹ to the reduction of nickel ion or nickel electrodeposition and hydrogen evolution upon the deposited nickel, respectively. The addition of QD to the electrolyte led the new reduction peak at -1.21 V, to be ascribed to the reduction of QD upon the nickel.

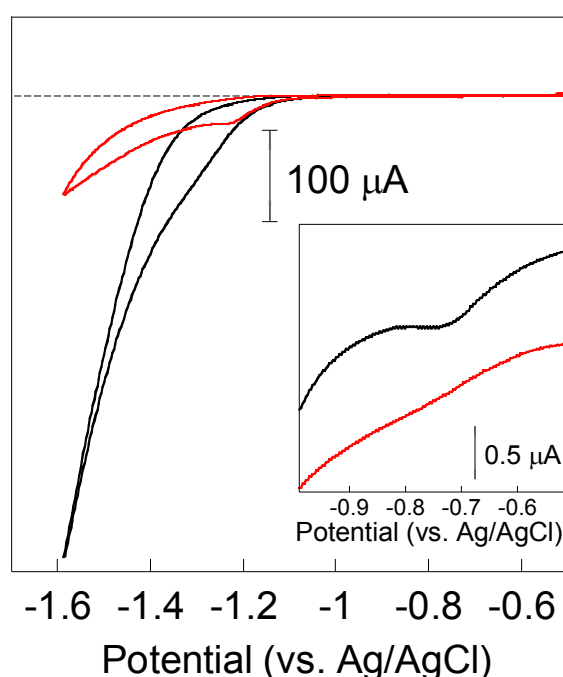


Figure 4.2.1 Cyclic voltammograms of 5 mM NiCl₂ in 2.5 M NH₄Cl water/methyl alcohol electrolyte (black line) and after the addition of 20 mM QD in the electrolyte (red line), scanned at 100 mV s⁻¹. Inset is the enlarged cyclic voltammogram at around -0.7 V.

The effect of the applied reduction potential on yield of the electrochemically reduced QD is given in Table 4.2.1. The reduction of QD or the HQD formation during electrochemical reduction was estimated by ¹H NMR on the reaction solution. The conversion of QD to HQD was almost 50% with the application of -0.9 V, and rather decreased with more negative potential application. During the electrolysis, nickel deposition on the working electrode was observed in conjunction with dissolution of nickel from the counter electrode (nickel mesh). Under the application of -0.5 V, the passed charge was consumed only for the nickel deposition, indicating that the applied potential of -0.5 V was more negative than that of

nickel reduction but more positive than that of hydrogen evolution. Most of the passed charge was consumed for hydrogen gas evolution under the application of -1.0–1.5 V. The total passed charge was used for nickel deposition and hydrogenation of QD with almost 100% efficiency upon the application of -0.9 V, suggesting that hydrogenation of QD to HQD preferentially proceeded under the application of turned potential.

Table 4.2.1 Electrochemical hydrogenation of QD by applying negative potential

| Applied potential (V vs. Ag/AgCl) | Conversion of QD to HQD ^{a)} (%) | Charge consumption for QD hydrogenation ^{b)} (%) | Weight of deposited nickel per unit electrode area (mg/cm ²) | Charge consumption for nickel deposition ^{c)} (%) |
|--------------------------------------|---|---|--|--|
| -0.5 ^{d)} | 0 | 0 | 1.7 | 98 |
| -0.9 ^{d)} | 46 | 22 | 1.2 | 73 |
| -1.0 ^{d)} | 21 | 10 | 0.2 | 11 |
| -1.5 ^{d)} | 18 | 9 | 0.1 | 4 |
| -0.9 ^{e)} | 91 | 45 | 2.4 | 49 |
| -0.9 ^{f)} | 26 | 13 | 1.4 | 83 |

a) Determined by ¹H NMR of the isolated samples

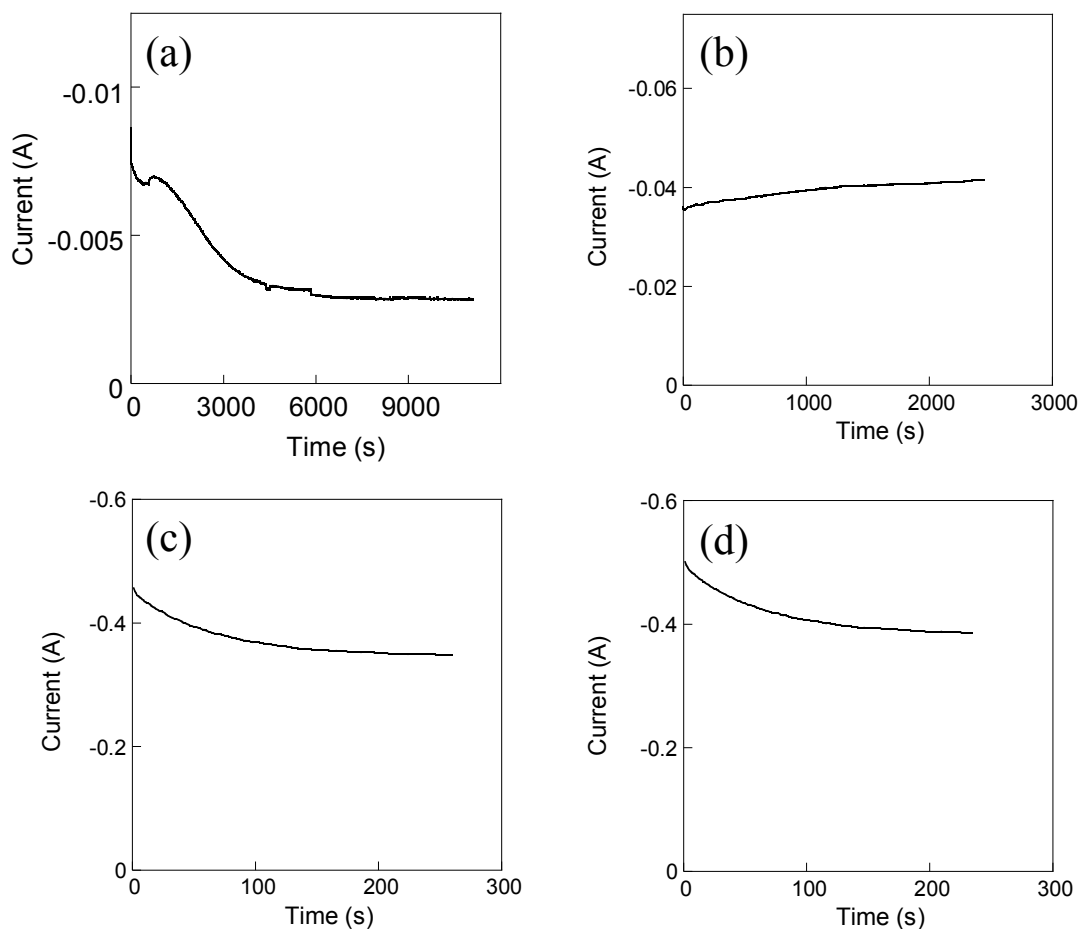
b) Ratio of the charge consumption estimated from conversion ratio of QD to the total passed charge

c) Ratio of the charge consumption estimated from weight of deposited nickel to the total passed charge

d) Electrochemical hydrogenation of 10 mM QD in 2.5 M NH₄Cl water/methyl alcohol (vol 4/1) with nickel counter electrode

e) Electrochemical hydrogenation of 30 mM QD in 2.5 M NH₄Cl water/methyl alcohol (vol 4/1) with nickel counter electrode

f) Electrochemical hydrogenation of 10 mM QD and 2 mM NiCl₂ in 2.5 M NH₄Cl water/methyl alcohol (vol 4/1) with nickel counter electrode



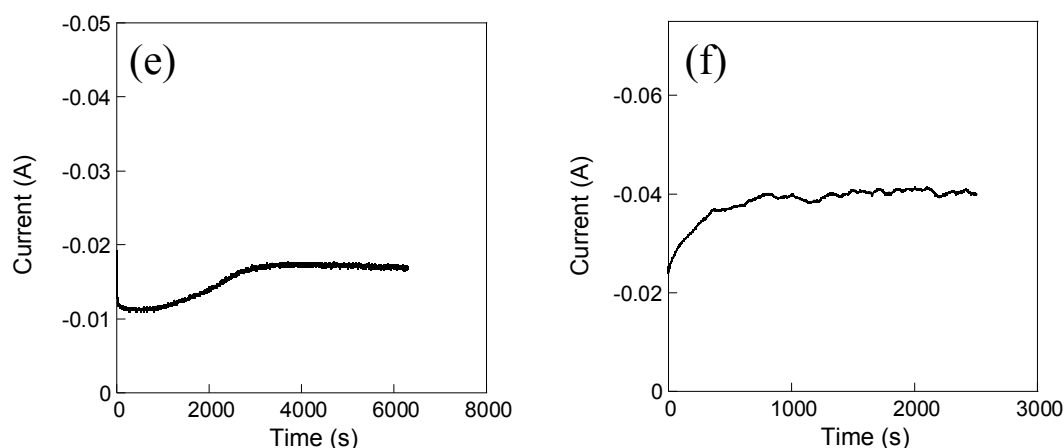


Figure 4.2.2 Chronoamperograms of Table 4.2.1 recorded under applying (a) -0.5 V to 10 mM QD, (b) -0.9 V to 10 mM QD, (d) -1.0 V to 10 mM QD, (d) -1.5 V to 10 mM QD, (e) -0.9 V to 30 mM QD, and (f) -0.9 V to 30 mM QD and 2 mM NiCl₂ in 2.5 M NH₄Cl electrolyte.

Figure 4.2.2 shows that the current density increased with applied potential. The nickel ions dissolved from the Ni mesh did not have enough time to diffuse to the working electrode in the conditions of applying -1.0 or -1.5 V. The decreasing of current applying -1.0 or -1.5 V supported the diffusion limitation of nickel ion at the early stage of electrolysis. However, electrolyte was sufficiently stirred during the electrolytic hydrogenation and few hundred seconds were probably enough time for nickel ion diffusion. Thus, we considered that nickel ions dissolved from the Ni mesh had enough time to diffuse to the working electrode and the decrease in the conversion of QD to HQD and an amount of nickel deposition in low potential, such as -1.5 V, were resulted from the predominant hydrogen evolution.

The conversion of QD to HQD was calculated from the integration ratio of ¹H NMR peaks of QD ($\delta = 7.23$, 1H, phenyl) and HQD ($\delta = 6.38$, 2H, phenyl). An example of the calculation in the case of applying -0.9 V to 10 mM QD electrolyte is shown as below. Integration ratio of QD ($\delta = 7.23$, 1H, phenyl) : HQD ($\delta = 6.38$, 2H, phenyl) was 1 : 1.7.

$$(\text{Conversion}) (\%) = \frac{\frac{1.7}{2}}{1.0 + \frac{1.7}{2}} \times 100 = 46$$

The current efficiency or charge consumption for QD hydrogenation was calculated from the conversion. An example of the calculation in the case of applying -0.9 V to 10 mM QD electrolyte is shown as below. The total passed charge was 80 C, and the amount of QD in the electrolyte was 0.1 mmol (10 mM).

$$(\text{Current efficiency})(\%) = \frac{0.0001 \times 4 \times 0.46 \times 96485}{80} \times 100 = 22$$

The current efficiency or charge consumption for nickel deposition was calculated from the deposited nickel weight. An example of the calculation in the case of applying -0.9 V to 10 mM QD electrolyte is shown as below. The surface area of the working electrode was 14.8 cm², and the molecular weight of nickel was 58.69 g mol⁻¹.

$$(\text{Current efficiency})(\%) = \frac{1.2 \times 14.8 \times 2 \times 96485}{58.69 \times 80 \times 1000} \times 100 = 73$$

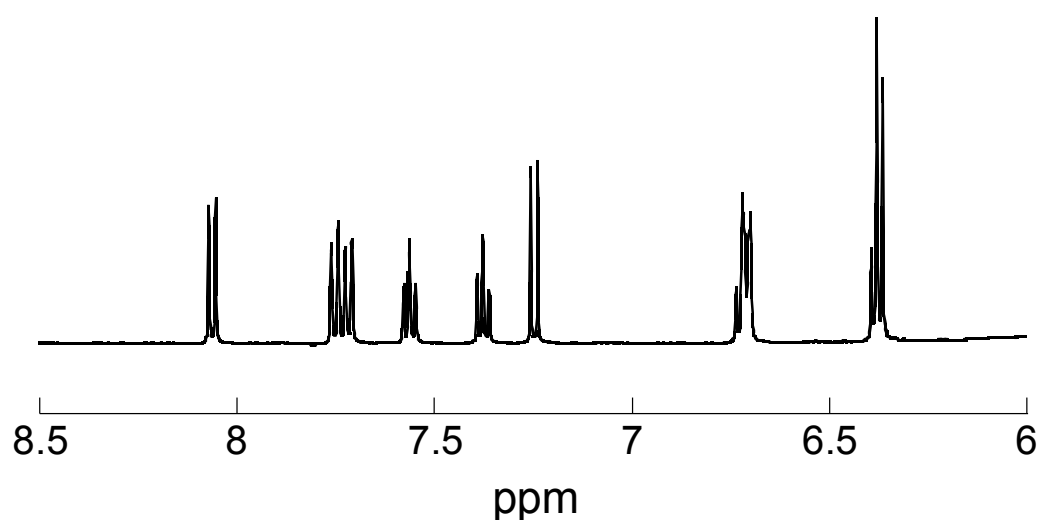


Figure 4.2.3. ¹H NMR spectra of the electrolysis products under the condition of applying -0.9 V to 10 mM QD electrolyte.

4.3 Ni-Electrodeposition-Assisted Hydrogenation of Quinaldine Polymer

A naked carbon plate was coated with the PQD layer with thickness of >500 μm which was applied as the working cathode. SEM images of the PQD layer after the electroreduction and nickel deposition are given in Figure 4.3.1. Nickel microparticles with 100–300 nm diameters were distributed throughout the PQD layer, indicating that nickel ion was interpenetrated into the swollen PQD layer and was electrochemically reduced and deposited in and upon the polymer layer.

After the nickel electrodeposition in the PQD-coated electrode, more than half of the QD unit was converted to the HQD unit, of which conversion efficiency was 5 times larger than

that of PQD solved in water/methyl alcohol electrolyte (Table 4.3.1). The improved conversion efficiency could be explained by the highly populated QD unit in the polymer layer (corresponded to 6.9 M and more than 3000 times higher than that (2 mM) of the PQD solved water/ methyl alcohol electrolyte), to enhance both the reaction rate of nickel microparticle-assisted hydrogenation of the QD unit and the reduction current efficiency upon the electrode. The poly(acrylic acid) backbone could also work as a protecting or surfactant residue on the microparticle formation of nickel to facilitate the electrodeposition and the electrochemical hydrogenation.

Finally, the conversion of QD to HQD in the polymer was enhanced up to 75% by adding NiCl_2 in the aqueous electrolyte. The increased concentration of nickel ion in the solution accelerated the nickel electrodeposition and the electrochemical hydrogenation of QD to HQD.

Table 4.3.1. Electrochemical hydrogenation of the PQD layer

| Working electrode | Aqueous solution | Conversion of QD to HQD ^{a)} (%) | Charge consumption for QD hydrogenation ^{b)} (%) | Weight of deposited nickel per unit electrode area (mg/cm ²) | Charge consumption for nickel deposition ^{c)} (%) |
|-------------------|--|--|--|---|---|
| Carbon | 2 mM PQD, 2.5 M NH_4Cl ^{d)} | 10 | 5 | 0.6 | 90 |
| PQD-coated carbon | 2.5 M NH_4Cl | 52 | 26 | 0.4 | 65 |
| PQD-coated carbon | 2 mM NiCl_2 , 2.5 M NH_4Cl | 75 | 38 | 0.4 | 55 |

a) Determined by ^1H NMR

b) Ratio of the charge consumption estimated from conversion ratio of QD to the total passed charge

c) Ratio of the charge consumption estimated from weight of deposited nickel to the total passed charge

d) The aqueous solution with methyl alcohol (vol 4/1)

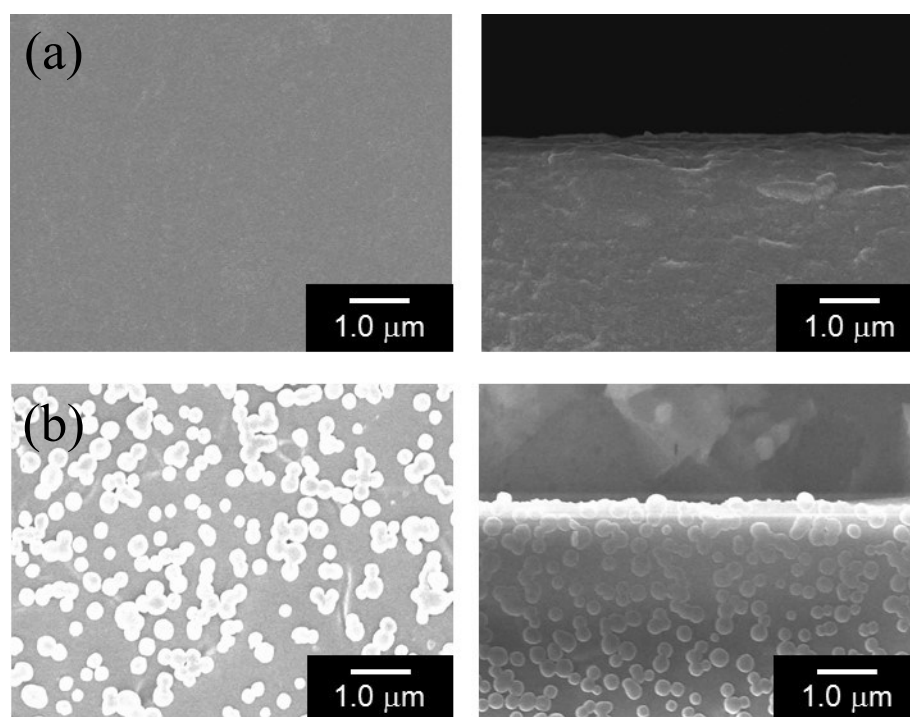


Figure 4.3.1 Surface and cross-sectional SEM images of the PQD layers (a) before and (b) after the electrodeposition of nickel in 2 mM NiCl_2 and 2.5 M NH_4Cl solution.

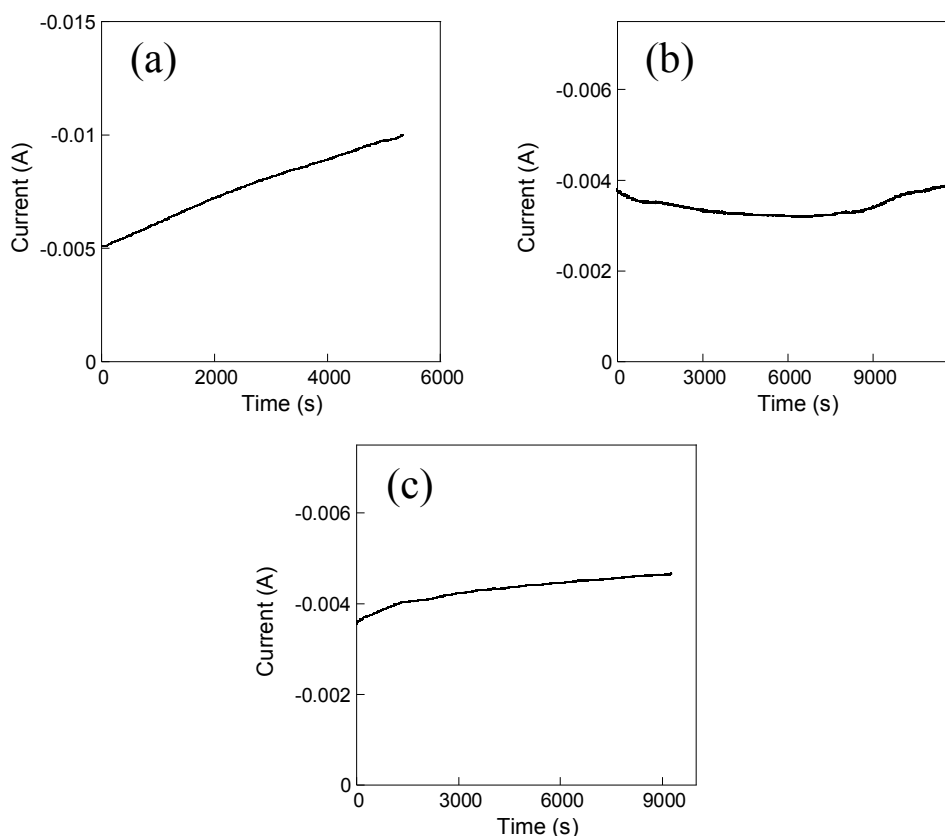


Figure 4.3.2 Chronoamperograms of Table 4.3.1 recorded by using (a) carbon working electrode in 2 mM PQD + 2.5 M NH_4Cl electrolyte, (b) PQD-coated working electrode in 2.5 M NH_4Cl , and (c) PQD-coated working electrode in 2 mM NiCl_2 + 2.5 M NH_4Cl electrolyte.

The PHQD-coated electrode, which was formed through the electrochemical hydrogenation, was soaked in the aqueous solution of the iridium catalyst and warmed at 80 °C. The rate of hydrogen evolution was almost similar to that of the neat PHQD and reached almost 100% after 5 h, indicating that almost all electrochemically hydrogenated QD units in the polymer eliminated hydrogen gas.

4.4 Hydrogen Evolution from the Hydrogenated Quinaldine Polymer

The PHQD flake (1.4 g) was soaked in 0.01 M aqueous solution (200 mL) of the iridium catalyst^{7,32} and warmed at 80 °C (Figure 4.4.1). Rapid gas evolution was ascribed to the eliminated hydrogen from the polymer and quantitatively analyzed by gas chromatography: The evolved hydrogen was amounted to be 225 ± 10 mL (at 25 °C) after 5 h and was $92 \pm 4\%$ of the formula weight-based mobile hydrogen amount. The hydrogen evolution rate from the PHQD polymer was more than 10 times larger than that from the monomeric HQD, which could be explained by the highly populated HQD unit in the polymer and by the limited solubility (1.7 mM) of HQD in the aqueous solution.

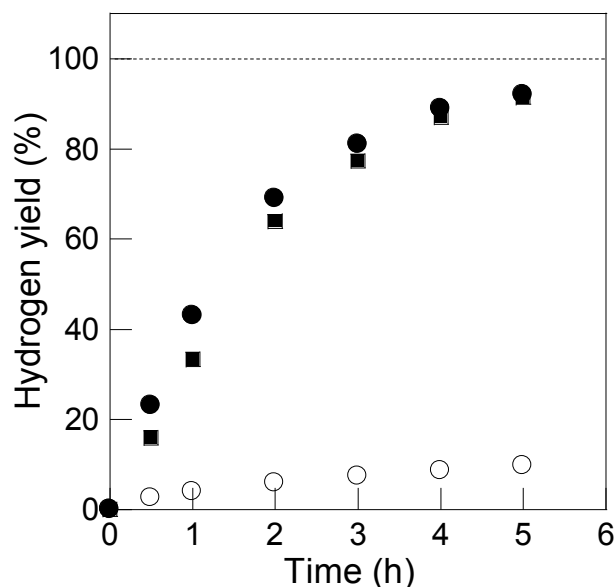


Figure 4.4.1 Time course of the hydrogen yield from HQD (○) and from the swollen PHQD polymer (●) in the aqueous solution of iridium catalyst. (■) for the hydrogen yield from the PQD layer coated on a carbon substrate after the electrochemical hydrogenation soaked in the aqueous solution.

The PHQD polymer evolved hydrogen by warming it at 80 °C in water containing the iridium complex catalyst, and its evolution rate was larger than that from the monomeric HQD. The PQD was coated on a carbon substrate as a scaffold of the nickel electrodeposition, to facilitate the electrochemical hydrogenation of the QD unit using water as a hydrogen source. The electrochemical hydrogenation efficiency of QD was enhanced by coating PQD on the substrate and the nickel ion dissolved in the aqueous electrolyte. The electrochemically hydrogenated PHQD polymer also evolved hydrogen by simply warming it with the aqueous solution. Three cycles of the hydrogen evolution from PHQD and the electrochemical hydrogenation of PQD were performed without any significant degradation. The hydrogen-releasing from the PHQD polymer proceeded under mild conditions. Direct electrolytic hydrogenation with water could be a potential process to reduce energy consumption for hydrogen-fixing. The PHQD/PQD polymer-based hydrogen-releasing and -fixing suggested a potentially new hydrogen storage system using polymers.

4.5 Experimental Section

Methods

1,2,3,4-Tetrahydroquinaldine, quinaldine, 6-aminoquinaldine and 4-(4,6-dimethoxy-1,3,5-triazin-2-yl)-4-methylmorpholinium chloride were purchased from Tokyo Chemical Industry Co. Aqua (6,6'-dihydroxy-2,2'-bipyridine)(pentamethylcyclopentadienyl)iridium(III)bis(triflate)³² was obtained from Kanto Chemical Co. Poly(acrylic acid) ($M_w = 25000$) was purchased from Wako Pure Chemical Industries.

6-Amino-2-methyl-1,2,3,4-tetrahydroquinoline (amino-HQD) was prepared as follows. Di- μ -hydridobis[chloro(pentamethylcyclopentadienyl)iridium]^{6,33} (182 mg) was added to a *p*-xylene solution (500 mL) of 6-amino-quinaldine (791 mg) and stirred under hydrogen (1 atm) for 20 h at 110 °C. After evaporation, the crude product was purified by silica gel column chromatography on Al₂O₃ with chloroform/hexane (2/1 in v/v) eluent, to give the amino-HQD as a white powder (365 mg): yield 45%. ¹H NMR (500 MHz, (CD₃)₂SO): δ 7.00 (s, 1H, ArH), 6.34 (d, 1H, ArH), 6.32 (d, 1H, ArH), 4.16 (b, 1H, NH), 3.42 (b, 2H, NH), 1.43–3.81 (m, 5H, CH), 1.12 (d, 3H, CH); MS(m/z) 161.6 [M]⁺, calcd for M = 162.2.

¹H NMR spectra were recorded on a JEOL ECX-500 spectrometer with chemical shifts downfield from tetramethylsilane as the internal standard. Mass spectra were obtained using a JMS-GCMATE II. Elemental analyses were performed using a Perkin-Elmer model PE-2400 II elemental analyzer. SEM observation was carried out using a HITACHI High-Tech S-4500S microscope.

Preparation of HQD- and QD-substituted poly(acrylic acid)

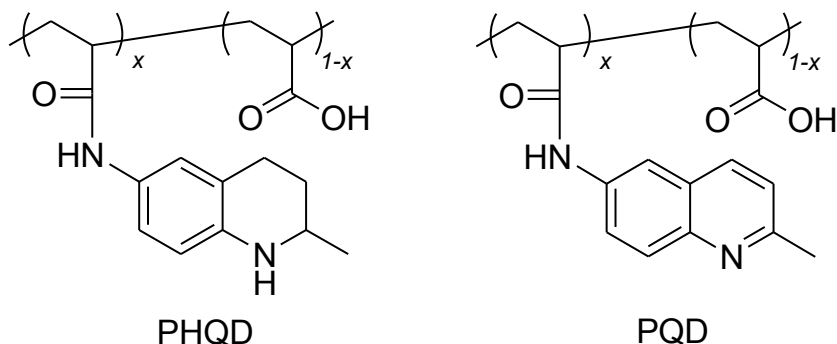
4-(4,6-Dimethoxy-1,3,5-triazin-2-yl)-4-methylmorpholinium chloride (2.76 g, 15 mmol) was added to a 200 mL DMF solution of poly(acrylic acid) (720 mg, 10 unit mmol) and amino-HQD (1.62 g, 10 mmol) or amino-QD (1.58 g, 10 mmol) and stirred for 24 h at room temperature. The mixture was poured into water. The precipitated powder was washed with water and reprecipitated twice from the DMF solution to water. The substitution degree of HQD or QD in the poly(acrylic acid) (*x* in Scheme 2) was determined with ¹H NMR spectroscopy to be 53% and 51% for PHQD and PQD, respectively. These almost coincided with 52% and 53% for PHQD and PQD estimated with the elemental analysis.

PHQD; ¹H NMR (500 MHz, (CD₃)₂SO): δ 1.01–1.39 (CH₃ (HQD)), 1.41–2.03 (CH₂ (poly(acrylic acid))), 2.70–2.36 (CH (poly (acrylic acid))), 2.56–3.42 (CH (HQD)), 5.32–5.67 (NH (HQD)), 6.31–6.88 (Ph (HQD)), 9.58–10.39 (CONH), 11.80–12.64 (COOH (poly(acrylic acid))).

PQD; ¹H NMR (500 MHz, (CD₃)₂SO): δ 1.41–2.03 (CH₂ (poly (acrylic acid))), 2.70–2.36

(CH (poly (acrylic acid))), 2.48–2.64 (CH₃ (QD)), 7.02–8.53 (Ph (QD)), 9.63–10.54 (CONH), 11.80–12.64 (COOH (poly(acrylic acid))).

The PHQD and PQD polymers were soluble in methyl alcohol, acetonitrile, and DMF, and were insoluble in but swollen with water. Methyl alcohol solutions of the polymers were spin-coated on an acrylic glass plate and immersed in water. Static contact angle was estimated with captive bubbles by using KRUSS DSA25s analyzer.



Scheme 4.5.1 HQD- and QD-substituted poly(acrylic acid).

Hydrogen evolution from PHQD and HQD

The PHQD flake (1.4 g) was soaked in the 0.01 M solution of the iridium catalyst (200 mL) and warmed at 80 °C, and the evolved gas was analyzed by using a gas chromatograph (Shimadzu GC-8AIT, Ar carrier) equipped with a 2 m long packed column of Molecular Sieve 5A and a recorder (Shimadzu C-R8A Chromatopac Data Processor). After the hydrogen evolution, the flake was washed with water and reprecipitated from DMF to water. Conversion of the HQD unit in the polymer to the QD unit was estimated with ¹H NMR spectroscopy on the isolated polymer.

The 0.01 M iridium catalyst aqueous solution (100 mL) saturated with HQD (25 mg) was warmed at 80 °C and the evolved gas was also analyzed as the control experiment.

Electrochemical measurements and electrochemical hydrogenation of QD and PQD

Cyclic voltammogram and chronoamperograms of QD in the aqueous 2.5 M NH₄Cl solution were carried out with a glassy carbon plate or disk electrode, a nickel mesh, and an Ag/AgCl electrode as the working, the counter, and the reference electrode, respectively, using an ALS700 electrochemical analyzer.

QD or PQD was dissolved in 2.5 M NH₄Cl water/methyl alcohol (vol 4/1) electrolyte and the electrolytic reduction was conducted by applying the each constant potential with a glassy carbon plate, a nickel mesh, and an Ag/AgCl electrode as the working, the counter, and the reference electrode, respectively. Twice charge amount of the theoretical one to hydrogenate

QD or the all quinaldine unit in the polymer layer was passed. After the electrochemical hydrogenation, the solution was mixed with DMSO- d_6 and measured with ^1H NMR.

The PQD-coated electrode was prepared by drop-casting the 0.2 wt% methyl alcohol solution of PQD on a glassy carbon plate. The PQD layer thickness was estimated using a KLA Tencor P-6 contact stylus profiler. The PQD-coated electrode was soaked overnight in a 2.5 M NH_4Cl aqueous solution, and then applied to the working electrode. A nickel mesh and an Ag/AgCl electrode were used as the counter and the reference electrode, respectively. The electrolytic reduction was conducted by applying the constant potential of -0.9 V. Twice charge amount of the theoretical one to hydrogenate the all quinaldine unit in the polymer layer was passed (the mass of the polymer layer on the carbon electrode was measured with a microbalance). During the electrolysis, a nickel microparticle was deposited on the polymer-coated electrode without peeling the polymer layer. After the electrochemical hydrogenation, the nickel-deposited working electrode was washed with water, dried, and soaked in DMSO- d_6 to extract the polymer.

References

1. Michael JP, *Nat Prod Rep* **2005**, *22*, 627–646.
2. Zahl IH, Samuelsen O and Kiessling A, *Fish Physiol Biochem* **2012**, *38*, 201–218.
3. Kaur K, Jain M, Reddy RP and Jain R, *Eur J Med Chem* **2010**, *45*, 3245–3264.
4. Yan Z, Xu H, Guang S, Zhao X, Fan W and Liu XY, *Adv Funct Mater* **2012**, *22*, 345–352.
5. Tomar M, Lucas NT, Kim H, Laquai F, Müllen K and Jacob J, *Polym Int* **2012**, *61*, 1381–1325.
6. Yamaguchi R, Ikeda C, Takahashi Y and Fujita K, *J Am Chem Soc* **2009**, *131*, 8410–8412.
7. Fujita K, Tanaka Y, Kobayashi M and Yamaguchi R, *J Am Chem Soc* **2014**, *136*, 4829–4832.
8. Chakraborty S, Brennessel WW and Jones WD, *J Am Chem Soc* **2014**, *136*, 8564–8567.
9. Xu R, Chakraborty S, Yuan H and Jones WD, *ACS Catal* **2015**, *5*, 6350–6354.
10. Crabtree RH, *Energy Environ Sci* **2008**, *1*, 134–138.
11. Ou L, *RSC Adv* **2015**, *5*, 57361–57371.
12. Li Z, Kelkar S, Lam CH, Luczek K, Jackson JE, Miller DJ and Saffron CM, *Electrochim Acta* **2012**, *64*, 87–93.
13. Vilar M, Oliveira JL and Navarro M, *Appl Catal A* **2010**, *372*, 1–7.
14. Pletcher D, *J Appl Electrochem* **1984**, *14*, 403–415.

15. Lain MJ and Pletcher D, *Electrochim Acta* **1987**, 32, 99–107.
16. Zhao J, Chen H, Xu J and Shen J, *J Phys Chem C* **2013**, 117, 10573–10580.
17. Lessard J, Belot G, Couture Y, Desjardins S and Roy C, *Int J Hydrogen Energy* **1993**, 18, 681–684.
18. Shigehara K, Oyama N and Anson FC, *Inorg Chem* **1981**, 20, 518–522.
19. Roncali J, *J Mater Chem* **1999**, 1875–1893.
20. Park MK, Deng S and Advincula RC, *J Am Chem Soc* **2004**, 126, 13723–13731.
21. Tsuboi A, Nakamura K and Kobayashi N, *Adv Mater* **2013**, 25, 3197–3201.
22. Oyaizu K, Ando Y, Konishi H and Nishide H, *J Am Chem Soc* **2008**, 130, 14459–14461.
23. Oyaizu K and Nishide H, *Adv Mater* **2009**, 21, 2339–2344.
24. Kato R, Kato F, Oyaizu K and Nishide H, *Chem Lett* **2014**, 43, 480–482.
25. Yu Y, Yan C and Zheng Z, *Adv Mater* **2014**, 26, 5508–5516.
26. Wang T, Zhuo J, Du K, Chen B, Zhu Z, Shao Y and Li M, *Adv Mater* **2014**, 6, 3761–3766.
27. Zhou W, Du Y, Zhang H, Xu J and Yang P, *Electrochim Acta* **2010**, 55, 2911–2917.
28. Mourato A, Wong SM, Siegenthaler H and Abrantes LM, *J Solid State Electrochem* **2006**, 10, 140–147.
29. Zouaoui A, Stephan O, Ourari A and Moutet J-C, *Electrochim Acta* **2000**, 46, 49–58.
30. Takano N, Nakade A and Takeno N, *Bull Chem Soc Jpn* **1997**, 70, 837–840.
31. Moutet J-C, Ouennoughi Y, Ourari A and Thibault SH, *Electrochim Acta* **1995**, 40, 1827–1833.
32. Kawahara R, Fujita K and Yamaguchi R, *J Am Chem Soc* **2012**, 134, 3643–3646.
33. Gill DS and Maitlis PM, *J Organomet Chem* **1975**, 87, 359–364.

Chapter 5

Electrolytic Hydrogenation of Carbonyl Compounds with Water and Dehydrogenation Using the Iridium Catalyst

Contents

- 5.1 Introduction
 - 5.2 Redox Properties of the Iridium Catalyst
 - 5.3 Hydrogen Storage Properties of the Carbonyl Compounds Using the Iridium Catalyst
 - 5.4 Experimental Section
- References

5.1 Introduction

Hydrogen fixing using nickel deposition and the application of the hydrogenation reaction to the hydrogen storage reaction was shown in chapter 4. However, coulombic efficiency was not so high using the nickel deposition system because of the charge consumption for nickel deposition. A homogeneous catalyst for the hydrogenation of polymers was required in order to apply the polymer to hydrogen storage materials and to store hydrogen at a high efficiency.

Transfer hydrogenation catalysts by metal complexes have been investigated and have attracted a lot of attention¹⁻¹¹. In particular, aqueous transfer hydrogenation catalysts have been developed due to the advantages of using water as a solvent. Water is an environmentally friendly solvent. Furthermore, the rate of hydrogenation could be improved using water, and side reactions could often be controlled or reduced by tuning the pH¹²⁻¹⁷.

Metal complexes bearing bipyridine have been studied as aqueous transfer hydrogenation complexes^{18,19}, and Fukuzumi's group has reported that an iridium complex bearing bipyridine ligand worked successfully as the catalyst for the hydrogenation of carbonyl compound²⁰. However, most of the system used sacrificial reductants such as formic acid, and the hydrogen of the sacrificial reductant was consumed as hydrogen source.

In this chapter, we focused on using the iridium complex bearing bipyridinediol as reported by Fujita's group as the catalyst for the ligand-promoted dehydrogenation of alcohols²¹⁻²⁵. We found that the iridium complex electrochemically reduced and hydrogenated carbonyl compounds using water as a hydrogen source. The iridium catalyst was applied to the redox catalyst for the electrolytic hydrogenation of the carbonyl polymer and also to the catalyst for the hydrogen evolution of the alcohol polymer.

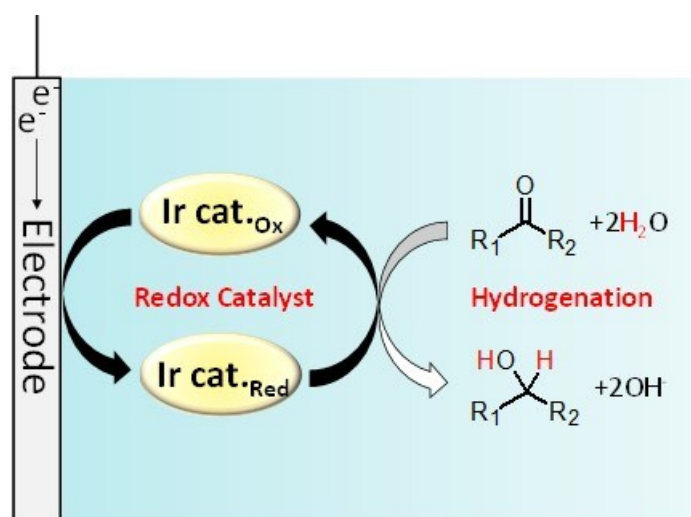


Figure 5.1.1 Schematic image of the electrolytic hydrogenation of carbonyl compound with the iridium redox catalyst.

5.2 Redox Properties of the Iridium Catalyst

First, the redox properties of Aqua (6,6'-dihydroxy-2,2'-bipyridine)(pentamethylcyclopentadienyl)iridium(III)bis(triflate)³ in water were investigated. A cyclic voltammogram of the iridium complex in 0.1 M Na₂SO₄ water/methanol (vol 4/1) gave one reduction peak at -1.2 V (vs. Ag/AgCl) and one oxidation peak at 0.2 V (Figure 5.2.2 (a)).

The results of the bulk electrolysis of the iridium complex in 0.1 M Na₂SO₄ water suggested that the iridium complex was reduced to two-electron by applying -1.2 V (Figure 5.2.2 (b)).

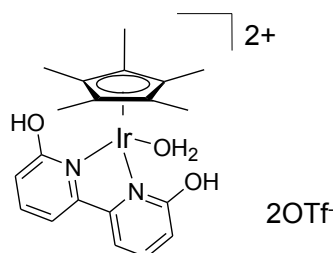


Figure 5.2.1 Structure of Aqua (6,6'-dihydroxy-2,2'-bipyridine)(pentamethylcyclopentadienyl) iridium(III)bis(triflate).

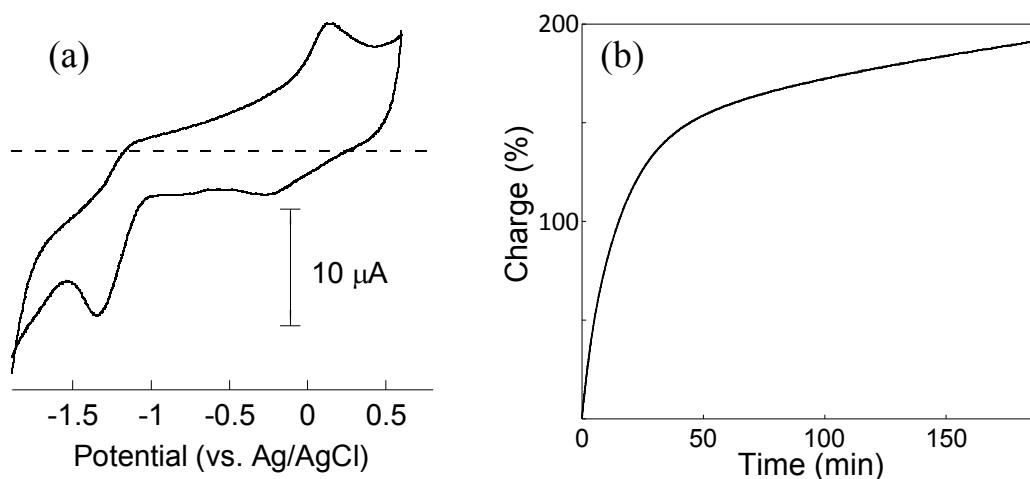


Figure 5.2.2 (a) The cyclic voltammogram of 10 mM iridium complex scanned at 100 mV s⁻¹ in 0.1 M Na₂SO₄ water/methanol (vol 4/1). (b) Bulk electrolysis with chronocoulometry of 0.5 M iridium complex in 0.1 M Na₂SO₄ water.

The electrolysis product was identified by ¹H NMR (Figure 5.2.3). The proton peaks of the bipyridine were shifted to the high magnetic field and proton peak of water as the ligand was depleted, suggesting an exchange or disengagement of the water ligand.

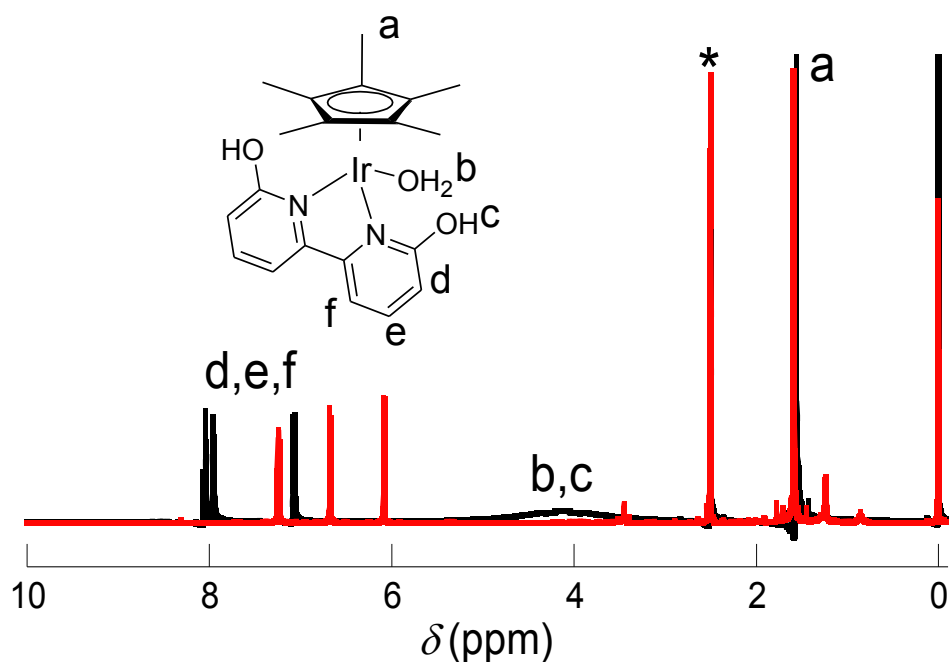


Figure 5.2.3 ^1H NMR spectra of the iridium complex (black) and the iridium complex after bulk electrolysis (red). The bulk electrolysis was carried out by applying the potential of -1.2 V (vs. Ag/AgCl) in a solution of 1 mM iridium complex in 0.1 M Na_2SO_4 water.

X-ray crystallographic structures of the iridium complex and the iridium complex reductant after electrolysis by applying -1.2 V demonstrated that the water ligand was exchanged to a hydrogen (proton or hydride) ligand with only one counter anion pairing with the iridium complex.

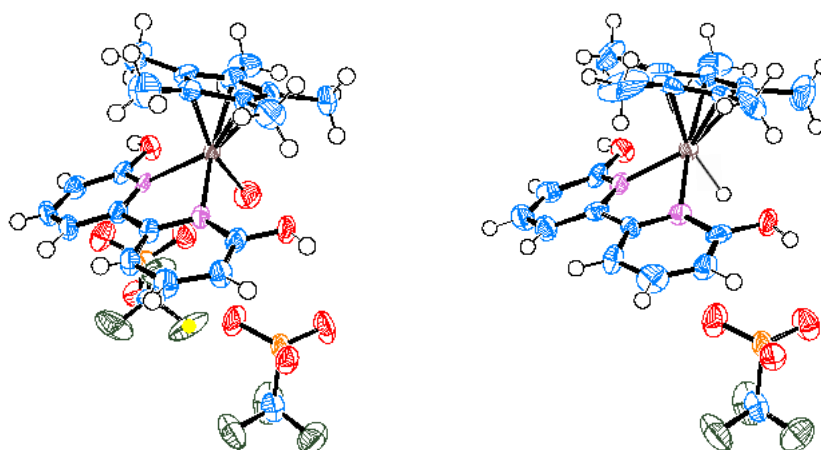


Figure 5.2.4 ORTEP view of the initial iridium complex (left) and the iridium complex after the bulk electrolysis (right).

5.3 Hydrogen Storage Properties of the Carbonyl Compounds Using the Iridium Catalyst

5.3.1 Electrochemical properties of the iridium complex with carbonyl compounds

As described in the previous section, cyclic voltammogram of the iridium complex in 0.1 M Na₂SO₄ water/methanol (vol 4/1) gave one reduction peak at -1.2 V (vs. Ag/AgCl). However, cyclic voltammogram gave two reduction peaks at -1.2 and -1.5 V (vs. Ag/AgCl) after adding acetophenone (100 mM) in the electrolyte. The reduction peak current at -1.2 V increased by adding acetophenone (Figure 5.3.1), suggesting that some another reaction proceeded by applying -1.2 V.

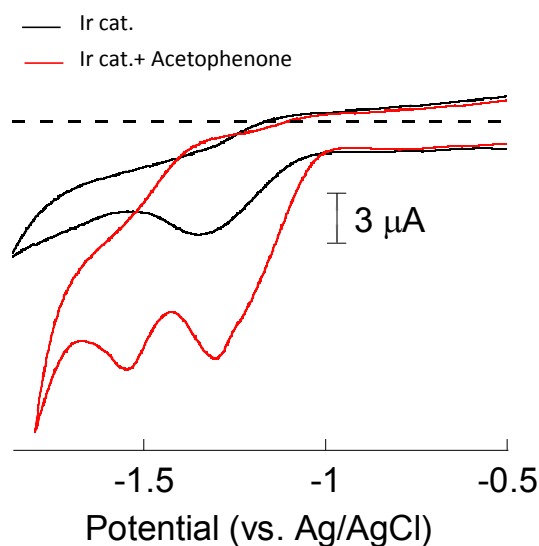


Figure 5.3.1 The cyclic voltammogram of 10 mM iridium complex scanned at 100 mV s⁻¹ in 0.1 M Na₂SO₄ water/methanol (vol 4/1).

Furthermore it was revealed that 1-phenylethyl alcohol, which was a hydrogen adduct of acetophenone, was produced after the bulk electrolysis by applying a potential more negative than the reduction potential of the acetophenone. The same reduction of acetophenone was carried out using the D₂O electrolyte, to almost quantitatively yield two-deuterated 1-phenylethyl alcohol (Figure 5.3.2).

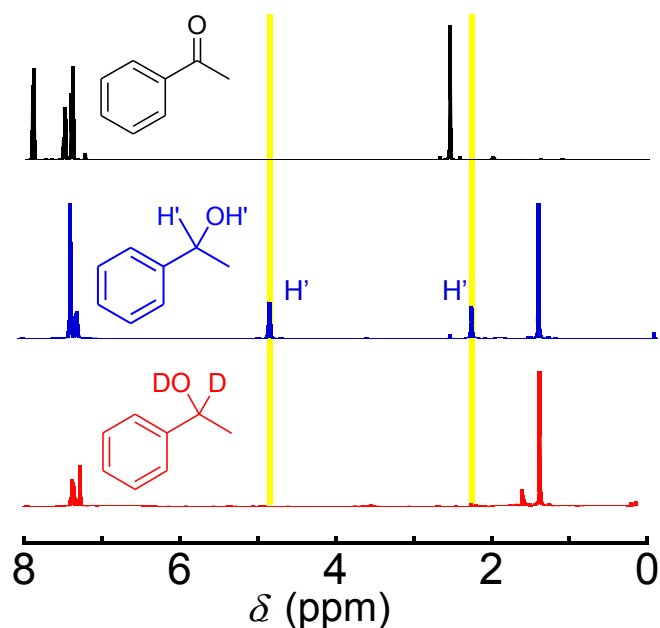


Figure 5.3.2 ^1H NMR spectra of acetophenone (black), 1-phenylethyl alcohol (blue), and the acetophenone after deuteration (red). Bulk electrolysis was carried out by applying potential of -1.2 V (vs. Ag/AgCl) in 0.1 M Na_2SO_4 water.

UV-vis spectra of the iridium complex after electrolytic reduction by applying -1.1 V (vs. Ag/AgCl) and after adding acetophenone are shown in Figure 5.3.3. Adsorption increased at 380 nm and decreased at 340 nm over time during the electrolytic reduction. After the absorption the wavelength became a steady state, and acetophenone was added in the electrolyte. The adsorption decreasing at 380 nm and increasing at 340 nm over time, indicated that the iridium complex reductant returned to the original iridium complex by a redox reaction with acetophenone. The result suggested that the iridium complex had the possibility of acting as a redox catalyst for the electrolytic hydrogenation of carbonyl compounds.

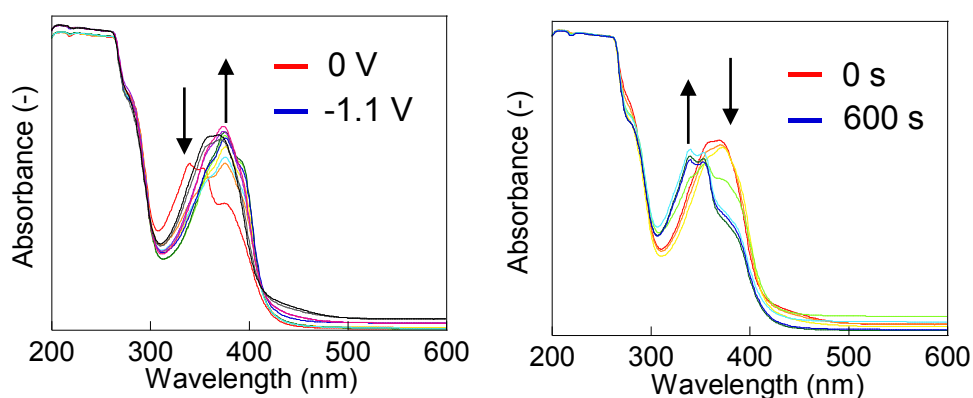
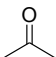
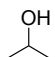
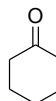
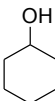
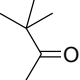
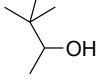
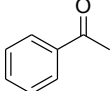
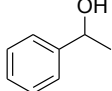
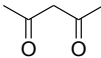
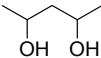
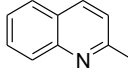
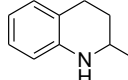


Figure 5.3.3 Electrolytic UV-vis spectra of the iridium complex after application at -1.1 V (left) and the addition of acetophenone (right) in 0.1 M Na_2SO_4 water/methanol electrolyte.

In order to search for a suitable structure to be used as for hydrogen storage by electrolytic hydrogenation, secondary alcohols or heterocyclic compounds were added to the electrolyte containing the iridium complex and -1.2 V were applied. Some samples were heated at 80 °C after electrolysis to evolve into hydrogen. The results of hydrogenation coulombic efficiency and dehydrogenation conversion efficiency are shown in Table 5.3.1.

Table 5.3.1 Electrolytic hydrogenation and hydrogen evolution of each substrate

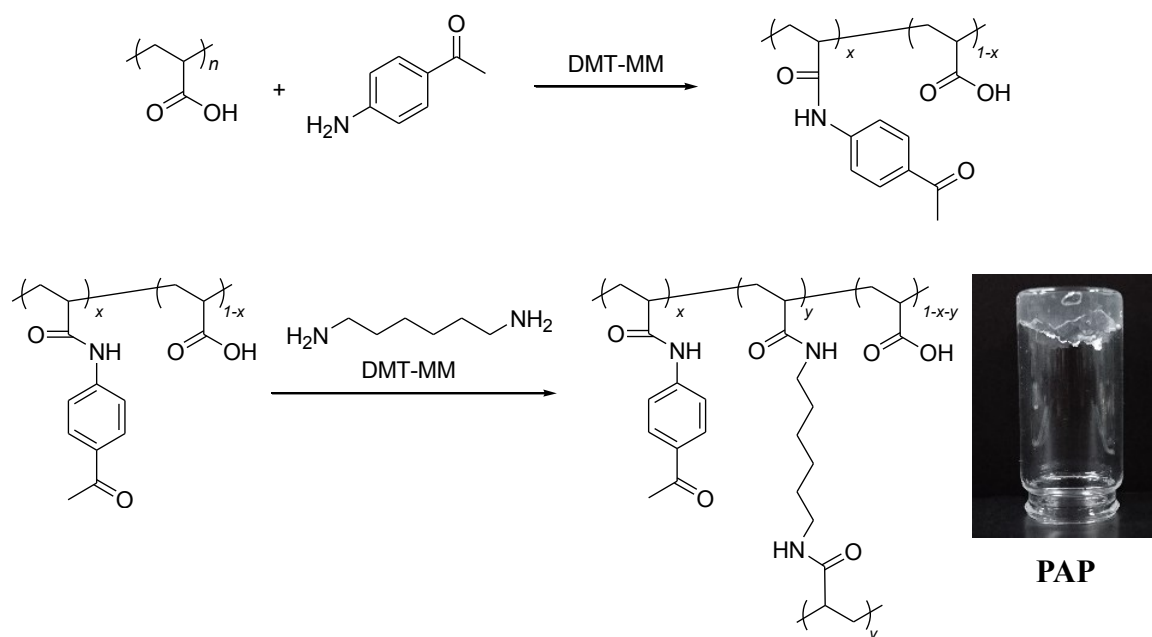
| Substrate | Product | Hydrogen density (wt%) | Hydrogenation coulombic efficiency (%) | Dehydrogenation conversion efficiency (%) |
|---|---|------------------------|--|---|
|  |  | 3.3 | >80 | >80 |
|  |  | 2 | >80 | >90 |
|  |  | 1.9 | >80 | >90 |
|  |  | 1.6 | >80 | >90 |
|  |  | 3.8 | <5 | - |
|  |  | 2.7 | <5 | - |

The iridium complex was precipitated by adding acetylacetone or quinaldine, indicating that these substrates acted as a ligand, to change the solubility of the complex and low conversion. The secondary alcohols were hydrogenated and dehydrogenated at a high efficiency with the iridium complex. The maximum hydrogen weight density (3.3 wt%) was achieved using acetone-propanol as a substrate.

5.3.2 Hydrogen storage properties of the crosslinked acetophenone polymer

Poly(acrylic acid) was selected as the hydrophilic main chain for introducing the acetophenone unit, to conduct dehydrogenation in aqueous solutions. 6-Amino-acetophenone was reacted with poly(acrylic acid) with a (unit) molar feed ratio of 1/1 in the presence of 4-(4,6-dimethoxy-1,3,5-triazin-2-yl)-4-methylmorpholinium chloride (DMT-MM) as a condensation reagent. The substitution degree of the acetophenone unit in the polymers was $x = 0.7$. Then, 1,6-diaminohexane (2 wt%) was reacted with the acetophenone-substituted

poly(acrylic acid) in the presence of DMT-MM, to prepare the crosslinked acetophenone polymer (PAP). The PAP uptook water with 75 wt% to be the gels.



The synthesized PAP was soaked in a 0.1 M Na_2SO_4 phosphate buffer electrolyte (pH = 7) containing the iridium complex (5 mol%), and bulk electrolysis was performed by applying -1.2 V (vs. Ag/AgCl). Four times the charge amount of the theoretical one to all acetophenone units in the polymer was passed.

The adsorption of infrared at 1750 cm^{-1} ascribed to $\nu_{\text{C=O}}$ disappeared after the electrolysis, which indicated the hydrogenation of the carboxyl group of the acetophenone units in the polymer. The electrolytic hydrogenation was also supported by a ^{13}C cross-polarization magic angle spinning–nuclear magnetic resonance (CP/MAS NMR) spectroscopy. The carbon peak of the carboxyl group disappeared and an alcohol group appeared after the electrolysis (Figure 5.3.4).

The electrolyte containing the iridium complex and the PAP after the electrolysis was heated at $100\text{ }^\circ\text{C}$ for 4 h, and the evolved gas was determined by gas chromatography analysis (GC). The result of the GC indicated a pure hydrogen gas evolved from the PAP, which amounted to >90% of the formula weight-based mobile hydrogen amount after 4 h (Figure 5.3.5). The quantitative and high efficient electrolytic hydrogenation of the polymer without a conductive additive was achieved using the iridium complex as a redox catalyst. Furthermore, the same iridium complex acted as both a hydrogenation and dehydrogenation catalyst of the polymer. The solvent doesn't need to be changed in order to store or release hydrogen.

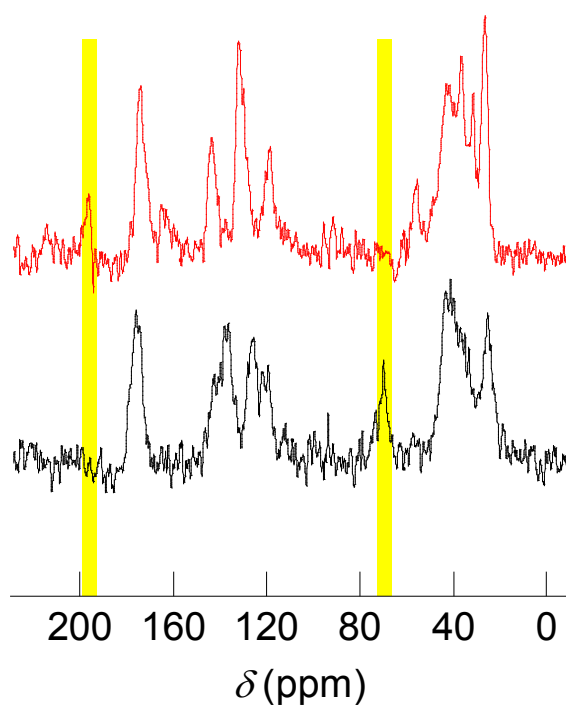


Figure 5.3.4 Solid-state ^{13}C NMR spectra of the PAP (red) and the PAP after the electrolysis (black).

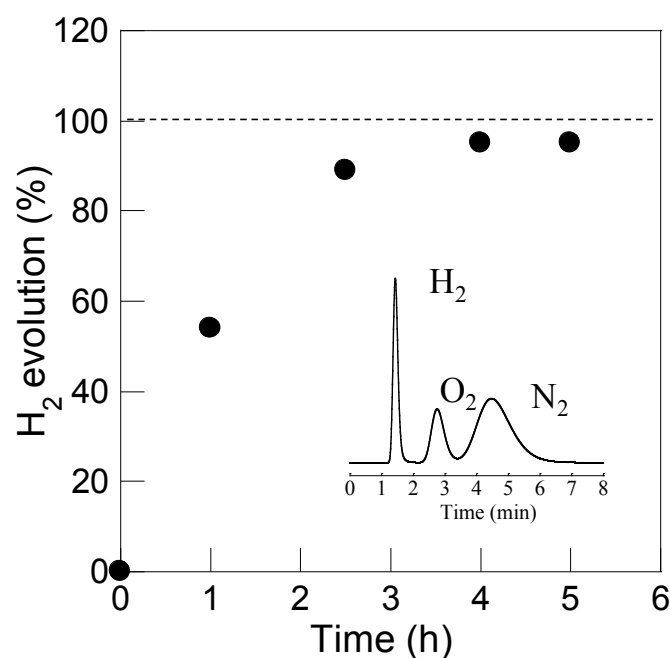


Figure 5.3.5 Time shift conversion of the dehydrogenation from the PAP. Inset: Gas chromatograph for evolved gas from the PAP.

5.4 Experimental Section

Methods

4'-Aminoacetophenone, acetophenone, acetone, 2-propanol, cyclohexanone, 2,4-pentanediol, 3,3-dimethyl-2-butanol, pinacolin and 4-(4,6-dimethoxy-1,3,5-triazin-2-yl)-4-methylmorpholinium chloride were purchased from Tokyo Chemical Industry Co. Aqua (6,6'-dihydroxy-2,2'-bipyridine)(pentamethylcyclopentadienyl)iridium(III)bis(triflate) was obtained from Kanto Chemical Co. Poly(acrylic acid) ($M_w = 25000$) was purchased from Wako Pure Chemical Industries.

^1H NMR spectra were recorded on a JEOL ECX-500 spectrometer with chemical shifts downfield from tetramethylsilane as the internal standard. Mass spectra were obtained using a JMS-GCMATE II. Elemental analyses were performed using a Perkin-Elmer model PE-2400 II elemental analyzer.

Preparation of crosslinked acetophenone alcohol-substituted poly(acrylic acid) (PAP)

4-(4,6-Dimethoxy-1,3,5-triazin-2-yl)-4-methylmorpholinium chloride (2.07 g, 7.5 mmol) was added to a 100 mL DMF solution of poly(acrylic acid) (360 mg, 5 unit mmol) and 4'-aminoacetophenone (676 mg, 5 mmol) and stirred for 24 h at room temperature. The mixture was poured into water. The precipitated powder was washed with water and reprecipitated twice from the DMF solution to water. The substitution degree of acetophenone in the poly(acrylic acid) was determined with ^1H NMR spectroscopy to be 70%.

^1H NMR (500 MHz, $(\text{CD}_3)_2\text{SO}$): δ 1.0–2.0 (CH_2 (poly(acrylic acid))), 2.0–2.3 (CH (poly(acrylic acid))), 2.4–2.5 (CH_3 (AP)), 7.5–78.0 (Ph (AP)), 9.8–10.4 (CONH), 11.7–12.6 (COOH (poly(acrylic acid))).

4-(4,6-Dimethoxy-1,3,5-triazin-2-yl)-4-methylmorpholinium chloride (276 mg, 1 mmol) was added to a 2 mL DMF solution of the yielded polymer (50 mg, 0.413 unit mmol) and 1,6-diaminohexane (8.60 μmol) and stirred for 24 h at room temperature. The mixture was poured into water. The precipitated powder was washed with water.

Crystal data and structure refinement for the iridium complex in Figure 5.2.4 (left)

| | |
|-------------------------|---|
| Empirical Formula | $C_{22}H_{22}F_6IrN_2O_9S_2$ |
| Formula Weight | 828.75 |
| Crystal Color, Habit | yellow, needle |
| Crystal Dimensions | 0.800 X 0.200 X 0.200 mm |
| Crystal System | triclinic |
| Lattice Type | Primitive |
| Lattice Parameters | $a = 9.2217(3) \text{ \AA}$ $b = 11.2664(4) \text{ \AA}$ $c = 15.3298(5) \text{ \AA}$ $\alpha = 83.9120(10)^\circ$ $\beta = 75.0880(9)^\circ$ $\gamma = 74.7600(10)^\circ$ $V = 1483.67(9) \text{ \AA}^3$ |
| Space Group | P-1 (#2) |
| Z value | 2 |
| D_{calc} | 1.855 g/cm^3 |
| F_{000} | 806.00 |
| $\mu(\text{MoK}\alpha)$ | 47.400 cm^{-1} |

| | |
|---|--|
| Diffractometer | R-AXIS RAPID |
| Radiation | MoK α ($\lambda = 0.71075 \text{ \AA}$) graphite monochromated |
| Voltage, Current | 50kV, 40mA |
| Temperature | -150.0°C |
| Detector Aperture | 460.0 x 256.0 mm |
| Data Images | 44 exposures |
| ω oscillation Range ($\chi=45.0$, $\phi=0.0$) | 130.0 - 190.0° |
| Exposure Rate | 40.0 sec./° |
| ω oscillation Range ($\chi=45.0$, $\phi=180.0$) | 0.0 - 160.0° |
| Exposure Rate | 40.0 sec./° |
| Detector Position | 127.40 mm |
| Pixel Size | 0.100 mm |
| $2\theta_{\max}$ | 54.9° |
| No. of Reflections Measured | Total: 14582 Unique: 6715 ($R_{\text{int}} = 0.0631$) |
| Corrections | Lorentz-polarization Absorption (trans. factors: 0.099 - 0.388) |

| | |
|---------------------------------------|---|
| Structure Solution | Direct Methods (SIR92) |
| Refinement | Full-matrix least-squares on F ² |
| Function Minimized | $\sum w (F_o^2 - F_c^2)^2$ |
| Least Squares Weights | $w = 1 / [\sigma^2(F_o^2) + (0.0664 \cdot P)^2 + 21.0455 \cdot P]$ where $P = (\text{Max}(F_o^2, 0) + 2F_c^2)/3$ |
| $2\theta_{\text{max}}$ cutoff | 54.9° |
| Anomalous Dispersion | All non-hydrogen atoms |
| No. Observations (All reflections) | 6715 |
| No. Variables | 399 |
| Reflection/Parameter Ratio | 16.83 |
| Residuals: R1 ($I > 2.00\sigma(I)$) | 0.0625 |
| Residuals: R (All reflections) | 0.0654 |
| Residuals: wR2 (All reflections) | 0.1621 |
| Goodness of Fit Indicator | 1.115 |
| Max Shift/Error in Final Cycle | 0.002 |
| Maximum peak in Final Diff. Map | 10.35 e ⁻ /Å ³ |
| Minimum peak in Final Diff. Map | -2.88 e ⁻ /Å ³ |

Crystal data and structure refinement for the iridium complex after the bulk electrolysis in Figure 5.2.4 (right)

| | |
|-------------------------|---|
| Empirical Formula | $C_{26}H_{25}F_6IrN_2O_9S_2$ |
| Formula Weight | 879.82 |
| Crystal Color, Habit | yellow, platelet |
| Crystal Dimensions | 0.200 X 0.100 X 0.100 mm |
| Crystal System | triclinic |
| Lattice Type | Primitive |
| Lattice Parameters | $a = 9.2399(4) \text{ \AA}$ $b = 11.3226(6) \text{ \AA}$ $c = 15.3632(6) \text{ \AA}$ $\alpha = 83.9385(15)^\circ$ $\beta = 75.0323(14)^\circ$ $\gamma = 74.7713(16)^\circ$ $V = 1496.99(12) \text{ \AA}^3$ |
| Space Group | P-1 (#2) |
| Z value | 2 |
| D_{calc} | 1.952 g/cm^3 |
| F_{000} | 860.00 |
| $\mu(\text{MoK}\alpha)$ | 47.042 cm^{-1} |

| | |
|---------------------------------------|--|
| Structure Solution | Direct Methods (SIR2008) |
| Refinement | Full-matrix least-squares on F ² |
| Function Minimized | $\sum w (F_o^2 - F_c^2)^2$ |
| Least Squares Weights | $w = 1 / [\sigma^2(F_o^2) + (0.0441 \cdot P)^2 + 0.0000 \cdot P]$ where $P = (\text{Max}(F_o^2, 0) + 2F_c^2)/3$ |
| $2\theta_{\text{max}}$ cutoff | 54.9° |
| Anomalous Dispersion | All non-hydrogen atoms |
| No. Observations (All reflections) | 6741 |
| No. Variables | 370 |
| Reflection/Parameter Ratio | 18.22 |
| Residuals: R1 ($I > 2.00\sigma(I)$) | 0.0701 |
| Residuals: R (All reflections) | 0.0847 |
| Residuals: wR2 (All reflections) | 0.2040 |
| Goodness of Fit Indicator | 2.158 |
| Max Shift/Error in Final Cycle | 0.000 |
| Maximum peak in Final Diff. Map | 10.83 e ⁻ /Å ³ |
| Minimum peak in Final Diff. Map | -1.84 e ⁻ /Å ³ |

| | |
|---|--|
| Diffractometer | R-AXIS RAPID |
| Radiation | MoK α ($\lambda = 0.71075 \text{ \AA}$) graphite monochromated |
| Voltage, Current | 50kV, 40mA |
| Temperature | -100.0°C |
| Detector Aperture | 460.0 x 256.0 mm |
| Data Images | 44 exposures |
| ω oscillation Range ($\chi=45.0$, $\phi=0.0$) | 130.0 - 190.0° |
| Exposure Rate | 500.0 sec./° |
| ω oscillation Range ($\chi=45.0$, $\phi=180.0$) | 0.0 - 160.0° |
| Exposure Rate | 500.0 sec./° |
| Detector Position | 127.40 mm |
| Pixel Size | 0.100 mm |
| $2\theta_{\max}$ | 54.9° |
| No. of Reflections Measured | Total: 14729 Unique: 6741 ($R_{\text{int}} = 0.0608$) |
| Corrections | Lorentz-polarization Absorption (trans. factors: 0.247 - 0.625) |

Hydrogen evolution from PAP

The PAP was soaked in the 0.01 M solution of the iridium catalyst (200 mL) and warmed at 80 °C, and the evolved gas was analyzed by using a gas chromatograph (Shimadzu GC-8AIT, Ar carrier) equipped with a 2 m long packed column of Molecular Sieve 5A and a recorder (Shimadzu C-R8A Chromatopac Data Processor). After the hydrogen evolution, the flake was washed with water and reprecipitated from DMF to water. Conversion of the PE unit in the polymer to the AP unit was estimated with ¹H NMR spectroscopy on the isolated polymer. The 0.01 M iridium catalyst aqueous solution (100 mL) saturated with PE was warmed at 80 °C and the evolved gas was also analyzed as the control experiment.

Electrochemical measurements and electrochemical hydrogenation of the carbonyl compounds

Cyclic voltammogram and chronoamperograms of the carbonyl compounds in the aqueous electrolyte were carried out with a glassy carbon plate, a Pt coil, and an Ag/AgCl electrode as the working, counter, and reference electrodes, respectively, using an ALS700 electrochemical analyzer.

Each carbonyl compound was dissolved in water electrolytes and electrolytic reduction was conducted by applying each constant potential with a glassy carbon plate, a Pt coil, and an Ag/AgCl electrode as the working, counter, and reference electrodes, respectively. The same charge amount as in the theoretical one to hydrogenate the carbonyl compound was passed. After electrochemical hydrogenation, the solution was mixed with DMSO-*d*₆ and measured with ¹H NMR.

References

- 1 R. H. Morris, *Chem. Soc. Rev.* **2009**, *38*, 2282.
- 2 P. E. Sues, K. Z. Demmans, R. H. Morris, *Dalton Trans.* **2014**, *43*, 7650.
- 3 R. Malacea, R. Poli, E. Manoury, *Coord. Chem. Rev.* **2010**, *254*, 729.
- 4 A. Mikhailine, A. J. Lough, R. H. Morris, *J. Am. Chem. Soc.* **2009**, *131*, 1394.
- 5 R. P. Linstead, E. A. Braude, P. W. D. Mitchell, K. R. H. Wooldridge, L. M. Jackman, *Nature*, **1952**, *169*, 100.
- 6 E. A. Braude, R. P. Linstead, P. W. D. Mitchell, K. R. H. Wooldridge, *J. Chem. Soc.* **1954**, 3595.
- 7 G. Brieger, T. J. Nestruck, *Chem. Rev.* **1974**, *74*, 567.
- 8 R. A. W. Johnstone, A. H. Wilby, *Chem. Rev.* **1985**, *85*, 129.
- 9 R. Noyori, S. Hashiguchi, *Acc. Chem. Res.* **1997**, *30*, 97.

- 10 S. E. Clapham, A. Hadzovic, R. H. Morris, *Coord. Chem. Rev.* **2004**, *248*, 2201.
- 11 T. Ikariya, A. J. Blacker, *Acc. Chem. Res.* **2007**, *40*, 1300.
- 12 P. E. Sues, K. Z. Demmans, R. H. Morris, *Dalton Trans.* **2014**, *43*, 7650.
- 13 U. M. Lindstöm, *Chem. Rev.* **2002**, *102*, 2751.
- 14 R. N. Butler, A. G. Coyne, *Chem. Rev.* **2010**, *110*, 6302.
- 15 S. Ribe, P. Wipf, *Chem. Commun.* **2001**, 299.
- 16 D. C. Rideout, R. Breslow, *J. Am. Chem. Soc.* **1980**, *102*, 7816.
- 17 S. Narayan, J. Muldoon, M. G. Finn, V. V. Fokin, H. C. Kolb, K. B. Sharpless, *Angew. Chem., Int. Ed.* **2005**, *44*, 3275.
- 18 Y. Himeda, N. Komatsuzaki, S. Miyazawa, H. Sugihara, T. Hirose, K. Kasuga, *Chem.-Eur. J.* **2008**, *14*, 11076.
- 19 S. Ogo, T. Abura, Y. Watanabe, *Organometallics* **2002**, *21*, 2964.
- 20 T. Abura, S. Ogo, Y. Watanabe, S. Fukuzumi, *J. Am. Chem. Soc.* **2003**, *125*, 4149.
- 21 K. Fujita, T. Yoshida, Y. Imori, R. Yamaguchi, *Org. Lett.* **2011**, *13*, 2278.
- 22 K. Fujita, N. Tanino, R. Yamaguchi, *Org. Lett.* **2007**, *9*, 109.
- 23 R. Kawahara, K. Fujita, R. Yamaguchi, *J. Am. Chem. Soc.* **2012**, *134*, 3643.
- 24 R. Yamaguchi, C. Ikeda, Y. Takahashi, K. Fujita, *J. Am. Chem. Soc.* **2009**, *131*, 8410.
- 25 K. Fujita, Y. Tanaka, M. Kobayashi, R. Yamaguchi, *J. Am. Chem. Soc.* **2014**, *136*, 4829.

Chapter 6

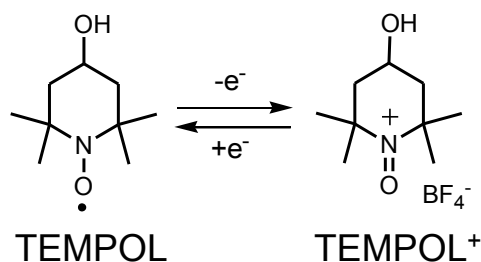
Fixing of Redox-Active Hydroxy-TEMPO Radical for a Dye-Sensitized Solar Cell

Contents

- 6.1 Introduction
 - 6.2 Redox Performance of the Fixed Hydroxy-TEMPO Radical in the Nafion Layer
 - 6.3 Aqueous Dye-Sensitized Solar Cell Performance using Nafion-Coated Electrode
 - 6.4 Experimental Section
- References

6.1 Introduction

Nitroxide radical molecules, such as TEMPO (2,2,6,6-tetramethylpiperidinoxy), have attracted much attention as an organic-based redox-active material based on their rapid and reversible one-electron transfer capability to form the corresponding oxoammonium cations.¹ 4-Hydroxy-2,2,6,6-tetramethylpiperidinoxy (TEMPOL) is one of the hydrophilic TEMPO derivatives and is often utilized in the spin-labeling and spin-trapping of biomolecules²; TEMPOL also possesses its reversible redox ability in aqueous solutions (Scheme 6.1.1). We have recently developed the TEMPO radical and its polymer extensions as a charge-transporting and -storage material in a rechargeable battery.³ We also reported an aqueous electrolyte-based organic battery using hydrophilic amide- and ether-substituted TEMPO radical polymers,⁴ which was characterized with ultrafast charging and discharging due to the high equivalent electrical conductivity of the aqueous electrolytes.



Scheme 6.1.1. Redox reaction of the TEMPOL.

Dye-sensitized solar cells (DSSCs) are being extensively studied as a photo-electrochemical device with still improving conversion efficiency.⁵ In DSSCs, a dye molecule is regenerated by a redox mediator in the electrolyte solution, the most widely-used one being the I_2/I_3^- redox couple in acetonitrile, which itself is regenerated on the counter electrode by electrons passed through an external loading. The redox mediator acts as the electron-transporting shuttle through its diffusion including its self-electron exchange reaction. Facilitation of the regeneration reaction of the mediator on the counter electrode is one of the unsolved issues to improve the DSSC efficiency. Coating of the counter with conductive polymers or carbon-polymer composites have been examined for the DSSC using iodide redox mediator.⁶ On the other hand, we have recently applied the acetonitrile solution of nitroxide radical derivatives as an organic-based redox mediator to DSSC: The DSSC cell fabricated with the mediator of a highly reactive nitroxide radical, azaadamantanoxy, yielded an 8.6% photovoltaic conversion which was ascribed to a low cell resistance due to the fast regeneration reaction of the mediator or the nitroxide radical cation on the counter electrode.⁷ One of the other unsolved issues to improve the DSSC is to replace acetonitrile with water as

the redox mediator solvent.⁸ High electrical conductivity of aqueous electrolyte solutions could contribute to the reduction of the DSSC cell resistance. The low volatility in comparison with that of acetonitrile and environmentally-benign characteristics are inherent advantages for an aqueous electrolyte-based cell.

It has been well-known that polymer electrolytes immobilize redox-active ionic species, such as $\text{Ru}(\text{bpy})_3^{3+}$ (bpy = 2,2'-bipyridine) and $\text{Fe}(\text{CN})_6^{3-}$, in their coating layers upon a current collector through the electrostatic interaction, producing redox-active modified electrodes.⁹ Nafion, which is one of the representative polymer electrolytes, is well studied to immobilize electroactive cations, including its application in sensing and photoelectric devices.¹⁰

In this chapter, we examined the electrostatic immobilization of an organic redox species in the Nafion layer by means of the TEMPOL/TEMPOL⁺ redox couple in an aqueous electrolyte solution and elucidated the redox performance of the immobilized and accumulated TEMPOL/TEMPOL⁺ in the Nafion layer. Application of the TEMPOL-redox modified counter electrode to DSSC resulted in an appropriate conversion efficiency of 2.1% by means of an environmentally-benign aqueous electrolyte. This chapter refer to the paper of Chemistry of Letters, 43, 480 (2014) written by the author.

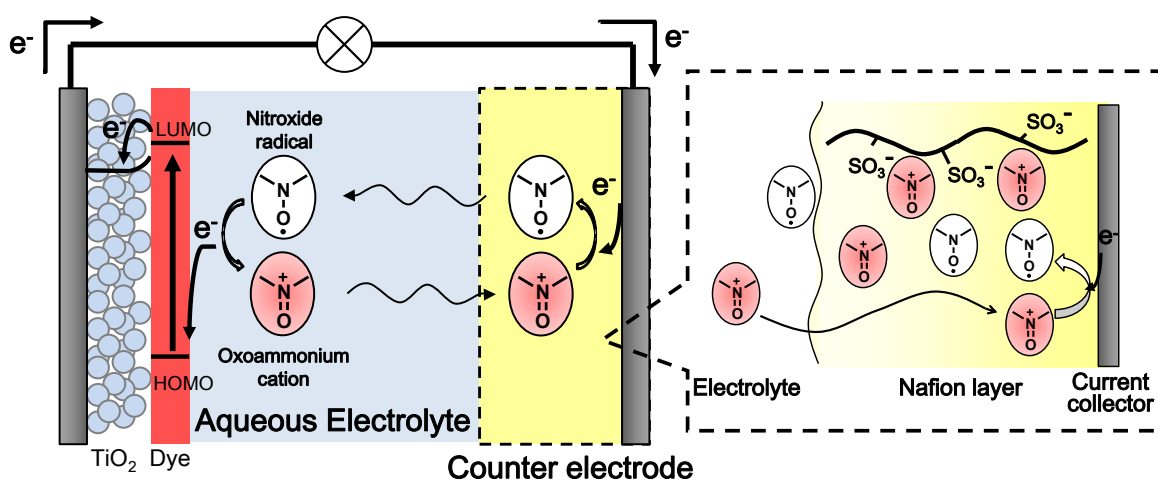


Figure 6.1.1 Schematic image of the DSSC composed with the Nafion coated counter electrode.

6.2 Redox Performance of the Fixed Hydroxy-TEMPO Radical in the Nafion Layer

An Nafion-coated electrode (NCE) was prepared by casting the Nafion propanol solution on a Pt plate with a layer thickness of 1.2 μm . Cyclic voltammogram (CV) of the aqueous TEMPOL solution was measured with the NCE as a working electrode, which gave 1.6 times-enhanced reduction peak current in comparison to that of the uncoated Pt electrode. The redox potential ($E_{1/2}$) was at 0.44 V vs. Ag/AgCl which was negatively shifted with 60 mV from that of the uncoated Pt electrode (Figure 6.2.1 (a)). A similar negative shift of $E_{1/2}$ had been reported for NCE in the aqueous solution of the ferrocene/ferricinium couple, which was explained with a localization of the ferricinium cation in the Nafion layer.¹¹ For the $\text{Ru}(\text{bpy})_3^{2+}/\text{Ru}(\text{bpy})_3^{3+}$ and $\text{Cu}(\text{bpy})_2^{2+}/\text{Cu}(\text{bpy})_2^{3+}$ couple in aqueous electrolytes, the NCE remarkably enhanced redox peak currents, which was ascribed to the immobilization of redox-active di- and tri-valent cations in the Nafion layer through an electrostatic interaction.^{9,12} On the other hand, the TEMPOL couple involves the neutral species and the mono-valent cation, a selective immobilization or accumulation of the cationic species in the NCE could be expected while the immobilization amount itself was lower than those of the multi-valent cationic redox couples in NCE.

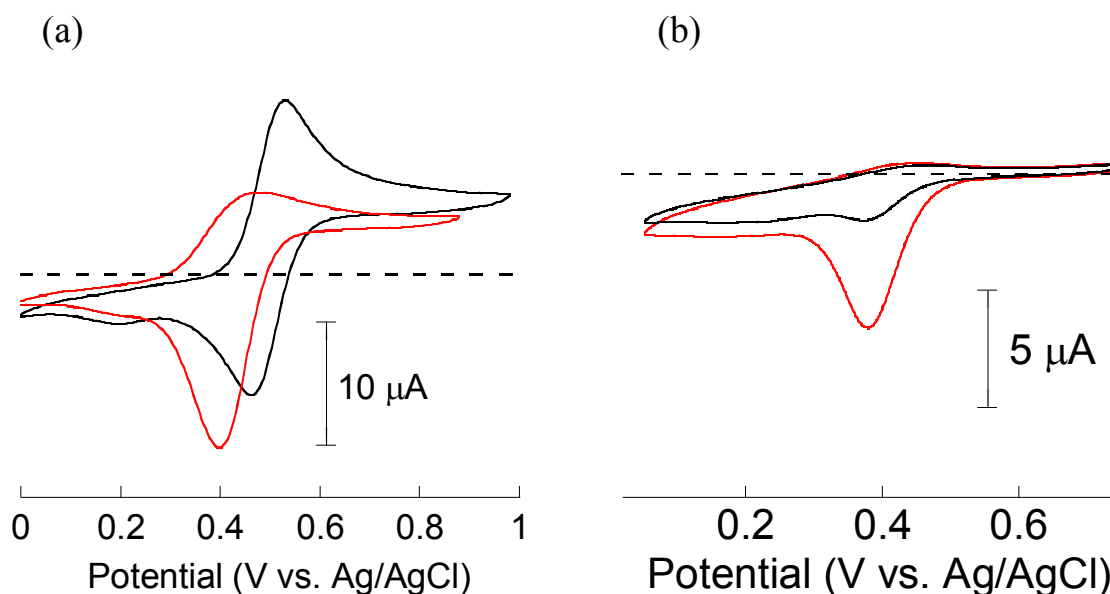


Figure 6.2.1. Cyclic voltammograms for the NCE (red line) and a Pt electrode (black line) in the 1.0 M NaBF_4 aqueous solution of 10 mM TEMPOL (a), and for the TEMPOL⁺-holding NCE immersed in the aqueous 1.0 M NaBF_4 solution at the first cycle (red line) and the second cycle (black line) (b); scan rate = 10 mV/s.

To estimate the amount of TEMPOL⁺ immobilized in the NCE, the NCE holding TEMPOL⁺ was prepared as follows: The potential of 0.8 V vs. Ag/AgCl was applied to the NCE as the working electrode in the aqueous electrolyte solution containing 1.0 M TEMPOL to oxidize TEMPOL to TEMPOL⁺, and the NCE was immersed in the aqueous electrolyte without TEMPOL for a half day. The reduction peak current in CV for the TEMPOL⁺-holding NCE disappeared at the second cycle (Figure 6.2.1 (b)), which suggested that the neutral TEMPOL radical molecule generated under the negative potential during the first cycle diffused out to the electrolyte from the Nafion layer. The amount of TEMPOL⁺ immobilized in the NCE was estimated to be as 2.3×10^{-8} mol/cm² from the reduction peak area at the first cycle, which was appropriate from the ion-exchange capacity of the Nafion and the previously reported data for the NCE with metal complexes.⁹

The effects of the TEMPOL⁺ immobilization in NCE were first analyzed on the enhanced reduction current density for the NCE by measuring the chronoamperometry (Figure 6.2.2). The TEMPOL⁺-holding NCE, used as the working electrode under the application of negative potential (0.1 V vs. Ag/AgCl), gave the steady-state reduction current which was enhanced more than that of the uncoated Pt electrode (Inset of Figure 6.2.2). It was suggested that the immobilization or accumulation of TEMPOL⁺ in NCE formed a steep concentration gradient in the Nafion layer and led to the reduction reaction enhancement.

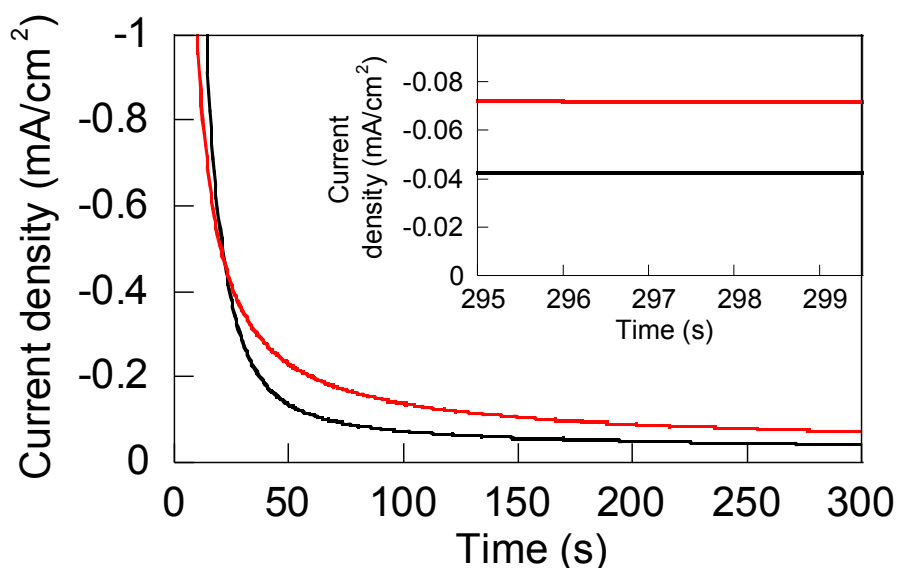


Figure 6.2.2. Chronoamperograms on the controlled-potential electrolysis at 0.1 V (vs. Ag/AgCl) for the NCE (red line) and a Pt electrode (black line) in the aqueous 1.0 M NaBF₄ solution of 1.0 M TEMPOL/TEMPOL⁺. Inset: The steady-state current density.

6.3 Aqueous Dye-Sensitized Solar Cell Performance using Nafion-Coated Electrode

Finally, the TEMPOL-based aqueous electrolyte and NCE were applied to the DSSC. The current density–voltage characteristics and the photovoltaic parameters of the DSSC cells utilizing the Nafion-modified counter electrode are given in Figure 6.3.1 and Table 6.3.1 along with those of the reference cell with Pt. The NCE-cell resulted in a significant increase of short-circuit current density (J_{SC}) and fill factor (FF) which could be ascribed to the low cell resistance resulting from the high efficiency in the regeneration reaction of mediator or the steep concentration gradient of the mediator cation. The higher J_{SC} was obtained by means of the electrolyte with a higher concentration of TEMPOL and responded to the conversion efficiency (η) beyond 2.1%. This η value is significant among those of the previously reported DSSCs based on aqueous electrolytes, and it could be improved by optimizing a combination of the supporting electrolyte composition and dye species.

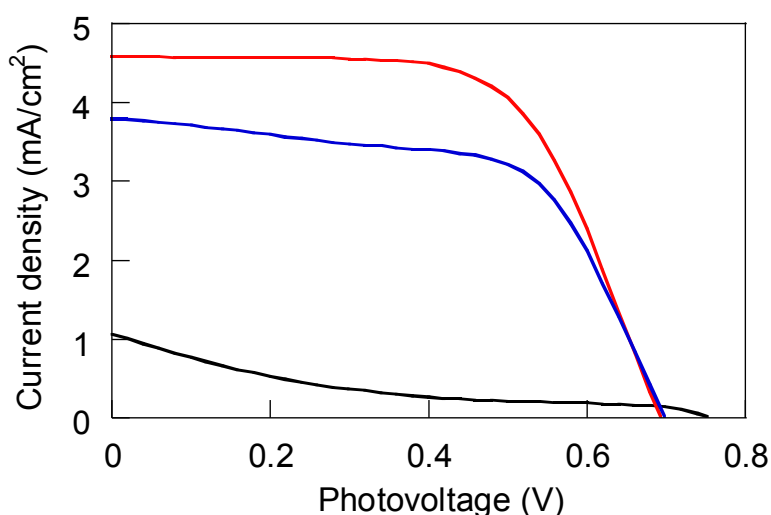


Figure 6.3.1. Current density-voltage characteristics fabricated with the Nafion-coated counter electrode by means of the aqueous electrolyte solution of 1.0 M TEMPOL (red line) and 0.5 M TEMPOL (blue line) as the redox mediator. The black line represents the control experiment using a Pt counter electrode with the electrolyte solution of 1.0 M TEMPOL.

Table 6.3.1. Photovoltaic parameters of the DSSCs fabricated with the Nafion-coated or Pt counter electrode using TEMPOL as the redox mediator, measured under 1 sun irradiation.

| Counter | TEMPOL (M) | J_{sc} (mA/cm ²) | V_{oc} (V) | FF (-) | η (%) |
|---------------|---------------|-----------------------------------|-----------------|-------------|---------------|
| Nafion-coated | 1.0 | 4.5 | 0.69 | 0.64 | 2.1 |
| | 0.5 | 3.8 | 0.70 | 0.61 | 1.6 |
| Pt | 0.5 | 1.1 | 0.76 | 0.14 | 0.11 |

6.4 Experimental Section

Methods

4-Hydroxy-2,2,6,6-tetramethylpiperidine 1-oxyl free radical (TEMPOL) was purchased from Tokyo Chemical Industry Co. Nafion 5 wt% dispersion was purchased from Aldrich. ¹H NMR spectra were recorded on a JEOL ECX-500 spectrometer with chemical shifts downfield from tetramethylsilane as the internal standard. Mass spectra were obtained using a JMS-GCMATE II. Elemental analyses were performed using a Perkin-Elmer model PE-2400 II elemental analyzer.

Electrochemical measurements of TEMPOL on the NCE

NCE was prepared by casting the Nafion propanol solution on a Pt plate with a layer thickness of 1.2 μm . Cyclic voltammogram and chronoamperograms of TEMPOL on the NCE in the aqueous electrolyte were carried out with a Pt disk electrode, a Pt coil, and an Ag/AgCl electrode as the working, the counter, and the reference electrode, respectively, using an ALS700 electrochemical analyzer.

Preparation of the cell and photovoltaic characteristics

The TEMPOL-based aqueous electrolyte and NCE were applied to the DSSC. The DSSC cell was fabricated as follows. The working electrode, a 2.8 μm TiO₂ layer and a 3.1 μm light-scattering layer, were heated at 450 °C for 1 h, and then immersed in a 0.3 mM dye (D205: (5-{1,2,3,3a,4,8b-hexahydro-4-[4-(2,2-diphenylvinyl)phenyl]cyclopenta[b]indole-7-ylmethylene}-3'-n-octyl-4,4'-dioxo-2'-[2,5']bithiazolidine-3-yl)acetic acid) solution in tert-butyl alcohol/acetonitrile (1/1 v/v) for 20 h at room temperature. The electrode and the TEMPOL⁺-holding NCE were dipped in an aqueous electrolyte for 1 day for fabricating in the DSSC cell. The electrolyte was the aqueous 1.0 M NaBF₄ solution containing 0.5 or 1.0 M TEMPOL.

References

- 1 T. Suga, Y. J. Pu, K. Oyaizu, H. Nishide, *Bull. Chem. Soc. Jpn.* **2004**, *77*, 2203.
- 2 G. Seber, R. S. Freitas, J. T. Mague, A. P. Filho, X. Gratens, V. Bindilatti, N. F. Oliveira, Jr., N. Yoshioka, P. M. Lahti, *J. Am. Chem. Soc.* **2012**, *134*, 3825.
- 3 T. Kaneko, H. Abe, M. Teraguchi, T. Aoki, *Macromolecules* **2013**, *46*, 2583.
- 4 K. Moonen, I. Laureyn, C. V. Stevens, *Chem. Rev.* **2004**, *104*, 6177.
- 5 H. Nishide, S. Iwasa, Y. J. Pu, T. Suga, K. Nakahara, M. Satoh, *Electrochim. Acta* **2004**, *50*, 827.
- 6 H. Nishide, T. Suga, *Electrochem. Soc. Interface* **2005**, *14*, 32.
- 7 T. Suga, H. Konishi, H. Nishide, *Chem. Commun.* **2007**, 1730.
- 8 H. Nishide, K. Oyaizu, *Science* **2008**, *319*, 737.
- 9 K. Oyaizu, Y. Ando, H. Konishi, H. Nishide, *J. Am. Chem. Soc.* **2008**, *130*, 14459.
- 10 K. Nakahara, K. Oyaizu, H. Nishide, *Chem. Lett.* **2011**, *40*, 222.
- 11 K. Koshika, N. Sano, K. Oyaizu, H. Nishide, *Chem. Commun.* **2009**, 836.
- 12 N. Sano, W. Tomita, S. Hara, C. Min, J. Lee, K. Oyaizu, H. Nishide, *ACS Appl. Mater. Interfaces* **2013**, *5*, 1355.
- 13 K. Takahashi, H. Nishide, *Chem. Lett.* **2013**, *42*, 218.
- 14 Trends in Advanced Sensitized and Organic Solar Cells, ed. T. Miyasaka, CMC, Tokyo, 2012.
- 15 B. O'Regan, M. Grätzel, *Nature* **1991**, *353*, 737.
- 16 A. Yella, H. Lee, H. N. Tsao, C. Yi, A. K. Chandiran, M. Nazeeruddin, E. W. Diau, C. Yen, S. M. Zakeeruddin, M. Grätzel, *Science* **2011**, *334*, 629.
- 17 T. Kinoshita, J.T. Dy, S. Uchida, T. Kubo, H. Segawa, *Nature Photonics* **2013**, *7*, 535.
- 18 T. N. Murakami, M. Grätzel, *Inorganica Chimica Acta* **2008**, *361*, 572.
- 19 F. Kato, N. Hayashi, T. Murakami, C. Okumura, K. Oyaizu, H. Nishide, *Chem. Lett.* **2010**, *39*, 464.
- 20 F. Kato, A. Kikuchi, T. Okuyama, K. Oyaizu, H. Nishide, *Angew. Chem.* **2012**, *124*, 10324.
- 21 T. Daeneke, Y. Uemura, N. W. Duffy, A. J. Mozer, N. Koumura, U. Bach, L. Spiccia, *Adv. Mater.* **2012**, *24*, 1222.
- 22 H. Tian, E. Gabrielsson, P. W. Lohse, N. Vlachopoulos, L. Kloo, A. Hagfeldt, L. Sun, *Energy Environ. Sci.* **2012**, *5*, 9752.
- 23 W. Xiang, F. Huang, Y. Cheng, U. Bach, L. Spiccia, *Energy Environ. Sci.* **2013**, *6*, 121.
- 24 N. Oyama, T. Shimomura, K. Shigehara, F. C. Anson, *J. Electroanal. Chem.* **1980**, *112*, 271.

- 25 C. R. Martin, I. Rubinstein, A. J. Bard, *J. Am. Chem. Soc.* **1982**, *104*, 4817.
- 26 A. Rastogi, S. Nad, M. Tanaka, N. D. Mota, M. Tague, B. A. Baird, H. D. Abruña, C. K. Ober, *Biomacromolecules* **2009**, *10*, 2750.
- 27 M. Krishnan, X. Zhang, A. J. Bard, *J. Am. Chem. Soc.* **1984**, *106*, 7371.
- 28 T. M. Downey, T. A. Nieman, *Anal. Chem.* **1992**, *64*, 261.
- 29 T. Tamura, H. Kawakami, *Nano Lett.* **2010**, *10*, 1324.
- 30 I. Rubinstein, *J. Electroanal. Chem.* **1985**, *188*, 227.
- 31 D. Rong, F. C. Anson, *J. Electroanal. Chem.* **1996**, *404*, 171.

Chapter 7

Conclusion and Future Prospects

Contents

7.1 Conclusion

7.2 Future Prospects

References

7.1 Conclusion

In this thesis, the synthesis and hydrogen storage properties of polymer-based hydrogen carriers were described. In this chapter, the characteristics of such polymer-based hydrogen carriers and important conclusions derived from this study are summarized.

In chapter 2, a hydrogen carrier polymer was prepared using the molecular design of fluorenone/fluorenol as a hydrogen-fixing and -releasing unit. The electrolytic reduction and protonation with water were successfully combined for the hydrogenation of the polymer, which is a largely different process from a water splitting; the hydrogenation of the polymer could fix hydrogen through the formation of chemical bonds, whereas a water-splitting process only releases hydrogen. Direct electrolytic hydrogenation with water could have great potential as a process to reduce energy consumption required for hydrogen-fixing and to eliminate many hydrogen production processes. The theoretical hydrogen storage capacity of the fluorenol polymer was 0.29 wt%.

In chapter 3, poly(vinyl fluorenone/fluorenol) was synthesized via radical polymerization. The fluorenone polymer fixed the charge in the aprotic solvent and hydrogen in the aprotic solvent by electrolytic reduction. After the charging and hydrogenation, the polymer reversely discharged and released hydrogen gas without any significant deterioration.

In chapter 4, a quinaldine polymer was prepared and coated on a carbon substrate as a scaffold of nickel electrodeposition, to facilitate the electrochemical hydrogenation of a quinaldine unit using water as a hydrogen source. The electrochemical hydrogenation efficiency of quinaldine was enhanced by coating the quinaldine polymer on the substrate, and the nickel ion was dissolved in the aqueous electrolyte. The hydroquinaldine polymer evolved hydrogen by warming it at 80 °C in water containing the iridium complex catalyst, and its evolution rate was larger than that from the monomeric hydroquinaldine. The electrochemically hydrogenated quinaldine polymer also successfully evolved hydrogen by simply warming it in the aqueous solution.

In chapter 5, the iridium complex, which had been used as a catalyst for hydrogen evolution from alcohols, was electrolytically reduced and oxidized through the hydrogenation of carbonyl compounds with water as hydrogen source. The hydrogenated product evolved hydrogen by warming in the same iridium catalyst. (Chapter 5)

In chapter 6, TEMPOL⁺ was adsorbed in the Nafion layer of an electrode and the adsorption amount of TEMPO⁺ was almost same as that of metal complexes J_{SC} , FF , and η which were improved for the Nafion-coated counter electrode, probably because the high concentration gradient facilitated the reductive reaction.

7.2 Future Prospects

In this thesis, electrolytic hydrogenation was examined as a methodology of organic hydride production operated under mild conditions using only water as a proton source. Furthermore, organic hydrides were polymerized and produced polymer-based hydrogen carriers having the inherent advantages of polymers, such as mouldability, non-flammability and low toxicity. In chapter 6, the iridium complex exhibited catalytic activities of both hydrogenation and dehydrogenation, as well as storing and releasing hydrogen in a one-pot reactor, indicating that the iridium or carbonyl compound acted as the catalyst for water splitting. If the reduction potential of fluorenone or iridium complex was lower than that of water, they could be applied to an organic water splitting catalyst. In that case, the introduction of the N-hetero structure into the fluorenone would be effective to positively shift the reduction potential of the compound.

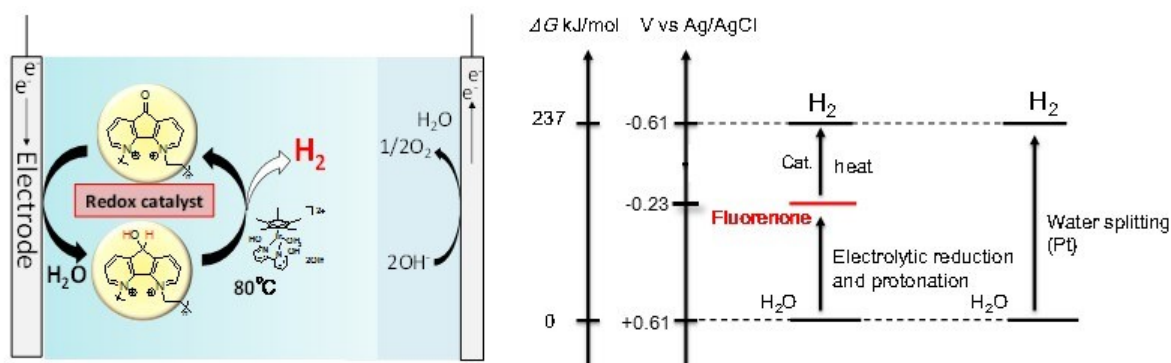


Figure 7.2.1 Schematic image of the water splitting with fluorenone derivative

In chapter 6, the iridium complex was electrochemically reduced and chemically oxidized with the hydrogenation of carbonyl compounds using water as a hydrogen source, suggesting that the structure of the carbonyl compound does not have to be electroactive and contain some special structure, such as an aromatic ring. The hydrogenation and dehydrogenation process with the iridium complex could be expanded to reactions with other, general alcohol/ketone polymers, such as poly(vinyl alcohol) and polysaccharide, and the iridium catalyst has potential to apply general polymers to polymer-based hydrogen carriers.

List of Publications

1. Ryo Kato, Keisuke Yoshimasa, Tatsuya Egashira, Takahiro Oya, Kenichi Oyaizu, Hiroyuki Nishide, “A Ketone/Alcohol Polymer for Cycle of Electrolytic Hydrogen-Fixing with Water and Releasing under Mild Conditions”, *Nature Communications*, **7**, 13032 (2016).
2. Ryo Kato, Fumiaki Kato, Kenichi Oyaizu, Hiroyuki Nishide, “Redox-Active Hydroxy-TEMPO Radical Immobilized in Nafion Layer for an Aqueous Electrolyte-Based and Dye-Sensitized Solar Cell”, *Chemistry Letters*, **43**, 480–482 (2014).
3. Ryo Kato, Takahiro Oya, Yuma Shimazaki, Kenichi Oyaizu, Hiroyuki Nishide, “A Hydrogen Storable Quinaldine Polymer: Ni-Electrodeposition-Assisted Hydrogenation and Hydrogen Evolution from the Polymer”, *Polymer International*, DOI: 10.1002/pi.5327.

Patent

Hiroyuki Nishide, Kenichi Oyaizu, Takeo Suga, Keisuke Yoshimasa, Ryo Kato, “Hydrogen carrier and hydrogen generation method”, WO2015005280.

List of Presentations

1. Ryo Kato, Keisuke Yoshimasa, Kenichi Oyaizu, Hiroyuki Nishide, “Poly(vinylfluorenone): A Novel Hydrogen Storage Material”, *16th IUPAC International Symposium on Macromolecular Complexes*, Wroclaw, Poland, August 2015.
2. Ryo Kato, Tatsuya Egashira, Kenichi Oyaizu, Hiroyuki Nishide, “Synthesize of Fluorenone-substituted Polymers and Their Charge and Hydrogen Storage Properties”, *64th Symposium on Macromolecules, the Society of Polymer Science, Japan*, Sendai, September 2015.
3. Ryo Kato, Keisuke Yoshimasa, Kenichi Oyaizu, Hiroyuki Nishide, “Charge Storage Characteristic of Poly(vinylfluorenone) and Its Electrolytic Hydrogenation”, *The 64th Annual Meeting of the Society of Polymer Science, Japan*, Sapporo, May 2015.
4. Ryo Kato, Fumiaki Kato, Kenichi Oyaizu, Hiroyuki Nishide, “Adsorption Behavior of Redox Active Species on Nafion-Coated Electrode and Its Application to Dye-Sensitized Solar Cell”, *The 62nd Annual Meeting of the Society of Polymer Science, Japan*, Kyoto, May 2013.
5. Ryo Kato, Fumiaki Kato, Kenichi Oyaizu, Hiroyuki Nishide, “Electrochemical Property of Nitroxide Radical Derivatives on Nafion-Coated Electrode”, *The 92nd Annual Meeting 2012, Japan*, Tokyo, March 2012.

Acknowledgements

The present thesis is the collection of the studies which have been conducted under the direction of Prof. Dr. Hiroyuki Nishide, Department of Applied Chemistry in Waseda University, during the 2011-2017. The author is extremely grateful to Prof. Dr. Hiroyuki Nishide for his valuable suggestion, advice, and continuous encouragement throughout this work.

The author is also extremely grateful to Prof. Dr. Kenichi Oyaizu (Waseda Univ.) for his valuable advice and efforts as members on judging committee for the doctoral thesis.

The author expresses the greatest acknowledgement to Prof. Dr. Yasushi Sekine (Waseda Univ.), Prof. Dr. Martin Sjödin (Uppsala University), and Dr. Hiroshi Mouri (Bridgestone Co.) for their efforts as members on judging committee for the doctoral thesis.

The author expresses the great acknowledgement to Prof. Dr. Yoshinori Nishikitani (Waseda Univ.) for his valuable advice, encouragement.

The author is great indebted to Assistant Prof. Dr. Takeo Suga for his useful technical advice, excellent discussion, and very kind support.

The author expresses the great acknowledgement to Dr. Fumiaki Kato (Samsung Co.), and Dr. Satoshi Nakajima (RICOH Co.), Dr. Wonsong Choi (Samsung Co.), Dr. Naoli Sano (Fuji Film Co.), Dr. Katsuyuki Takahashi (GS Yuasa Co.), Dr. Natsuru Chikushi (Fuji Film Co.), Dr. Takashi Sukegawa (Asahi Kasei Co.), and Dr. Fuyuki Aida (JX Nippon Oil & Energy Co.).

The author express special thanks to all active collaborators, namely Mr. Keisuke Yoshimasa (Fuji Film Co.), Mr. Tatsuya Oka (Toppan Printing Co.), Mr. Tatsuya Egashira (DIC Co.), Ms. Yuma Shimazaki (JX Nippon Oil & Energy Co.), Mr. Takahiro Oya, Ms. Ayaka Iwawaki, Mr. Masataka Nakajima, and Mr. Hiroki Sumi.

The author acknowledges Mr. Yoshito Sasada and Mr. Hiroshi Tokue for their exciting discussion and kind assistance. The author also acknowledges Mr. Hirofumi Maruo for his kind support. The author sincerely thanks to all members of the laboratory.

The author acknowledges the Leading Graduate Program in Science and Engineering, Waseda University, from MEXT, Japan.

Special thanks to the Society of Applied Chemistry of Waseda Univ. scholarship, the Scholarship for Young Doctoral Students of Waseda Univ., Toshiyuki Mizuno Memorial Scholarship, and Nakasone Scholarship for the financial support.

Finally, the author expresses his deepest gratitude heartily to his family, Mr. Shinichi Kato, Mrs. Atsuko Kato, and Ms. Eriko Kato for their heartfelt supports.

January, 2017

Ryo Kato